Mobil Tyco Solar Energy Corporation
16 Hickory Drive
Waltham, Massachusetts 02154

LARGE AREA SILICON SHEET BY EFG

Program Manager: F.V. Wald

Second Quarterly Report - Subcontract No. 954355

Covering Period: April 1, 1977 - June 30, 1977

June 15, 1977

ABSTRACT

During the quarter on which this document reports significant amounts of 2" wide
ribbon have been grown from both growth systems at speeds up to 2"/min. Solar cells
prepared from the material have shown conversion efficiencies up to 8% (AM1).

Thus, we believe that the basic effort to produce reasonably clean conditions in
these resistance heated furnaces has succeeded. However, the ribbons produced show
a cross-sectional structure which is significantly different from that of induction
furnace grown ribbon (1" wide at a rate of 1"/min). Also, the ribbon produced in
this program has unusually large inhomogeneities across its width. Some hypotheses
to explain both of these features are advanced in the report and the possible implica-
tions for solar cell performance are touched upon.

The multiple ribbon growth system (JPL No. 3A) has shown a number of flaws with
respect to the reliability of the basic furnace design. These definitely need to be
rectified before any significant demonstration of multiple ribbon growth can proceed.
The cartridges, however, have performed quite well. The work on 3" cartridge design
and automatic controls has proceeded nearly on schedule and the report contains a
detailed description of the approach and the equipment to be used for automatic control
of ribbon width.

Table of Contents

List of Figures

List of Tables

# I. INTRODUCTION

The present program is part of a total Mobil Tyco Solar Energy Corporation objective to produce silicon ribbon for solar cells at a cost which will allow their wide scale use for generation of electric power. On February 14, 1977, it was significantly expanded with the addition of several new tasks. In order to carry out these tasks, major pieces of equipment which have been designed and built under in-house funded programs were made available for use under the contract, namely a multiple EFG ribbon growth station and automatic growth control devices.

The edge-defined, film-fed growth process itself was initially developed for the commercial production of continuous, shaped single crystals of sapphire from the melt and was applied to growth of silicon for solar cells partly under NSF Grant GI37067X via Harvard University, JPL Contract 953365, and under NSF Grant GI433873. The basic feasibility of the application of EFG to the growth of silicon ribbon has been proven and the theoretical base for extending the technique to the efficient production of single crystal silicon sheet has been established. There are three fundamental objectives which are now being pursued:

1. Demonstrate that, from an improved resistance heated EFG crystal growth station (JPL No. 1), it is possible to obtain growth of single, continuous ribbons, 3 inches wide at a rate of 3 inches per minute. These ribbons furthermore are to be of a quality sufficient for fabrication of solar cells between 8% and 12% AM1 efficiency.

2. Demonstrate, by using the resistance heated multiple growth station made available to the program by Mobil Tyco (Machine No. 16, now JPL No. 3A), that it is possible to grow simultaneously 5 ribbons of 2 inch width at 3 inches per minute, using automatic control systems which have been developed also by Mobil Tyco and which are likewise made available to the program to be mated with the growth station.

3. Characterize the material grown not only in terms of its electrical and crystallographic properties, but more particularly as a solar cell. The aim here is to identify any fundamental barrier which might prevent the material from achieving 12% AM1 solar conversion efficiency when grown from the crystal growth stations employed here.

In summary, the program is now entering into a greater engineering research and development effort. Thus, the crystal growth machines now being used can be considered forerunners of true production machines because of their capability for wide (2" - 3") high speed (3"/min) multiple (5 ribbons) growth under automatic control. Also, with respect to the capability of the material to produce solar cells, the

1

question is no longer whether EFG material is fundamentally capable of yielding solar cells of more than 10% AM1 efficiency, but, rather whether crystal growth machines operating at the high speeds required for economic reasons and with the complexity necessary for multiple growth can be designed such that they produce material from which large (e.g., 3" x 3") cells of good efficiency can be fabricated at high yields.

## II. WORK ON CRYSTAL GROWTH STATION JPL No. 1 by J. Kalejs and T. Surek

### A. Overview

Two series of four growth runs each in the material quality program proposed earlier[1] have been completed in Station JPL No. 1 during this quarterly period. Comprehensive new clean procedures and uniformity in material handling have been instituted with the aim of upgrading material quality. Geometrical, electrical, chemical, and structural studies of as-grown material and of fabricated solar cells are being carried out to establish a baseline material characterization for the JPL No. 1 growth system.

Ribbon grown from JPL No. 1 in the first series of runs has been processed into solar cells. Overall average values of power density, generally above 6 mW/cm$^2$ for AR coated cells, show significant improvement over those for cells fabricated from previously grown material. Several distinguishing features of JPL No. 1 as-grown material have been identified. A central grain structure (in the thickness dimension) appears in all of the ribbon examined. Infrared absorption measurements have revealed absorption peaks attributed to substitutional aluminum in the ribbon. Neither of these features is present in "good" solar cell material produced in induction furnaces. In addition, material inhomogeneity over distances much smaller than a typical full-size cell (2 cm by 10 cm) is reflected in large variations of diffusion length obtained from SPV measurements, as well as from analysis of solar cell spectral response. Further investigation will be necessary to determine the origin of these features and how they contribute to degradation of cell performance.

The emphasis in the ongoing material quality program has now been shifted to concentrate on identifying the origins of material inhomogeneity, of the central structure, and of the substitutional aluminum impurities. Experiments are planned with modified dies and cartridges which will allow variations of growth parameters to study the effect of interface shape and fluid flow changes on material structure and quality. Structural, electrical, and analytical studies are being continued to attempt to correlate changes in growth parameters to cell performance. Graphite crucibles have been designed to replace the fused silica which is suspected to be the major source of aluminum.

The fabrication of the 7.5 cm cartridge and puller is proceeding nearly on schedule. Assembly of the cartridge has started; both systems will be tested during the next quarterly period.

3

## B. Crystal Growth

### 1. Experimental

Data for the runs made in this reporting period appears in Table I. Each of the two series of four growth runs was preceded by a dismantling and thorough cleaning of the furnace. The runs within each series differed only in limited component replacements. Crucible covers were used in all the runs. Except for runs 18-15 and 18-18, the covers consisted of a graphite plate slotted on the melt side to reduce the tendency to warp. The two exceptions had a solid graphite plate with an inner grafoil liner. The presence of a crucible cover was observed to cool the die ends, more so when the grafoil liner was in place. Since the latter did not appear to offer any advantage, it was not used in the second series of clean runs, 18-19 to 18-23.

This second series differed in several respects from the first. A 4 in. long fused silica crucible replaced the 6 in. long crucible used previously. The combination of the shorter crucible with approximately the same 270 gm charge should lead to a lower value of the crucible surface-to-melt-volume ratio, and hence to less contamination of the melt by impurities from the crucible. An additional difference was an increase in the melt doping level (p-type) to give 1 $\Omega$-cm material in runs 18-19 to 18-23 instead of the 10 $\Omega$-cm material of runs 18-15 to 18-18. Solar cells made from 1 $\Omega$-cm material are expected to have higher values of open circuit voltage than obtained with 10 $\Omega$-cm doping.

The growth runs reported in Table I were notable in the low incidence of system failures and a high success rate in obtaining stable growth conditions. Interruptions in growth occurred once as a result of die heater failure. A broken heater in run 18-23 was thought to be a consequence of silicon flooding from the die top to nearby radiation shields. Only limited growth was achieved after the flooding because of unstable thermal conditions. Water flooding at the top of the cartridge resulted in the termination of run 18-21 without growth. The water damage was confined to the cartridge, and normal operation with a rebuilt cartridge was resumed the next day. The heater element and power studs functioned reliably throughout this period.

A total of 34 meters (112 feet) of ribbon was grown in eight successful growth runs. Included in these runs were several periods of operator training. The crucible was emptied of melt on two occasions (runs 18-16 and 18-20). The most stable growth configuration was found to be at about seven-eighths of the full width of the 5 cm die. This width was usually achieved after one to one and a half feet of growth. It has been observed that ribbon growth is generally more stable when the ribbon edges

4

Table I. JPL No. 1 Ribbon Data

| Ribbon No. | Desired Resistivity Ω·cm (P-Type) | Growth Speed (cm/min) | Maximum Width (cm) | Length (cm) | Thickness (Mils) Min. | Max. | Diffusion Length* $L_D$ (μ) Range | Average | Comments |
|---|---|---|---|---|---|---|---|---|---|
| 18-15-1 | 10 | 3.8 | 4.8 | 46 | 12 | 15 | 0 | 0 | Many SiC particles |
| 18-15-2 | | 4.1 | 5.1 | 46 | 11 | 15 | 0-11† | 5.5 | Many SiC particles |
| 18-15-3 | | 4.1 | 5.1 | 127 | 8 | 13 | 0 | 0 | Many SiC particles |
| 18-15-4 | | 4.1 | 5.1 | 43 | 8 | 13 | - | - | Difficult to spread |
| 18-16-1 | 10 | 4.0 | 4.8 | 28 | 15 | 19 | 0-2 | 0.5 | Cold ends |
| 18-16-2 | | 4.0 | 3.8 | 23 | 10 | 18 | - | - | End heater fuse blew |
| 18-16-3 | | 3.1 | 3.8 | 19 | 10 | 20 | - | - | Grew slowly on purpose |
| 18-16-4 | | 4.0 | 5.1 | 43 | 10 | 20 | - | - | |
| 18-16-5 | | 4.0 | 5.1 | 46 | 13 | 20 | 0-3 | 1.4 | |
| 18-16-6 | | 4.3 | 5.1 | 127 | 11 · | 18 | 0-5 | 1.8 | Stable conditions |
| 18-16-7 | | 4.2 | 3.8 | 22 | 15 | 20 | 0-1 | 0.5 | |
| 18-16-8 | | 4.2 | 3.8 | 10 | 15 | 18 | 0-3 | 2.5 | |
| 18-17-1 | 10 | 4.0 | 5.1 | 77 | 12 · | 18 | 0 | 0 | Difficult to keep full width |
| 18-17-2 | | 4.0 | 5.1 | 146 | 12 | 15 | 3-8 | 5.0 | Known $L_D$ seed |
| 18-17-3 | | 4.1 | 4.8 | 47 | 10 | 14 | - | - | Cold ends |
| 18-17-4 | | 4.1 | 4.5 | 125 | 10 | 15 | 0-15 | 6.8 | Full stroke, 3/4 width |
| 18-17-5 | | 4.5 | 4.4 | 66 | 8 | 12 | - | - | High speed |
| 18-18-1 | 10 | 3.7 | 5.1 | 74 | 10 | 19 | 2-3 | 2.5 | Very difficult to spread |
| 18-18-2 | | 3.6 | 4.5 | 56 | 13 | 18 | 1-5 | 3.3 | Stable at 3/4 width |
| 18-18-3 | | 4.0 | 2.2 | 40 | - | - | - | - | Cold ends; operator training |
| 18-19-1 | 1 | 3.8 | 4.3 | 135 | 12 | 19 | 0-3 | 0.8 | Stable growth |
| 18-19-2 | | 5.0 | 4.3 | 137 | 10 | 13 | 0-1 | 0.2 | Stable growth |
| 18-19-3 | | 5.7 | 4.3 | 69 | 9 | 15 | 0 | 0 | Not stable at this speed |
| 18-19-4 | | 3.8 | 4.3 | 51 | 12 | 15 | 0 | 0 | Froze on quartz tube; operator training |
| 18-19-5 | | 3.8 | 2.5 | 10 | - | - | - | - | Froze while spreading; operator training |
| 18-20-1 | 1 | 4.5 | 4.6 | 85 · | 10 | 15 | 2-4 | 2.7 | Froze on left |
| 18-20-2 | | 4.6 | 4.6 | 127 | 9 | 13 | 0-3 | 2.2 | Stable growth |
| 18-20-3 | | 5.1 | 4.6 | 125 | 10 | 13 | 1-7 | 2.4 | Stable growth |
| 18-20-4 | | 5.2 | 4.6 | 125 | 9 | 13 | - | - | Stable growth |
| 18-20-5 | | 5.1 | 4.6 | 125 | 9 | 13 | - | - | Stable growth |
| 18-20-6 | | 5.0 | 4.6 | 127 | 9 | 11 | 0-4 | 2.0 | Stable growth |
| 18-20-7 | | 4.8 | 4.6 | 51 | 8 | 12 | - | - | Die beginning to be coated with SiC |
| 18-20-8 | | 4.5 | 4.6 | 91 | 10 | 13 | 0 | 0 | Crucible almost empty |
| 18-21 | 1 | - | - | - | - | - | - | - | Water flood in cartridge |
| 18-22-1 | 1 | 5.0 | 4.6 | 127 | 9 | 12 | 3-5 | 4.2 | Stable growth |
| 18-22-2 | | 5.0 | 4.6 | 127 | 9 | 11 | - | 8.8 | Stable growth |
| 18-22-3 | | 5.0 | 4.6 | 33 | 8 | 11 | - | - | Sudden freeze |
| 18-22-4 | | - | - | - | - | - | - | - | Many freezes |
| 18-22-5 | | 5.0 | 4.6 | 122 | 9 | 12 | 4-8 | 6.1 | |
| 18-22-6 | | 5.0 | 4.6 | 127 | 9 | 13 | - | - | |
| 18-22-7 | | 4.9 | 2.5 | · 81 | - | - | - | - | |
| 18-22-8 | | 5.0 | 3.8 | 31 | - | - | - | - | }Operator training |
| 18-22-9 | | 5.3 | 2.0 | 61 | - | - | - | - | |
| 18-23-1 | 1 | 4.5 | 5.0 | 123 | 11 | 15 | 3-8 | 3.9 | End heaters very hot |
| 18-23-2 | | 3.8 | 2.0 | <10 | - | - | - | - | Cold ends, cannot spread |
| 18-23-3 | | 3.8 | 3.0 | 116 | 8 | 16 | 2-5 | 3.8 | Cold ends, cannot spread |

* SPV method. A value of 0 denotes that diffusion lengths were too low to measure accurately.

† One of two measurements gave $L_D$ = 11 μm, the other $L_D$ = 0 μm.

are anchored at some distance from the die ends. This also permits the operator to perform minor adjustments to offset effects of changes in the growth variables (i.e., $h_{eff}$). In the reported experiments, growth at less than full width was caused by cold die ends because of reduced heating due to the presence of the crucible cover. This problem has already been encountered in Station JPL No. 3A and was alleviated there by modification to the cartridge floor. On the other hand, it is also possible to take advantage of the increased stability of growth at less than full width and of the cooler die ends by using oversize dies, e.g., dies wider than 5 cm for 5 cm wide ribbon growth.

A concentrated effort was made in the second series of runs to determine the limits to which growth parameters can be pushed in the present system so as to increase meniscus height, with an attendant reduction in ribbon thickness. These limits were sought in an attempt to change the shape of the growth interface, and thus perhaps to reduce or eliminate the central grain structure. Stable growth at increasing growth rates could be attained during growth at less than full width by simultaneously increasing the helium flow rate to the cartridge as the growth speed was increased. Speeds of 5 to 5.5 cm/min were routinely reached in this manner in runs 18-19, 18-20, and 18-22. Attempts to increase the meniscus height by simultaneously increasing die top temperatures and the helium gas flow rate were not so successful because of the onset of tapering in the ribbon width. This end instability (i.e., tapering) limited the range of growth parameter variations that were possible if stable growth were to be maintained. Changes in meniscus height that were realized are reflected in the minimum ribbon thicknesses given for runs 18-19, 18-20, and 18-22 in Table I. Typically, these were reduced to 9 - 10 mils at the highest growth speeds, 5 cm/min and above.

### 2. Discussion

Criteria for success in the present effort to upgrade material quality have been established on the basis of diffusion lengths in as-grown material and the performance of fabricated solar cells. In both of these areas, significant progress from earlier levels has been made in the two series of clean runs toward quality goals set for the JPL No. 1 growth system. Work toward a related objective, to identify any fundamental barrier which might prevent the material from achieving 12% AM1 solar conversion efficiency, has now also been recognized in the concern over the central grain structure and the aluminum content observed in JPL No. 1 grown material.

a.  Solar Cells

To date, solar cells have been made from material grown in the first series of clean runs only. Full size cells have been chosen for comparison of overall performance improvement in JPL No. 1 material in order to minimize the effect of material inhomogeneity. Average cell power densities, P (mW/cm$^2$), before and after the institution of new clean procedures are summarized in Table II. Improvements of over 50% in P, both with and without antireflection coatings, have been realized in the recent series of runs. It should be noted that the average for the antireflection coated cells from the clean runs includes four cells from run 18-15 which exhibited very poor electrical cell behavior due to an abnormally high SiC particle density. More details on cell performance can be found in Section IV.B.

b.  Diffusion Lengths

Representative sections of as-grown material were taken for diffusion length measurements using the surface photovoltage (SPV) method. Ranges of values and averages of the SPV diffusion length, $L_D$, for ribbons are given in Table I. They represent the first measurable values of SPV diffusion lengths reported for JPL No. 1 material.

Two trends in diffusion length data may be noted: the average $L_D$ values are lower in the first run of each series than in later runs, and the averages are generally highest in the latter part of the second series. However, for reasons given in the section on material characterization, SPV diffusion lengths are at the present time only useful as a qualitative indication of material improvement. However, since the method allows a fast turnaround on many samples, it is still judged to be a valuable aid in determining the direction of crystal growth experiments.

c.  Interface Shape

As explained in a previous report,[2] the presence of the central grain structure in JPL No. 1 ribbon (also discussed in Section IV.B) is felt to be related to the shape of the solid-liquid interface in the thickness cross-section, viz., an interface which is concave toward the solid should lead to the central grain structure. Efforts to influence the central structure through the variation of growth parameters, as discussed in the experimental section above, were not successful. Although the meniscus height was varied by more than 50% (in the 10 - 15 mil range), which led to a decrease in ribbon thickness from an average 12 - 15 mils to 9 - 10 mils, this had no measurable effect on the occurrence of the central structure. It should be remembered these changes were also accompanied by an increase in growth speed from 3 - 4 cm/min

7

Table II.  Averages of Solar Cell Performance of Ribbon from
Station JPL No. 1 Before and After System Cleanup
and Institution of First Level Clean Handling
Procedures.

Before Clean-Up:

| | | P (Cell Quantity) | |
|---|---|---|---|
| Run Number | No AR | | With AR |
| 18-5 | 1.98 (2) | | 2.98 (6) |
| 18-8 | 3.97 (4) | | 3.28 (1) |
| 18-11 | 2.90 (8) | | 3.80 (4) |
| 14 Cell Average: 3.07 | | 11 Cell Average: 3.31 | |

After Clean-Up:

| | | | |
|---|---|---|---|
| 18-15 | | | 3.66 (4) |
| 18-16 | | | 6.61 (8) |
| 18-17 | 4.52 (11) | | |
| 18-18 | 5.75 (3) | | |
| 14 Cell Average: 4.78 | | 12 Cell Average: 5.63 | |

to above 5 cm/min; thus, even though the ribbon thinned considerably, the concavity of the interface was perhaps not affected to any great extent.

Further attempts to change interface shape will now center on modifications to the flat-topped die currently in use. Preliminary tests have shown that complementary modifications to the die heater configuration will in all probability be needed before growth is possible. Other experiments planned are growth with a standard 2.5 cm two-piece die and growth with 5 cm dies with radiused tops. In addition, growth with a modified cartridge to change the thermal conditions above the interface is being planned.

### d. Impurity Distribution

Another series of experiments will incorporate die modifications designed to explore possible effects of lateral fluid flow on impurity distribution along the width of the solid-liquid interface. It has already been suspected that the impurity distribution across the thickness dimension of the ribbon can vary with the interface concavity. Generally speaking, convection should not influence this thickness distribution at the typical ribbon thicknesses (~10 mils) and expected values of impurity diffusion rates (D ~$10^{-4}$ to $10^{-3}$ cm$^2$/sec) in liquid silicon. However, lateral fluid flow appears to be vigorous enough at the liquid silicon flow rates encountered in the present experiments to allow convection to compete with diffusion over distances typical of the die width. If this is the case, the impurity distribution in the width dimension will be sensitive to the arrangement of the capillary feed slots and the die top fluid recess. Conventional 5 cm dies are being modified to allow several capillary flow investigations to be explored.

An important change for the second series of runs has been the use of 4 in. instead of 6 in. long fused silica crucibles. The impetus for this change came about as a result of observations relating to the presence of substitutional aluminum in ribbon grown on Stations JPL No. 1 and No. 3A, as discussed in Section IV.A. The decrease in crucible length brings the ratio of the crucible surface-to-melt volume closer to that existing in induction furnace growth systems in which the aluminum absorption is rarely observed. Further work in this area will involve replacing the fused silica crucibles with purified graphite crucibles. The drawing for the latter appears at the end of this report.

### e. Analysis

Further analysis of ribbon material and solar cells is underway in a continuing effort to relate structure, impurity distribution, and electrical properties to growth parameters. Correlations are being sought between SPV and spectral response

diffusion length variations and the occurence of the cross-sectional grain structure (see also Section IV.B). Samples have been prepared for analysis of the distribution of impurities in the ribbon cross-section by quantitative emission spectroscopy. Additional analyses are being planned to examine the impurity distribution in the ribbon width dimension.

## C. Machine Design

Work on fabrication and assembly of the three inch wide cartridge and belt puller is proceeding on schedule. Several minor design errors were corrected in each assembly. These necessitated minimal rework of parts already made. All components for the cartridge have been fabricated, and it is now in the initial stages of assembly and testing. Components for the belt puller are scheduled to be completed by the beginning of July. The remaining work is being done in-house. It is expected the puller will be incorporated into the system in July.

A new crucible cover with stress relief slots and a dog-bone opening (to prevent flooding) has been designed. The design made use of data gathered in auxiliary experiments to examine warping and in growth runs. Prototype testing showed little deformation and an acceptable recycling lifetime. One cover has been cycled for four runs with no apparent degradation.

A new top cover plate for the furnace chamber was also designed during this quarterly period. This has a larger opening to admit the three inch cartridge. It is also water cooled to prevent overheating.

Finally, as noted in the above discussion, a graphite crucible has been designed (see Fig. 1 in the Appendix). The crucibles have been ordered and should be available for experiments in July.

III. CRYSTAL GROWTH MACHINE JPL MODEL 3A  by B. Mackintosh

A. Overview

. The work on the multiple ribbon growth system in the past three months was directed toward the intermediate milestone of demonstrating the simultaneous growth of three ribbons of 5 cm width at growth speeds approaching 5 cm/min.

The goal was not achieved, however, due to a variety of failures in the furnace which made it clear that the reliability of the system as presently designed is far too low to qualify it as a prototype for a production system. Surprisingly though, the failures occurred not in the complicated cartridges as expected, but rather in the furnace proper. This is satisfying since it does again prove the validity of the cartridge concept, but also quite dismaying because the advantage of a multiple growth machine vis-à-vis several single growth stations largely rests in the assumption that the basic furnace system is extremely reliable and failures thus occur only in the cartridges which are designed for quick fix maintenance. Therefore, the ribbon output per unit time should be only slightly affected. It is obvious then that the reliability of the basic furnace setup must be significantly increased if the five ribbon multiple growth demonstration which is the basic goal of the present contract is to have any larger significance. Thus, the furnace hot zone will be redesigned for greater stability and precision, and with changes in details to accommodate more readily the melt replenishment setup, which will soon be a feature of this system. These changes are discussed below.

Finally, solar cells have been prepared from material grown in the multiple furnace. Although the numbers produced are not statistically significant, we still feel that it is reasonable to state that material from the multiple furnace is not inferior to that produced from JPL No. 1, and therefore the furnace cleanup which was also a goal of the first months of this contract has succeeded at least to the extent that this large resistance heated furnace seems comparable with the much smaller No. 1 single ribbon unit.

B. Summary of Furnace Operation

Table III lists the significant data pertaining to all ribbon growth runs in the past quarter.

1. General Discussion

Of the ten runs of routine nature (exclude 16-066, 067, 068, and 074), four were ended by silicon floods which destroyed heating elements and damaged the insulation. One run was seriously hindered by the effects of leaving off the crucible cover

11

Table III. Run Data: Machine No. 3A (Multiple Furnace).

| Run No. | Duration (Days) | No. of Cartridges | Purpose | Comments |
|---|---|---|---|---|
| 16-063 | 2 | 1 | Evaluate modifications to dies and cartridge floors. | - |
| 16-064 | ½ | 1 | Evaluate modifications to die heaters. | Major flood - no ribbon growth. |
| 16-065 | 2 | 1 | Repeat 16-064. | - |
| 16-066 | 1 | 1 | First trial, suspended crucible. | Excellent growth performance. |
| 16-067 | ½ | 1 | Evaluate suspended crucible. | - |
| 16-068-1 | ½ | 1 | Evaluate suspended crucible. | - |
| 16-068-2 | ½ | 1 | Evaluate suspended crucible. | - |
| 16-069 | 1 | 2 | First attempt to grow two ribbons simultaneously. | Good growth - cartridge No. 1. Minor flood - cartridge No. 2. |
| 16-070 | 2 | 2 | Repeat 16-069. | Two ribbons full width for 15 minutes. One ribbon on AWC for one hour. |
| 16-071 | ½ | 3 | First attempt to grow three ribbons simultaneously. | Cartridge cooling water failure - run short duration. |
| 16-072 | ½ | 3 | Repeat 16-071. | Major flood. |
| 16-073 | 3 | 3 | Repeat 16-071. | Crucible cover left off. Growth problems related to SiO. |
| 16-074 | 1 | 1 | Growth parameter measurements for automatic controls work. | |
| 16-075 | 1 | 3 | Triple growth demonstration. | New design of crucible cover with central support. Major flood caused by broken piece of insulation. |
| 16-076 | 2 | 3 | Repeat 16-075 | Broken insulation prevented insertion of one cartridge. |

12

as a precaution against floods. One triple cartridge run was not fully successful because the furnace insulation was falling apart and blocking a cartridge opening. As was stated in the May Monthly Report, these failures were related to lack of rigidity and precision of the main furnace components. These problem areas were recognized in early April and modifications to the heaters and crucible holders were designed to lessen the tendency for silicon to flood to the heaters and insulation. The modified parts ordered at that time have been repeatedly delayed and have still not arrived as of the end of June.

A particularly difficult problem has been the design of a satisfactory cover for the long trough crucible of this system. The crucible cover serves the triple purposes of 1) shielding radiation from the melt surface so that the melt does not have to be so strongly heated from the bottom, 2) "absorbing" (reacting with) some of the silicon monoxide produced by the large melt, and 3) protecting the melt surface, except at openings for the dies, from small contaminating particles and large objects (broken pieces of insulation).

The crucible cover must be thin and the cartridge bottom must be positioned close to the crucible cover, so as not to add unduly to the height of the die tip above the melt. Graphite, the material used to date for fabrication of crucible covers, has several drawbacks. It warps when exposed to SiO, and thus is neither mechanically stable nor sufficiently durable to warrant sophisticated design; a graphite crucible cover is a one-shot item. Dense, highly purified graphite is not available in stock sizes large enough to make single-piece crucible covers for this large system, but the thinness required of the covers makes joining small sections difficult. Grafoil* sheet overcomes the problems of stock size availability and cost, and has been used to make crucible covers for System 3A. Its main shortcoming is its great tendency to absorb and wick molten silicon. Once in contact with a source of silicon either from the melt below or the dies passing through, the grafoil quickly conducts large quantities of the melt to adjacent components.

The addition of continuous melt replenishment which is planned for the near future can be seen as salutory to the present problems with crucibles and crucible covers. A reduced requirement of crucible capacity will permit thicker crucible holders, shorter dies, and smaller unsupported spans of covers over the melt. The smaller silicon/quartz contact area will reduce the quantity of SiO generated.

---

* Union Carbide Co.

The following comments are pertinent to the runs which were completed without major mishap.

The mechanical and electrical reliability of the cartridges has been good in both this system and in JPL No. 1. Growth performance in terms of percent of ribbon grown at essentially full width, and yield in terms of average ribbon length grown per operating hour, have both been markedly better in System 1 than in System 3A for at least three reasons. The most immediately apparent reason is the total devotion of the crystal grower's attention in the case of the single ribbon machine vs. divided attention in the multiple machine. During whatever time is required to attain full width growth in one of multiple cartridges, the others are either awaiting startup or growing without the human surveillance that can foresee and correct faulty growth far more effectively than can any presently existing automatic device.

The second reason, strongly suspected but not yet proven, has to do with the different ways in which the two furnaces are started up. Furnace 1 is heated from cold condition with the cartridge in place and the die inserted into a pocket in the solid silicon charge. Immediately upon melting, the silicon begins to fill the die. Furnace 3A is brought to temperature with cartridges outside; these are then lowered so that the dies dip into molten silicon. A finite resistance of the cartridge parts to thermal shock limits the rate at which they can be lowered into place. During this lowering operation, the relatively cold dies are exposed to SiO over the melt. It is believed that the SiO condenses on the dies and disproportionates to form a layer or matrix of $SiO_2$, which inhibits wetting of the dies. This would be a contributory factor to the 15 to 30 minute "break-in period" experienced with new dies before growth behavior becomes stabilized. The break-in period for dies used in No. 1 is not so long.

The third reason for the higher yield and productivity of Furnace 1 is not fundamental. Much greater electrical power is available to the cartridge heating elements of this system, which allows a wider range of variation of growth parameters while maintaining good control. The power supplies of Furnace 3A were built before the power requirement of the cartridge was accurately known. They are adequate, but 25 to 50 percent greater power would at times be useful.

During the three cartridge growth runs, No. 3, No. 4, and No. 5 of six equally spaced furnace openings were used for growth. Optical pyrometer and thermocouple measurements did not show significant temperature differences among these furnace positions, and growth performance did not differ in consistent manner among the three "holes". Pyrometer readings have shown, however, that the two endmost positions, No. 1 and No. 6, are colder. When the full five cartridges are used later in the

year, it may be necessary to trim the main heating elements to create hot spots in the cold ends. The experience to date with multiple cartridge operation does not permit a conclusion to be drawn about the feasibility of replacing a cartridge while growth is maintained in adjacent positions. It is known, however, that when multiple cartridges are in place, growth in any of them may be initiated and worked up to full speed and width without affecting growth in the others.

## 2. Diffusion Length Measurements and Solar Cell Results

SPV diffusion lengths have been measured on a number of ribbons from Furnace No. 3A before and after cleanup. The results, although not as numerous as those obtained from JPL No. 1, show exactly the same trends, ranges, and inhomogeneities as reported for samples from that furnace. Since correlations of these numbers with solar cell results are not possible (as discussed in the other sections of this report), a table of numbers is not included here.

Solar cells have also been prepared from a number of ribbons from this furnace. They are shown in Table VII (Section IV.B). Here it is apparent, too, that the material produced is of a quality quite comparable at the present time with material produced in JPL No. 1.

## C. Design Work in Progress

The final design work is being done at the end of the present quarter on a continuous melt replenishment system for Model 3A, to be procured and evaluated in the next quarter. It is designed to allow several different modes of operation to be evaluated. Structurally, it is a two-part system with a mechanical section analogous to the belt puller, and a thermal control section constructed similarly to a growth cartridge, which inserts into one of the six identical furnace openings. It is designed to feed either solid rod of 1¼" diameter or chunk silicon into the crucible in a molten state, as it is provided with three heating elements to supply heat for melting. When using rod as feed material, feed rate will be controlled by a mechanical lowering drive. Chunk material can be used if a melting funnel can be designed which reliably stops and starts flow by controlling heaters. A melt level probe will provide for closed-loop control of feeding rate.

Design work is also presently underway on the task of developing the performance of the two inch cartridge to a higher growth rate, nominally to be 7.5 cm/minute by the end of the contract. The same techniques which were incorporated into the design of the yet untried three inch cartridge are to be applied to the two inch version; namely, colder heat removal elements just above the die, helium fed directly to the faces of these elements adjacent to the ribbon, and better radiation shielding between

15

the closely spaced hot and cold elements. A program of experimental development is being planned to optimize the growth system in its new speed range.

D. Plans for Coming Quarter

A set of performance criteria for the end-of-year demonstration of multiple ribbon growth is being formulated so that the level of reliability required of each system component will be better understood and corrective design work can be carried out where necessary. It is already known that redesign of the hot zone is a high priority task. The new design will probably include, as a minimum, the following elements:

1. Water-cooled main structural elements to eliminate overall lengthwise thermal expansion.

2. Elimination of the stainless steel shell which in the present design is both "dirty" and mechanically imprecise.

3. Greater strength and precision in heating element mounts.

4. Greater clearance between heating elements and insulation, and around cartridges.

5. Insulation material installed in samll segments which are individaully replaceable.

A different insulation material will be sought which is more durable and/or more efficient and/or more cost-effective.

A satisfactory design must be found for a crucible to run the full 28 in. length of the five-ribbon furnace. An evaluation of graphite crucibles soon to be made in Furnace No. 1 may demonstrate their superiority over quartz crucibles.

The melt replenishment system will be developed to a satisfactory state of operation within the next quarter.

We will attempt to increase the growth rate of the two inch cartridge using the techniques mentioned above; however, basic growth process development is the primary purpose of JPL No. 1, while the demonstration of multiple growth is the purpose of JPL No. 3A which may take precedence over the task of achieving a 7.5 in./minute growth rate in two inch ribbon.

E. Automatic Controls by D.A. Yates

1. Introduction

In order to maintain the steady-state growth of a uniform cross-section crystal, one of the requirements is to maintain a predetermined meniscus height (as a function of melt level); this gives a constant ribbon thickness. The relationship

16

between meniscus height and ribbon thickness has previously been predicted theoretically and verified experimentally; but only a theoretical relationship between die top temperature and meniscus height has been developed. In ribbon growth, however, the most critical consideration is to maintain the edges in a constant position with respect to the ends of the die. This is not only necessary to maintain a constant width, but also to sustain growth itself since "freezes" frequently occur if the ribbon grows too closely to the ends of the die. Observations suggest that excellent temperature control is very important near the ends of the die on account of the marginal stability that exists at the ribbon edges. To obtain this temperature control, special end heaters have been incorporated into the design of ribbon growth systems. During ribbon growth, the operator (or the control system) needs to carefully watch and control the edges of the ribbon. Typically, increasing the temperature at the end of the die will inhibit the spreading of the ribbon edge towards the end of the die; decreasing the temperature at the end of the die will inhibit the tapering of the ribbon edge with respect to the end of the die.

· A sensitive technique for the determination of the process status has been developed. The sensing system uses direct optical sensing of meniscus height and edge position; this information is used to control power to the edge heaters, after steady-state growth is obtained by the operator. For a typical thermal geometry, use of this technique with associated control systems apparently has not required a direct temperature distribution determination in the growth system for control purposes.

In order to assess the acceptability of a cartridge control system, standards that it must meet should be established - especially since one operator must be able to supervise the operation of five cartridges by the end of the contract period. Additionally, as problems develop with control of the growth, it is useful to analyze the control signals at various points in the system. In particular, initial experience with the control system indicates that "freezes" are an important failure mode of the controlled growth. To gather appropriate data, a cartridge testing procedure for the measurement of electrical, geometrical and thermal variables has been developed. In these systems there is a large set of variables that might be measured, and some simplification is necessary to facilitate data taking and analyses. Efforts to implement the procedure during growth runs have been delayed since the multiple growth demonstration has taken priority and since various problems with the basic furnace have occurred as described in the previous section.

During this quarter, three growth runs have used the AWC system; successful automatic control for periods up to an hour has now been accomplished. During these runs, various parts of the testing procedure have been used. For the next quarter we will

17

attempt to use the complete testing procedure during some growth runs. Additionally, we will test the performance in the presence of adjacent cartridges.

## 2. Automatic Width Control System Description

The specific system designed and constructed to control the ribbon edge positions has been called the Automatic Width Control (AWC) system. In this system the position of each edge is optically monitored by forming a real image of the growing crystal and placing a linear imaging device at the position of the image of the ribbon edge. Figure 1 shows a superposition of the heater, the die, the growing ribbon, the image of the growing ribbon, and the two linear imaging devices (LID). Typically, the ribbon appears bright against the dark background of the relatively cool radiation shields surrounding the die. The output from the LID is a clocked series of pulses, each of which corresponds to an optical sensor in the array. The amplitude of each pulse is proportional to the photon flux that falls on the corresponding sensor. By the use of sampling techniques, a comparator, and a digital-to-analog converter, an analog representation of the position of the image of each edge of the ribbon is generated. This is also schematically indicated in Figure 1. Figure 2 shows, in block diagram form, how the edge position sensing circuitry is used to control the power to the end heaters. In this particular configuration of control circuitry, each edge position sensor independently controls (except for a manual power adjustment) the power applied to the respective end heater. The power to the face heater has been typically controlled by a thermocouple placed close to the face heating element near the center of the element. To operate the system, the mode switch is switched to "man" so that the edge position sensors are switched out of the circuit, then zero volts appear on the switch. The operator initiates growth and subsequently obtains full width steady-state growth. At this point an electrical offset adjustment in the edge position sensing circuit is made to bring the output of the circuit to zero volts. The auto-man switch is positioned to "auto" and subsequent edge position deviations will initiate control action.

Some potential shortcomings to this simple control system are readily recognized. For example, the position of the edges is responsive not only to end heater power changes but also to face heater power changes. Furthermore, the thermocouple which controls the face heater power also is somewhat responsive to changes in end heater power; this is referred to as the thermal interaction, and has been observed in earlier resistance furnaces. Additionally, some power leads are common to the face and end heater systems so the potential for an electrical interaction exists. Solutions to these problems generally introduce additional system complexity. Thus, it

18

Gated Scaler output (after D → A)

Output from comparator

Resolved output from array

Comparator threshold setting

Time

⊢→ Scan

Dark | Bright

LID array No. 1

LID array No. 2

19

← Interface

Meniscus

End heater

$H_1$

End heater

$H_2$

$H_3$

Die width (typically 2")
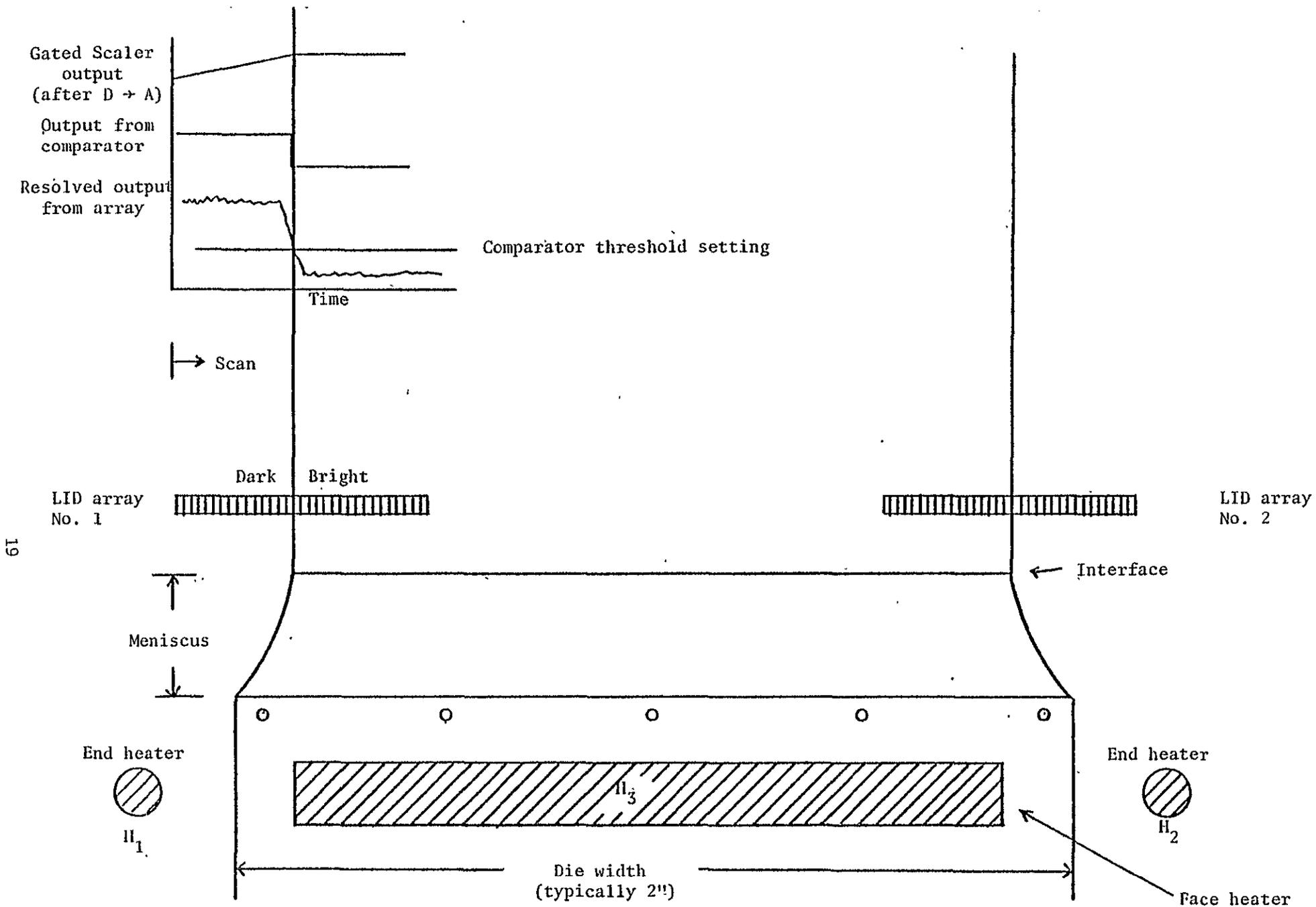
Face heater

Fig. 1.  Automatic ribbon width control.  Schematic showing die, end heaters and face heaters.  Superimposed is the optical image of the growing ribbon with LID arrays located in the image plane. Electrical outputs are also shown.

Sensor o/p           Controller o/p         Heater current

```
┌──────────┐        Auto. ┌──────────┐         ┌──────────┐         ┌──────────┐
│Right edge│              │Summer/   │         │SCR       │         │Right end │
│position  │────────○  ○─▶│controller│────────▶│controller/│───────▶│heater    │
│sensor    │         ●    │          │         │SCR       │         │          │
└──────────┘        Man.  └──────────┘         └──────────┘         └──────────┘
                               ▲
                       Operator power adj.
```

Die top temp.
on right

Sensor o/p           Controller o/p      · Heater current

```
┌──────────┐        Auto. ┌──────────┐         ┌──────────┐         ┌──────────┐
│Left edge │              │Summer/   │         │SCR       │         │Left end  │
│position  │────────○  ○─▶│controller│────────▶│controller/│───────▶│heater    │
│sensor    │         ●    │          │         │SCR       │         │          │
└──────────┘        Man.  └──────────┘         └──────────┘         └──────────┘
                               ▲
                       Operator power adj.
```

Die top temp.
on left

Sensor o/p           Controller o/p      Heater current

```
┌──────────┐              ┌──────────┐         ┌──────────┐         ┌──────────┐
│Upper     │              │L & N PID │         │SCR       │         │Face      │
│control   │─────────────▶│controller│────────▶│controller/│───────▶│heater    │
│thermocouple│            │          │         │SCR       │         │          │
└──────────┘              └──────────┘         └──────────┘         └──────────┘
                               ▲
                       operator power
                       (set point) adj.
```

Die top temp.
across die

Fig. 2.  Simplified block diagram of cartridge control systems.

20

appears reasonable to investigate the utility of the current system.

### 3. Standards of Performance

Standards for geometrical control performance relate to the ability of the control system to maintain the ribbon cross-section within prescribed limits. The ideal cross-section for the minimal usage of silicon would, of course, be rectangular. However, in practice, ribbons have been grown which are thicker or thinner in the center portions than near the edges. It is not the present purpose of this contract to be concerned with the minimum usage of silicon; thus, a strong effort will not initially be made to control the thickness, that is, the meniscus height, except insofar as the cessation of growth ("freezes") is concerned. In practice, maintaining a relatively constant meniscus height does not require much operator attention in ribbon growth. The main concern and control problem is keeping the edge positions relatively fixed.

A specification on the desired performance of an automatic width control system should be imposed so that the acceptability of a given system can be ascertained. This has been chosen to be ±15 mils per edge. Our concern here is, of course, the loss of surface area for cell production. For a 2 in. width ribbon, the average silicon volume loss would be 1.5% in straightening the edge by allowing a ±15 mil variance.

The length of time that the control system can keep the ribbon growth within geometrical specifications is also important. Typically, during early testing of the AWC systems it has been observed that the system slowly drifts. This might be expected of a simple control system and is probably allowable (initially) if adequate warning of the drifting is given to the human supervisor, and if he can make an easy adjustment to correct for the drift. If the operator is to supervise a multiplicity (at least five) of growth stations, and if it takes about three minutes to make and check an adjustment, then each controlled growth station should be able to stay in bounds for at least fifteen minutes on the average. However, a safety factor of 2 is reasonable. Thus, we could consider that automatic control for thirty minutes should be acceptable to meet the minimum goals of the contract.

There is perhaps one exception to this goal. If a cartridge is removed or inserted adjacent to an automatically controlled cartridge, then severe thermal disturbances can be probably expected. Thus, constant operator attention may be required during this interim period.

### 4. Cartridge Testing Procedure

An appropriate way to determine the geometrical performance of a given

control system is to continuously record the position of each edge. In addition, we want to be able to determine the causes of control problems. There are numerous possible signals in the control loop that might be monitored as indicated in Fig. 2 (dotted lines). In addition to these, other relevant parameters are the meniscus height along the whole interface, the pulling speed, the power applied to the after-heater, the gas flow rate in the afterheater, the water flow rate in the cooling shoes, etc. The difficulty in developing the testing procedure has been to select a subset of all these parameters that would contain adequate information yet be small enough to be readily measured. During recent growth runs, it has been observed that the termination of growth (after typically one-half hour) has been caused by a "sudden freeze". During the few minutes preceding this event, both edge control systems appeared to be operating in a stable condition. Thus, the testing procedure must emphasize the determination of the cause of the freezes.

Some of the signals indicated in the figure appear to be redundant. For example, the controller output would be expected to correspond directly to the heater current; however, this is only true if the resistance of the contacts remains constant during the run. We have observed contact variations in earlier resistance furnaces. The controller output of the end heater is affected by manual adjustments of the operator as well as by the edge sensor output. Typically, the operator has never had the need to make such an adjustment once the system is put into automatic control (also indicating that the edge control systems probably work well). Additionally, only propor-tional control is used in the end heater controller; thus, measurement of the sensor output and of the controller output is indeed redundant for the end heater control system. Direct measurement of the die top temperature distribution is, of course, necessary since the reduction of the temperature somewhere along the die top precedes the freeze (assuming that the speed is not decreased). This reduction is to be corre-lated with either a reduction in heat input from the heater elements or (by default) to a change in the heat loss mechanism in the system. In order to optically measure temperature, cavities have been machined in some die tops as shown in Fig. 1. The bottoms of the cavities (they are not "ideal" cavities) are machined to be perpendicu-lar to the optical axis to minimize the observation of reflected light. The selected cavity diameter (32 mils) is the smallest that can be observed by the radiometer (Ircon Modline 2000 Series). The average depth of the cavity is one-half of the diameter; thus, if the emissivity of the die surface is 0.90, the cavity emissivity should be about 0.96. The center of the cavity will initially be 45 mils below the die top surface; this has necessitated lowering the die radiation shields 20 mils from their "normal" position. Variations on this scheme will probably be tried.

Initially, the use of an Ircon for a radiometer presents the difficulty of needing an unobstructed light path one inch in diameter at the furnace window. This is not possible in System 3A. Since it is wise to have a reliable optical aperture in radiometry, we have placed a 125 mil aperture disc in front of the Ircon lens. The Ircon was tested with this modification on a surface in another furnace after that system was temperature-stabilized for several hours. Drift and noise in the (reduced) output were low enough so that one degree relative measurements should be possible (although some difficulty from convection currents and window clouding is expected). An extra mount on the operator's side of the furnace has been installed so that the Ircon can be slipped into (and out of!) position quickly.

We have adopted the following test procedure. The variables measured continuously during growth are the left and right edge positions, the control thermocouple signal and the face heater controller output; these are plotted on chart recorders. Additionally, the occurrence of a freeze (as determined optically) will be indicated on the charts. Periodically, the heater currents, controller outputs and the die top temperature distribution at five points along the top will all be measured sequentially with a digital voltmeter as the output device. As outlined in Fig. 3, the cartridge is first lowered into the furnace and die filling is obtained. Then the quality of the heater connection system is checked by manually varying the controller outputs over the appropriate operating range and measuring the heater currents by the current measuring transformers and RMS-to-DC converter; a curve for this data is plotted. This is done for all four heaters by switching the digital voltmeter to sequentially measure the appropriate signal. A patch panel circuit has been constructed to perform these measurements more readily. Since cartridges are expected to be identical, the appropriate heater in each cartridge should produce identical data. Periodically during the run, the controller signal and the heater current will be checked to determine whether the heater system is still operating on the curve. This procedure is called the "contact testing mode". Then the Ircon pyrometer is calibrated by lowering the die top temperature until a freeze indicates that the Ircon signal corresponds to $1412^{o}C$. The calibration curve above the melting point is then determined by alternately using the Ircon and a Leeds and Northrop optical pyrometer on the same cavity. Growth is initiated, automatic control is started when steady-state growth is obtained, and the chart recorders are turned on. Periodically, say every 10 minutes, the controller output signals, the currents in the heater elements, and the die top temperature distribution are sequentially checked.

## S. Results

Certain parts of this procedure have already been used during various growth
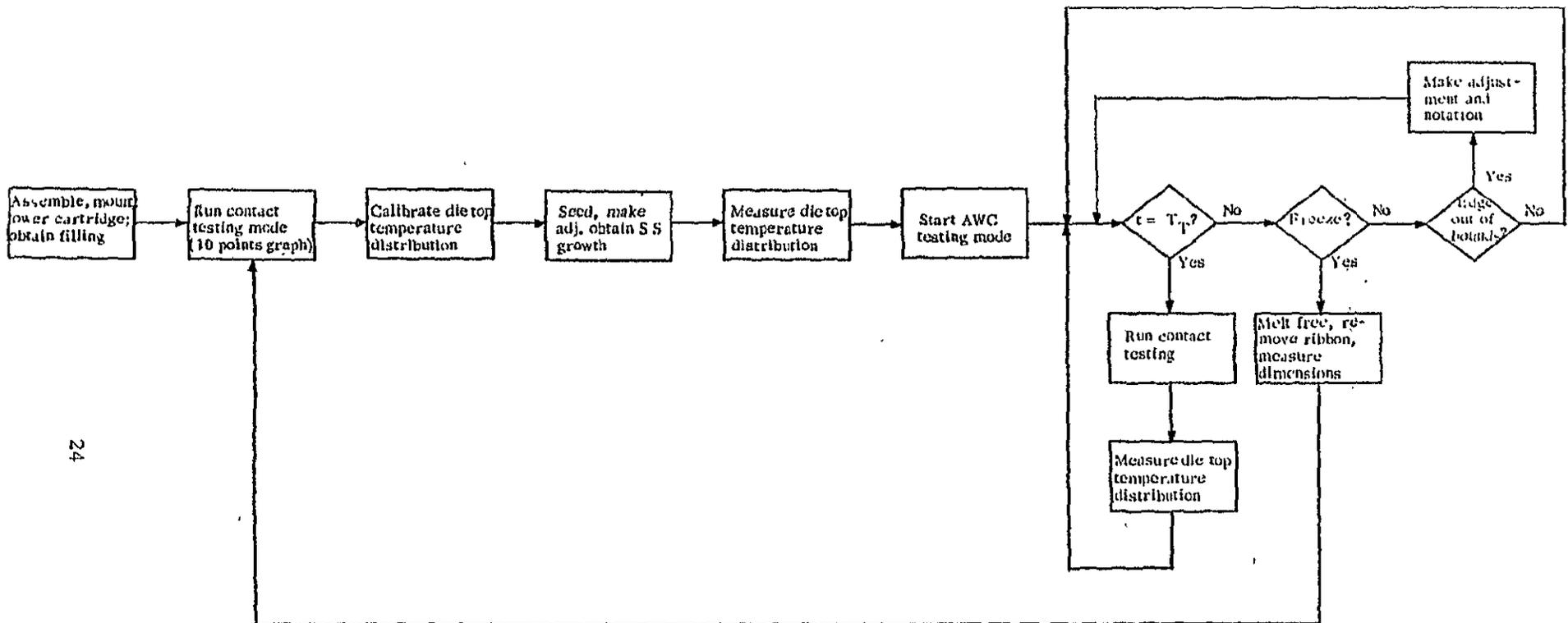
Fig. 3. Cartridge testing procedure.

runs. During run 16-065, we observed the face heater controller output signal, one edge position signal, and the power to that end heater. A "sudden freeze" terminated the controlled period after 24 minutes. During the 11 minutes preceding the freeze, the average face heater controller signal gradually increased; the average end heater power increased very slightly. Some oscillatory behavior in these signals also occurred. It is possible that the freeze might have occurred near the unmonitored end; die top temperature measurements would have been useful. The width was controlled to within a 7 mil variation. During run 16-072, we ran the contact testing procedure at the beginning of the run. Unfortunately, a flood terminated the run soon thereafter. However, we did observe a difference in the controller output vs. heater current curves for the two end heaters. This has led us to begin studying the heater system more closely. Another interesting observation on the heater system is that there is some electrical interaction between the end and face heaters since they share some common leads. We found up to a 5.7% change in face heater power for a 90% change in end heater power. This is probably not too serious since during steady-state growth, probably not more than about a 10% change in end heater power is made.

Automatic width control has been used this past quarter during two other runs, 16-069 and 16-070. Since the main purpose of these runs was to demonstrate multiple growth with three cartridges, there was no opportunity to use the testing procedure described above. However, during run 16-070, the AWC on one cartridge was in continuous operation for one hour.

During the next quarter, efforts will be made to continue tuning the system and to use the complete testing procedure during some growth runs. Also, we will be using the testing procedure to monitor the controlled cartridge in the presence of adjacent operating cartridges.

IV. CHARACTERIZATION by H. Rao and J. Ho

Detailed characterization of the structure of ribbons grown from JPL systems was carried out during this quarterly period. Specifically, structural features on the surface and in the cross-section of ribbons were examined. EBIC studies were carried out on solar cells fabricated on these ribbons. Infrared absorption measurements have also been undertaken.

A. Materials Characterization

1. Crystallographic and Metallographic Evaluation

Ribbons grown from JPL No. 1 and No. 3A machines were sectioned, polished and Sirtl etched to reveal the cross-sectional structure. Figure 4 shows typical cross-sectional views of ribbon 18-15-3 and 18-18-1. Figure 4(c) is a cross-sectional view of ribbon 18-15-3. Figure 5 shows similar photomicrographs of ribbons 16-060-9-2 and 16-042. The growth conditions of the ribbons are reported in the crystal growth sections. The important finding in structure, pertaining to the ribbons grown in the resistance-heated systems, is the presence of grain boundaries in the middle of the ribbon cross-section. The distance of the grain boundaries from the ribbon surface is typically 40 - 50 µm. In some cases, the grains extend to the ribbon surface. The grain structure is found to be present along the entire width of the ribbon in the majority of cases. Ribbons from run 18-15 were found to be exceptions, in that only a small fraction of the ribbon width displayed grain boundaries in the cross-sectional structure. Typical structure of the ribbons grown in the induction-heated systems is shown in Figure 6 for comparison with the ribbons grown from resistance-heated systems.

2. Diffusion Length Measurements

Representative sections of as-grown material were taken for diffusion length ($L_D$) measurements using the surface photovoltage (SPV) technique. Diffusion lengths were measured using the SPV technique after fabricating Schottky barriers on the ribbon surface. Ranges of values and the average diffusion lengths are reported in Table I, in the crystal growth section. As can be seen, in a majority of cases, the diffusion lengths were less than 2 µm. This could be due to the fact that the error in the measurement of $L_D$ is quite large in cases where the diffusion lengths are very low. In addition, the diffusion length measurements using the SPV technique assume that the material is quite homogeneous through the thickness. Thus, the presence of a cross-sectional grain structure, with the attendant possible impurity segregation effects, may also lead to errors in the measurement.

That the ribbon could be inhomogeneous through the thickness dimension can be inferred from the non-homogeneity observed in the width dimension (see the section on

27
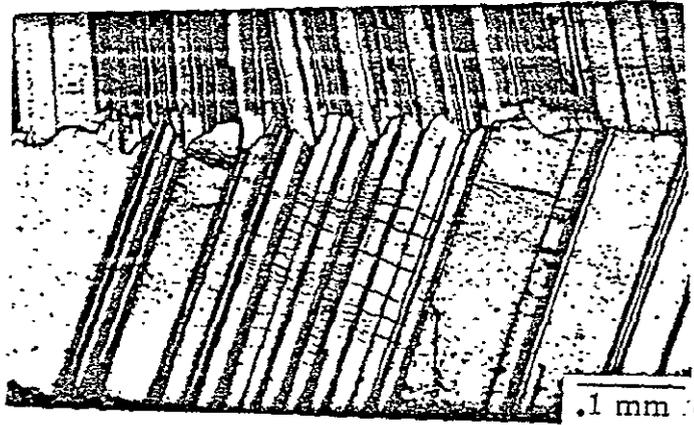
(a)
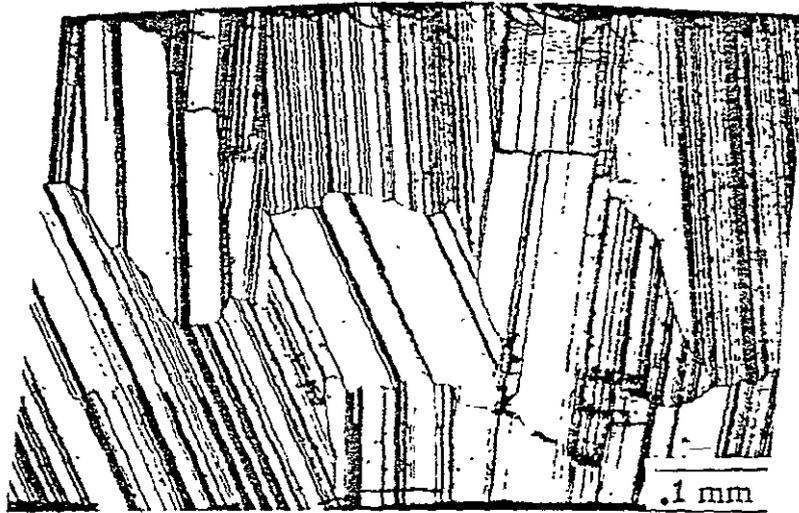
(b)
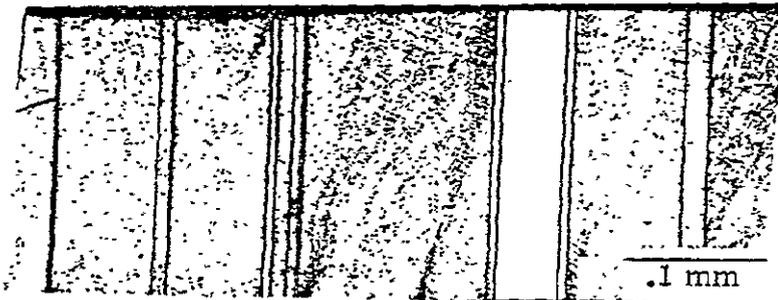
(c)

Fig. 4.  Typical cross-sectional views of ribbons (a) 18-8-2, (b) 18-18-1,
and (c) 18-15-3, grown from JPL Machine No. 1 (Sirtl etched for
20 seconds).

28

(a)

(b).
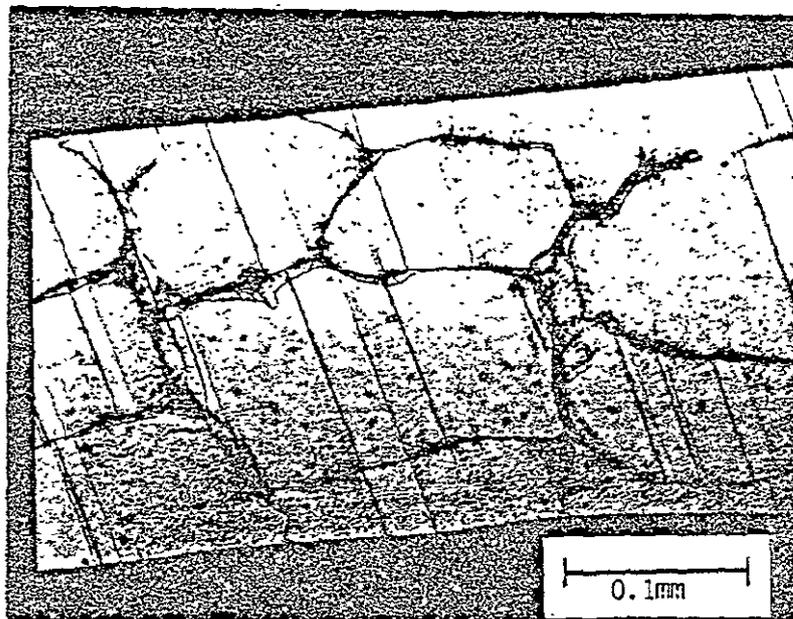
Fig. 5. Typical cross-sectional views of ribbons (a) 16-060-8-2 and (b) 16-042, grown from JPL Machine No. 3A (Sirtl etched for 20 seconds).
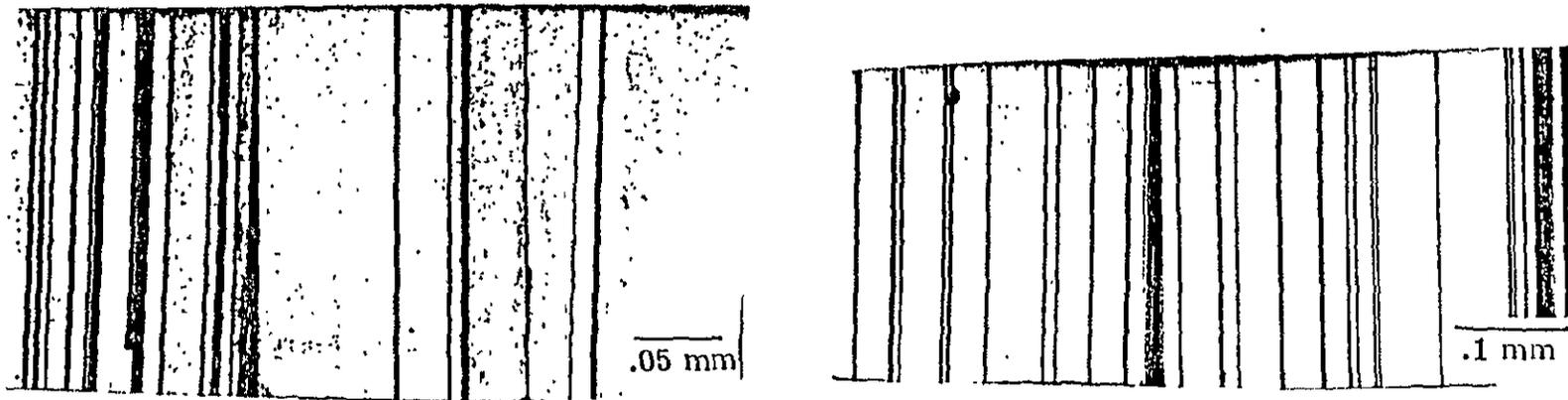
Fig. 6.  Typical cross-sectional views of ribbons
grown in induction heated systems.

infrared scans). Large variations in the power output of solar cells made on adjacent ribbon sections also show that the material is inhomogeneous. Solar cells fabricated from ribbon 18-16-6 showed power density values of 7.51 and 7.34 mW/cm$^2$ in sections adjacent to those where very low diffusion lengths were measured (<2 μm). On the other hand, the cell fabricated on a section adjacent to the region with a 4.5 μm diffusion length had a lower P value of 4.78 mW/cm$^2$. Two adjacent regions of ribbon 18-17-4 yielded $L_D$ values of 14.0 μm and 2.4 μm. All the above indicate that the material has a non-homogeneous distribution of impurities. The correlations between diffusion lengths obtained under essentially 'dark' conditions and the solar cell parameters (measured under AM1 sun conditions) are further complicated by the "light enhancement" effect referred to in previous reports.

The measurement of diffusion length in the as-grown material can, however, be used to gauge the improvements in crystal quality. Increasing values of $L_D$ do tend to go along with improvements in solar cell performance. As can be seen from Table I, the diffusion lengths in the as-grown material tend to improve with time in each run. Once a system is cleaned, later ribbon runs seem to yield higher diffusion length material (hence, higher purity material). This appears to indicate that the growth system needs a "bakeout period" after each system assembly operation.

### 3. Infrared Absorption Measurements

Infrared absorption measurements have been carried out in ribbons grown in JPL Stations Nos. 1 and 3A, both at room temperature (300°K) and at liquid nitrogen temperature (80°K). Figure 7 shows a typical room temperature scan of an as-grown ribbon (unpolished). Included is a scan of the same sample at 80°K. Figure 8 is a scan at 80°K, measured on an expanded (5X) ordinate scale. All the scans were made against air reference. The presence of the absorption peaks at 520 cm$^{-1}$, 478 cm$^{-1}$, 320 cm$^{-1}$, 278 cm$^{-1}$, and 245 cm$^{-1}$ should be noted in the figures.

Table IV lists the origins of the absorption peaks in silicon along with the references in the literature. It should be pointed out that the absorption peaks corresponding to aluminum were measured, in the present experiments, at 80°K, while the literature data were obtained at 4.2°K. In order to ascertain that the observed absorption peaks can indeed be attributed to aluminum, a Czochralski sample doped with ~5 x 10$^{16}$ atoms/cm$^3$ of aluminum was examined at 300°K and at 80°K. The IR scans are shown in Fig. 9. One can readily observe that the Czochralski sample containing aluminum as an impurity shows additional absorption peaks when examined at 80°K; these peaks occur at the same wave numbers as the peaks attributed to aluminum in the ribbon.

All the evidence obtained thus far leads us to believe that the absorption peaks (at 520 cm$^{-1}$ and at 478 cm$^{-1}$) observed at 80°K are caused by the presence of substitu-
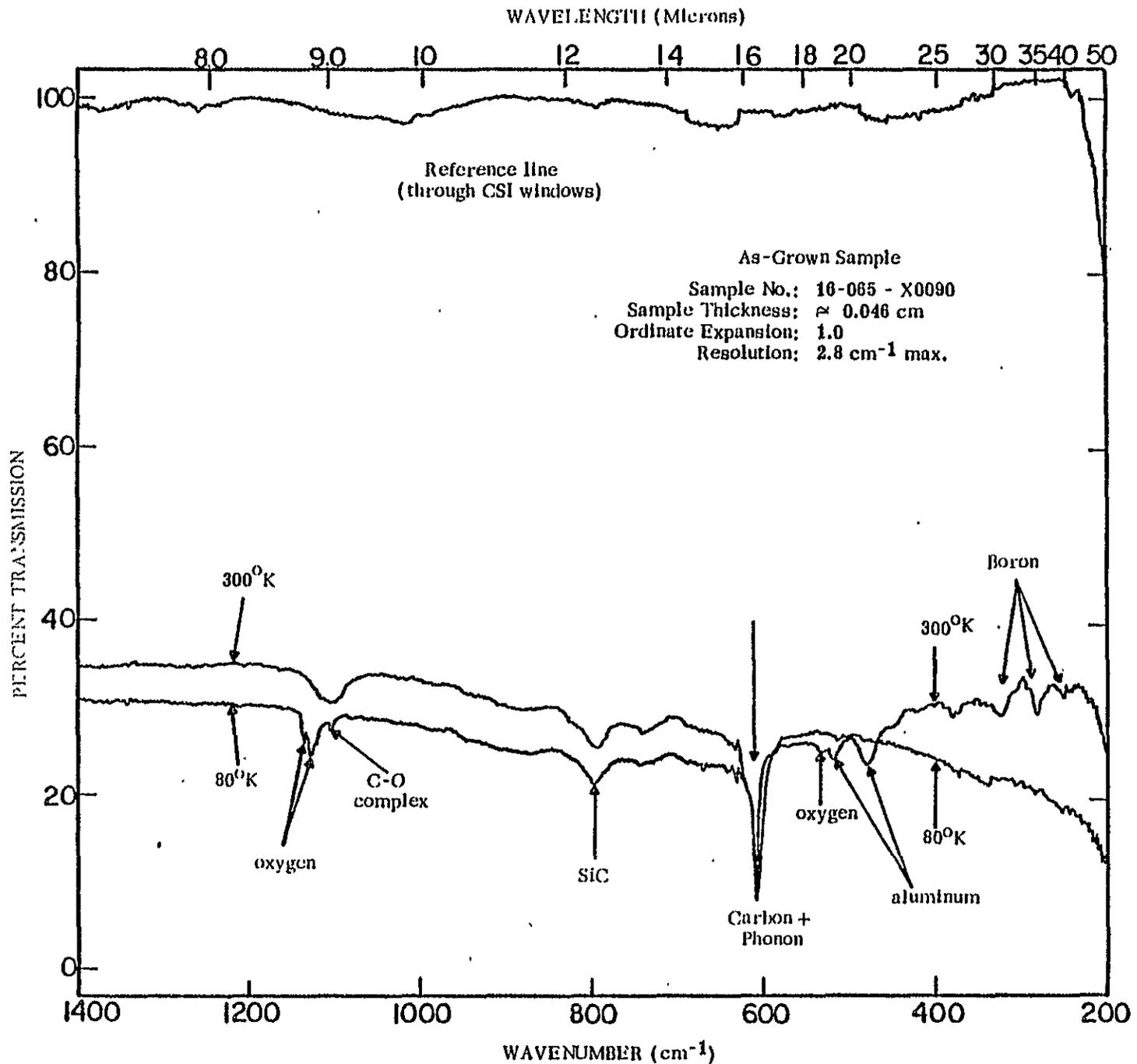
Fig. 7. IR absorption spectrum, at 300°K and 80°K, of ribbon 16-065-X0090.
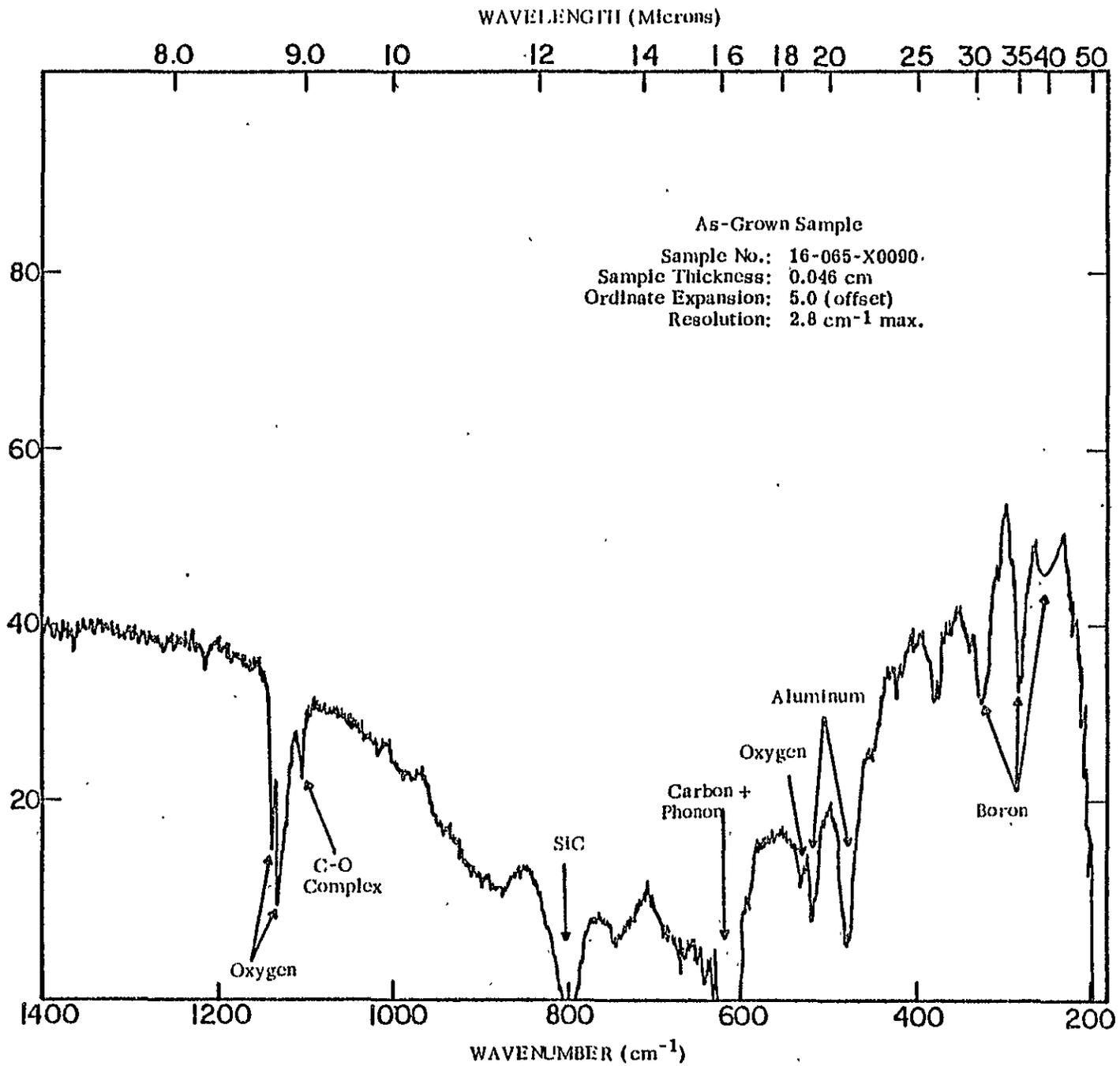
Fig. 8. IR absorption spectrum at 80°K of ribbon 16-065-X0090 with 5X ordinate expansion.

Table IV. Infrared Absorption Peaks Observed in Silicon
(Summary of Literature Data).

| Wave Number $(cm^{-1})$ | Origin | Temperature of Observation | References |
|---|---|---|---|
| 1136, 1128 | Interstitial oxygen | $80^{\circ}K$ | 4 |
| 1106 | Interstitial oxygen | $300^{\circ}K$ | 4 |
| 1104 | Carbon-oxygen complex | $80^{\circ}K, 77^{\circ}K$ | 4, 5 |
| 795 | SiC | $290^{\circ}K$ | 6 |
| 610 | Substitutional carbon and 2-phonon lattice band of Si | $300^{\circ}K$ | 5 |
| 604 | Substitutional carbon | $77^{\circ}K$ | 5 |
| 524 | Al (1s → 2 $p^4$ transition) | $4.2^{\circ}K$ | 7, 8 |
| 517 | Si-O bending mode | $4.2^{\circ}K$ | 7, 9 |
| 516 | Al (1s → 2 $p^3$ transition) | $4.2^{\circ}K$ | 7, 8 |
| 472 | Al (1s → 2 $p^2$ transition) | $4.2^{\circ}K$ | 7, 8 |
| 320 | Boron (1s → 2 $p^4$ transition) | $4.2^{\circ}K$ | 7, 8 |
| 278 | Boron (1s → 2 $p^2$ transition) | $4.2^{\circ}K$ | 7, 8 |
| 245 | Boron (1s → 2 $p^1$ transition) | $4.2^{\circ}K$ | 7, 8 |
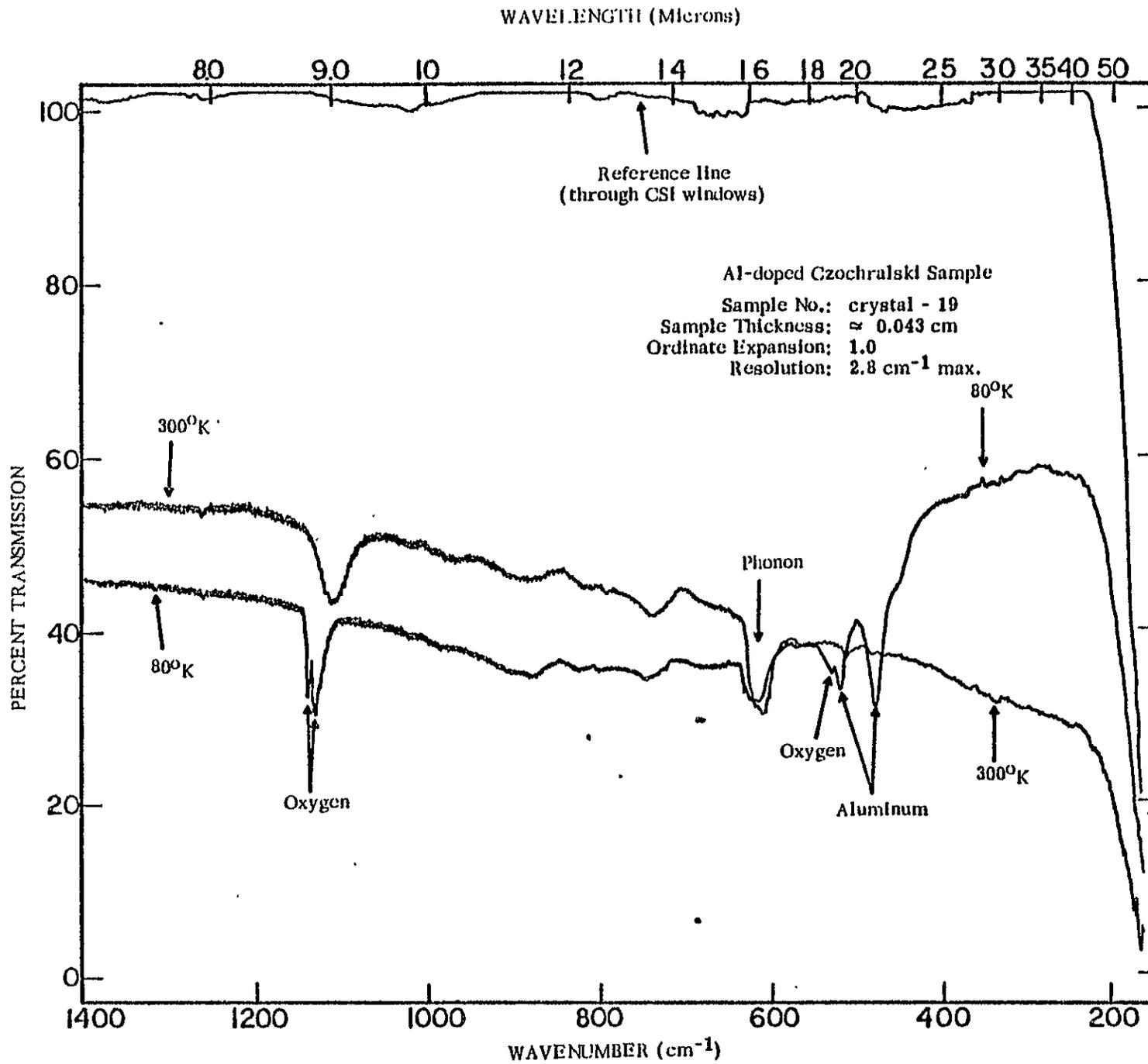
Fig. 9. IR absorption spectrum of Al-doped Czochralski sample.

tional aluminum in the silicon lattice. Table V presents the absorption coefficients (at 80°K) of the peak at 478 cm$^{-1}$. Also included in the table are the average thicknesses of the samples. Since measurements were made on unpolished samples, the surface roughness of the ribbon contributes to the total thickness; thus, the average thickness values refer to the upper limit of sample thickness. This uncertainty in the thickness of the samples leads to an error in the calculation of the absorption coefficients. However, we do not yet know how to exactly quantify this error.

Figure 10 shows absorption data at 80°K for a ribbon grown in an induction heated system for comparison with the above results. In general, ribbons grown in induction furnaces do not show the absorption peaks that can be attributed to substitutional aluminum. In addition, the 9.0 μm absorption peak corresponding to interstitial oxygen is observed infrequently in ribbons grown in the induction heated systems.

Why these differences between the two types of systems exist is not yet clear because a readily apparent major source of both aluminum and oxygen in both the resistance and induction heated growth systems is the fused silica crucible. Table VI shows data on the impurity levels in GE-204 fused silica. In addition to aluminum, it is quite likely that other elemental impurities are also incorporated into the melt as the fused silica crucible dissolves. The aluminum concentration thus should serve as a measure of total impurity incorporation into the melt from the crucible. However, semiquantitative analyses (using emission spectroscopy) of silicon ribbon samples showed that the general levels of major impurities in ribbons grown in the JPL stations[4] and in induction heated systems are comparable.

A possible explanation for these results can be made if cognizance is taken of the fact that spectrochemical analyses reveal the total amount of aluminum (as well as the other impurities) in the ribbon samples, whereas infrared spectroscopy is sensitive only to substitutional aluminum. Thus, aluminum present in the form of oxides, silicides or carbides, for example, will not be detected by infrared absorption techniques. There are significant differences in growth conditions (e.g., die configuration, growth rate, thermal profiles, etc.) between the JPL stations and the induction heated systems. This could lead to differences in the distribution of impurities in the ribbon during growth, and hence in the form the impurities are present in the ribbon. Further chemical analyses and infrared absorption measurements are in progress. In addition, growth experiments using graphite crucibles are planned.

B. Solar Cell Evaluation

During the reporting period a total of 64 cells were fabricated from both JPL No. 1 and No. 3A grown materials. The AM1 test results are summarized in Table VII.

Table V. Interstitial Oxygen Content and Absorption Coefficient at 478 cm$^{-1}$ in EFG Silicon Ribbon.

| Ribbon No. | Thickness (cm) | Interstitial $O_2$ Content (atoms/cm$^3$)* | Absorption Coefficient @ 478 cm$^{-1}$ ($\alpha$) |
|---|---|---|---|
| 16-058 | 0.065 | $8.7 \times 10^{17}$ | 1.0 |
| 16-063 (Phase I, Sect. I) | 0.047 | $3.5 \times 10^{18}$ | 1.5 |
| 16-063 (Phase III, Sect. VI) | 0.036 | $4.2 \times 10^{17}$ | 3.6 |
| 16-063 (Phase III, Sect. VII) | 0.037 | $5.9 \times 10^{17}$ | 5.2 |
| 16-065-X-0023 | 0.0355 | $2.3 \times 10^{18}$ | 2.4 |
| 16-065-X-0077 | 0.050 | $2.4 \times 10^{18}$ | 5.6 |
| 16-065-X-0085 | 0.044 | $1.8 \times 10^{18}$ | 2.6 |
| 16-065-X-0090 | 0.046 | $1.9 \times 10^{18}$ | 2.8 |
| 16-066-011 | 0.029 | – | 2.4 |
| 16-068-009 | 0.035 | $1.7 \times 10^{18}$ | 4.2 |
| 18-12-5 | 0.055 | $4.9 \times 10^{18}$ | 9.2 |
| 18-15-1 | 0.0395 | $4.4 \times 10^{18}$ | 0.8 |
| 18-16-5b | 0.043 | $2.3 \times 10^{17}$ | 2.0 |
| 18-17-1c | 0.0365 | Trace | 0.6 |
| 18-17-2f | 0.035 | Trace | – |
| 18-18-1e | 0.046 | $3.1 \times 10^{18}$ | 1.5 |
| 18-19-2f | 0.030 | $1.7 \times 10^{18}$ | 1.9 |

*These values were calculated in accordance with ASTM Standard No. F 121 70T from the 9 μm absorption peaks. Note that there is an uncertainty in these numbers caused by the sample thickness uncertainties, as discussed in the text.
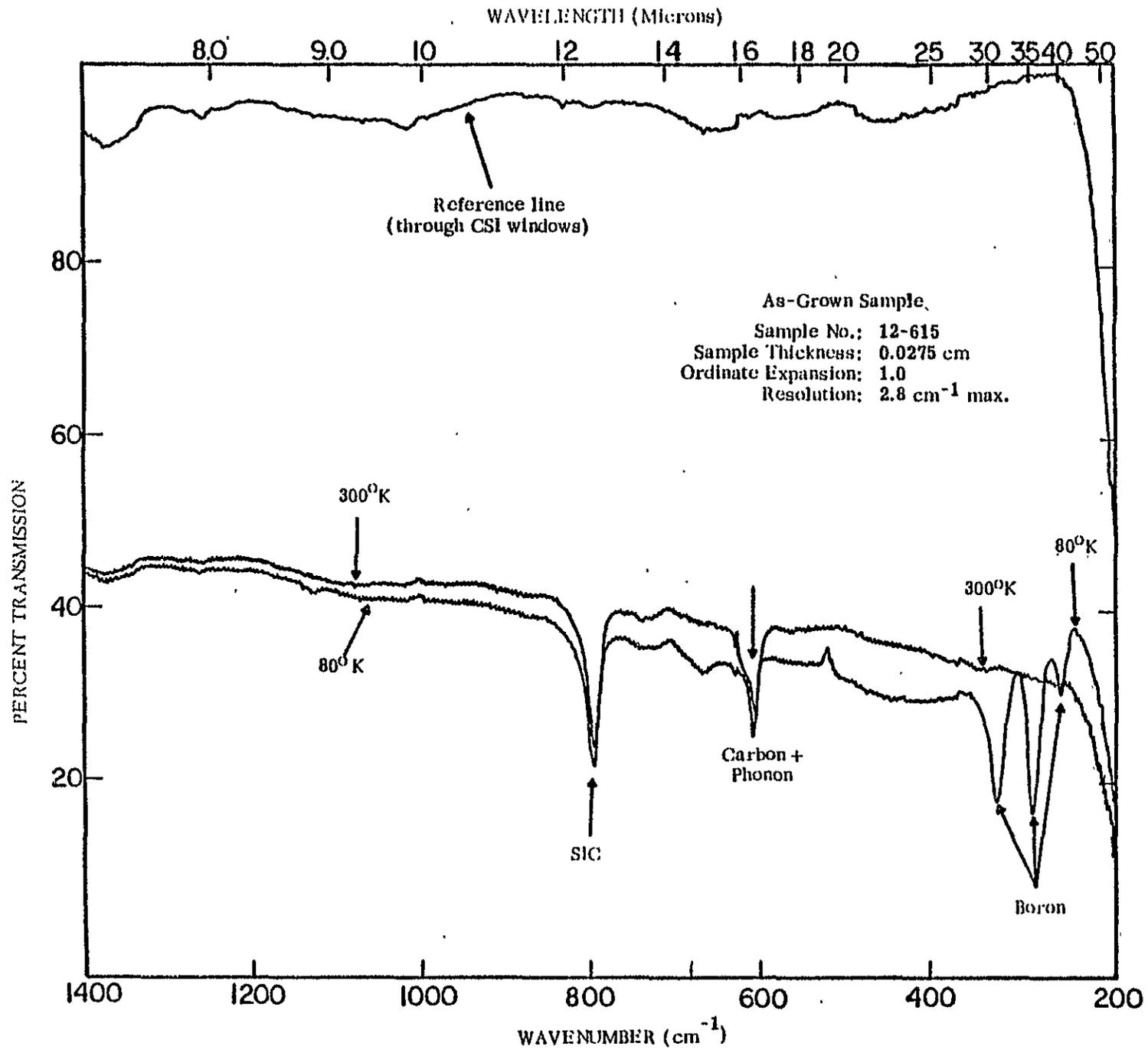
Fig. 10. IR absorption, at $300^{\circ}$K and $80^{\circ}$K, of a ribbon grown from induction heated system.

Table VI.  Typical Chemical Analysis of General Electric
           Type 204 Fused Silica Tubing.[+]

| Element | PPM Average | Range | Element | PPM Average | Range |
|---|---|---|---|---|---|
| Aluminum | 27 | 22-35 | Titanium | 2 | 1-2 |
| Iron | 4 | 1-6 | Zirconium | 2 | .7-4 |
| Calcium | 3 | 1-4 | Boron | 1 | - |
| Magnesium | 1 | 1-2 | Chromium | 1 | 1-3 |
| Potassium | 3 | .8-6 | Copper | 1 | - |
| Sodium | 3 | 2-4 | Manganese | 2 | 2-3 |
| Lithium | .5 | 0-1 | TOTAL | 50.5 | 32.5-70.0 |

*Data supplied by manufacturer.

Table VII. Summary of Solar Cell Results Obtained on Ribbons from JPL No. 1 and JPL No. 3A.

| Material | No. of Cells | $J_{sc}$ (mA/cm$^2$) [Max.] [Min.] | $V_{oc}$ (Volt) [Max.] [Min.] | F.F. [Max.] [Min.] | P (mW/cm$^2$) [Max.] [Min.] | Remarks |
|---|---|---|---|---|---|---|
| 16-063 | 2 | 15.40 [17.62] [11.10] | 0.353 [0.479] [0.167] | 0.362 [0.622] [0.252] | 2.24 [5.25] [0.47] | 4 Ω·cm No AR |
| 16-065 | 11 | 24.32 [25.43] [22.51] | 0.510 [0.516] [0.502] | 0.608 [0.651] [0.514] | 7.55 [8.37] [6.11] | 4 Ω·cm AR coated |
| 16-070 | 4 | 19.23 [19.61] [18.88] | 0.496 [0.500] [0.492] | 0.616 [0.722] [0.564] | 5.88 [6.93] [5.39] | - No AR |
| 18-15 | 5 | 21.07 [23.15] [19.08] | 0.436 [0.513] [0.338] | 0.399 [0.582] [0.283] | 3.92 [6.78] [1.82] | 4 Ω·cm AR coated |
| 18-16 | 14 | 22.93 [24.85] [17.82] | 0.486 [0.496] [0.474] | 0.581 [0.637] [0.506] | 6.49 [7.75] [4.78] | 15 - 16 Ω·cm AR coated |
| 18-17 | 19 | 16.40 [18.79] [14.93] | 0.467 [0.496] [0.435] | 0.547 [0.679] [0.366] | 4.24 [5.88] [2.68] | 7 - 13 Ω·cm No AR |
| 18-18 | 3 | 17.68 [18.07] [17.14] | 0.485 [0.490] [0.481] | 0.669 [0.702] [0.615] | 5.75 [6.22] [5.10] | 10 Ω·cm No AR |
| 18-20 | 4 | 15.26 [16.74] [13.83] | 0.97 [0.506] [0.491] | 0.67 [0.721] [0.570] | 5.08 [6.10] [4.37] | ? Ω·cm No AR |

We have chosen three cells for further examination; each cell is a representative one from the high, medium, and low performance groups. These cells have the following photovoltaic output characteristics:

| Ribbon No. | Cell No. | $J_{sc}$ (mA/cm$^2$) | $V_{oc}$ (Volt) | F.F. | Pm/A (mW/cm$^2$) |
|---|---|---|---|---|---|
| 18-18-2e | Good cell (No. 11889) | 18.07 | .490 | .702 | 6.22 |
| 18-17-5f | Medium cell (No. 11911) | 17.95 | .487 | .669 | 5.84 |
| 18-17-4j | Poor cell (No. 11913) | 14.93 | .467 | .541 | 3.77 |

They are not antireflection coated and have a full size of 20 cm$^2$. Spectral response, diffusion length, light enhancement, and IR scan measurement are used for the evaluation.

### 1. Spectral Response Measurement

The short circuit current spectral response is made and the collection efficiency $Q(\lambda)$ is calculated according to the procedures described in the First Quarterly Report.[1] The results for these cells are shown in Fig. 11. In the figure both a CZ cell (minority carrier diffusion length $L_D \approx 70$ µm) and an rf grown ribbon cell ($L_D \approx 20$ µm) are included for comparison. As seen in the figure, the decrease in $Q(\lambda)$ of each cell in the long wavelength region is consistent with the reduction in diffusion length. There is no evidence for any abnormality in the near surface region of the cells as indicated in the short wavelength response of $Q(\lambda)$.

### 2. Diffusion Length Enhancement Measurement

The schematic diagram for the diffusion length enhancement measurement setup is shown in Fig. 12. The short circuit spectral responses from a chopped ac mono-chromatic light of low intensity ("dark"), with a superimposed dc white light of AM1 (100 mW/cm$^2$) intensity, were obtained. Then the diffusion lengths are deduced from the long wavelength responses.[4] The measurement results are shown as follows:

| | $L_D$ ("Dark") | $L_D$ (AM1) | Enhancement Factor $L_D$ (AM1)/$L_D$ ("Dark") |
|---|---|---|---|
| Good cell (No. 11889) | 11.1 µm | 34.3 µm | 3.09 |
| Medium cell (No. 11911) | 7.30 | 33.6 | 4.60 |
| Poor cell (No. 11913) | 7.37 | 24.5 | 3.32 |
| Typical rf cell (No. 54A) | 17.5 | 44.0 | 2.51 |

On the average the enhancement factor, defined as the ratio of $L_D$ (AM1)/$L_D$ ("dark"), is higher for cells fabricated from resistance furnace grown material when compared with material grown in the rf furnaces. This result is still quite preliminary,
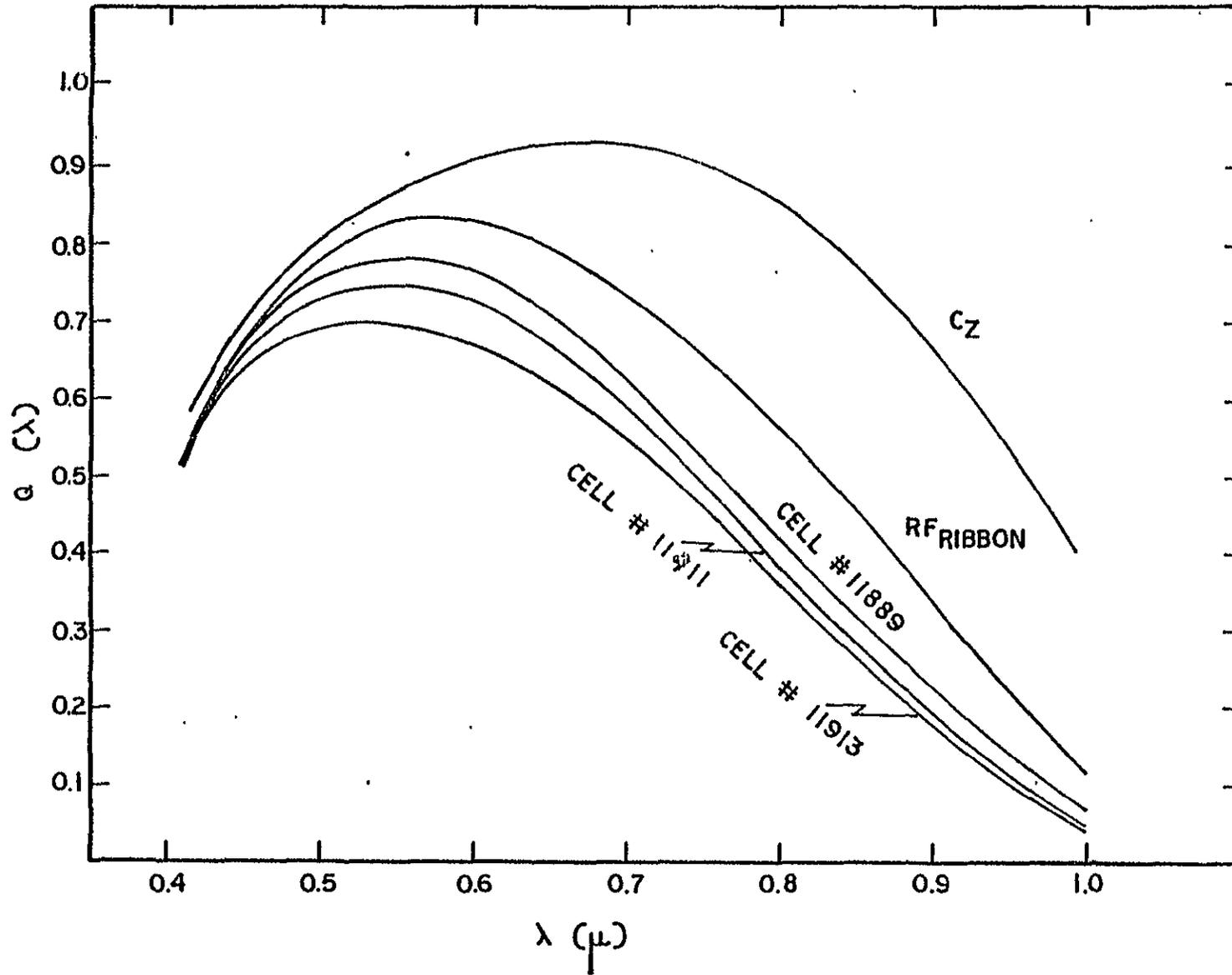
Fig. 11.  Collection efficiencies of good, medium and poor cells fabricated from resistance furnace grown materials.  A typical CZ cell and an rf furnace grown ribbon cell are included for comparison.
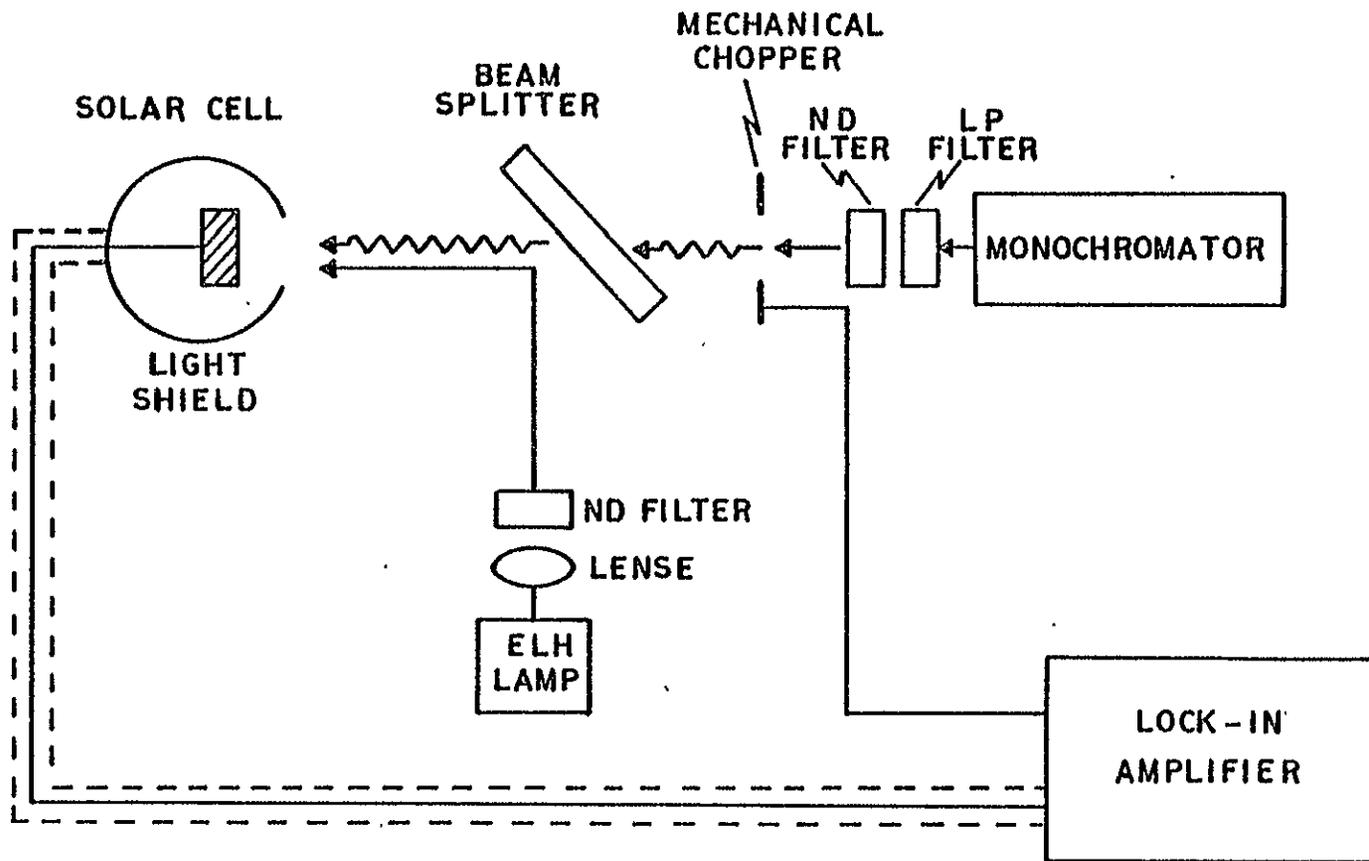
Fig. 12. Schematic of the diffusion length enhancement apparatus.

though, due to the small number of samples investigated; a more detailed study is in progress.

### 3. IR Scan Measurement

IR light of wavelength $\lambda = 0.95$ μ from a monochromator is scanned across the 2 cm width of each cell. The photovoltage response is recorded as shown in Figures 13 - 15. A calculated scale of diffusion length is also shown in the figures. The striking feature of this measurement is that there exists a periodicity of heavy recombination regions ($L_D \leq 1$ μm) near the central portion of the cells. For the poor performance cell, this periodicity is largely masked by the strong overall recombination in the cell. The scans along the length (or growth) direction do not show nearly as large a fluctuation. In general, the variation of diffusion length along the 20 cm length is about ±50% from the mean value. However, it can be as high as two to three times, and as low as near zero along the width direction.

The solar cell samples were polished at the same sections corresponding to the IR scans, preferentially etched and the cross-sectional structure was examined. The correlations between IR scans and structure are shown in Figures 13, 14, and 15. Figure 13(a) shows the IR scan of cell 11747. On examination of the cross-section, Figure 13(b), the structural features remain essentially constant, i.e., grain boundary structure in the center of the ribbon cross-section, throughout the width of the ribbon. Yet the IR scan reveals a non-uniformity in the diffusion length. However, closer examination reveals that in the regions exhibiting higher diffusion lengths, the grain structure is at a larger distance from the diffused surface (average distance of grains from surface ≈130 μm) compared to the lower diffusion length regions (average distance of grains from surface ≈50 μm). It is reasonable to assume that for the grain structure to have a significant effect on the solar cell performance, it should be present within one diffusion length from the surface exposed to solar radiation (i.e., from the junction region). Figures 14(b) and 15(b) do not reveal a grain structure in the middle of the ribbon. However, IR scans reveal significant variations in the photovoltage in these cells. Correlations reveal that high dislocation densities in the ribbon interior could lead to local recombination effects. Dislocations and twin boundary structure such as those seen in Figs. 14(b) and 15(b) have been observed in ribbons grown from rf systems. The dislocation densities are, however, lower. Yet, the ribbons grown from rf systems have produced good quality (>8%) cells consistently. Therefore, it is reasonable to speculate that the material grown in resistance systems has (a) more impurity content, or (b) that the state in which the impurities are present in the resistance grown ribbons is different from that in ribbons grown

44

Poor Cell (#11747)
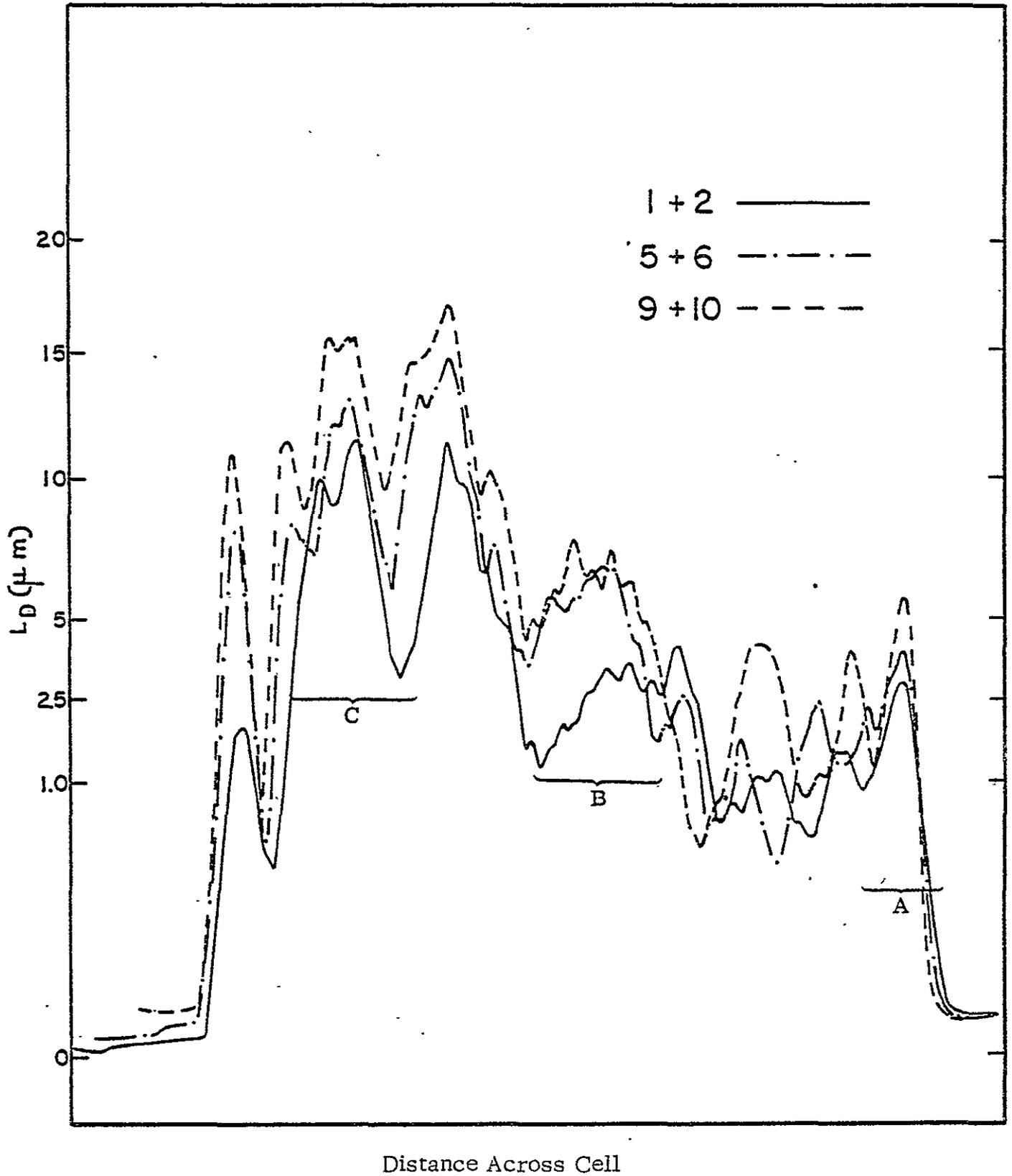


Fig. 15(a). IR scan of Cell No. 11747. (1 + 2, 5 + 6, etc., refer to scans taken between those respective contact fingers.) The data for this cell are: $J_{sc}$ = 23.36 mA/cm$^2$, $V_{oc}$ = 0.502 volts, F.F. = 0.521, Pm/A = 6.11 mW/cm$^2$.
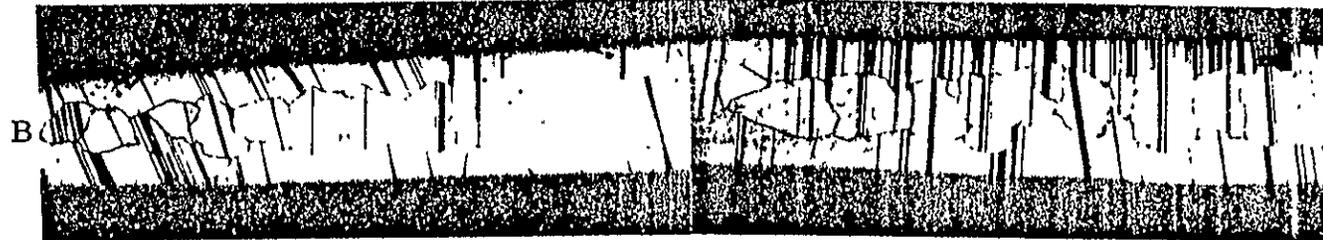
Fig. 13(b). Cross-sectional view of selected areas of Cell No. 11747, between metal contacts 5 and 6. A, B, and C refer to the corresponding regions in Fig. 13(a).

Good Cell (#11889)



Distance Across Cell
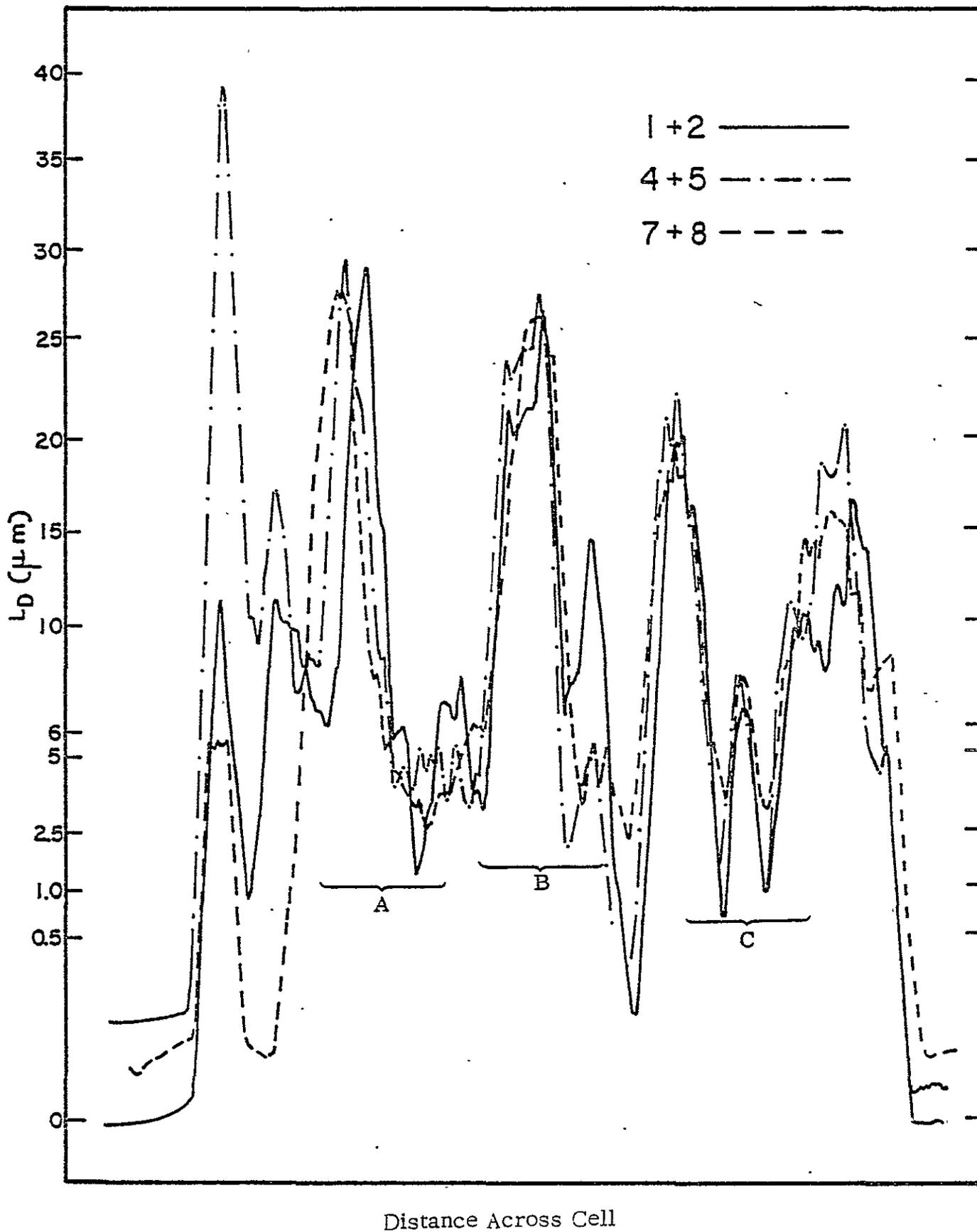
Fig. 14(a). IR scan of Cell No. 11889. (1 + 2, 4 + 5, etc., refer to scans taken between those respective contact fingers.)
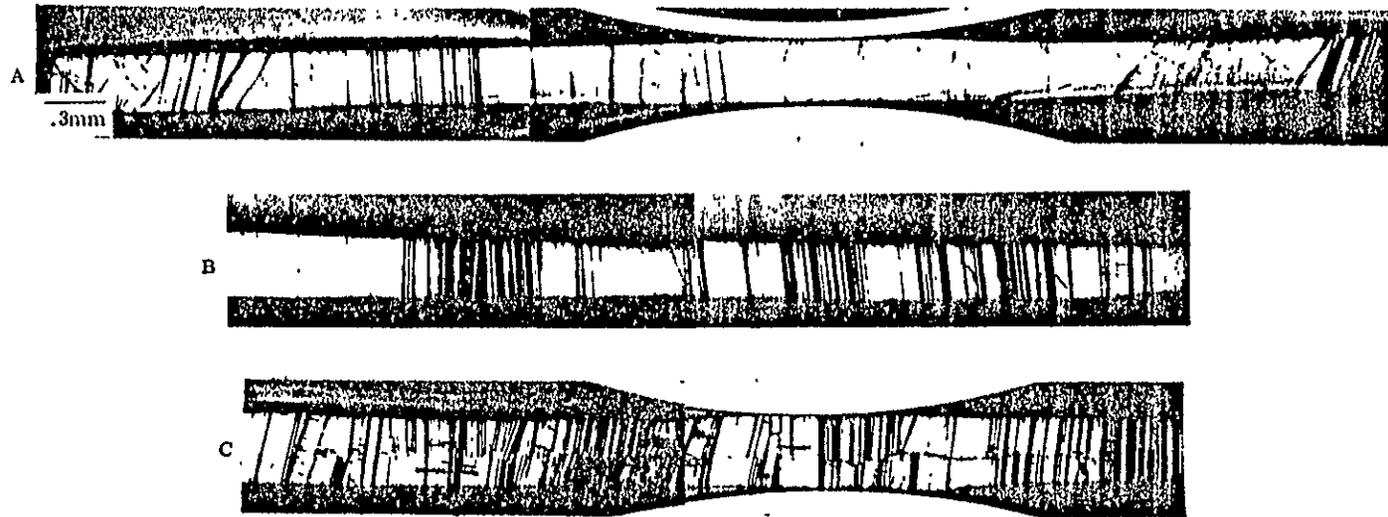
Fig. 14(b). Cross-sectional view of selected areas of Cell No. 11889, between metal contacts 1 and 2. A, B, and C refer to the corresponding regions in Fig. 14(a).

Poor Cell ( #11913)
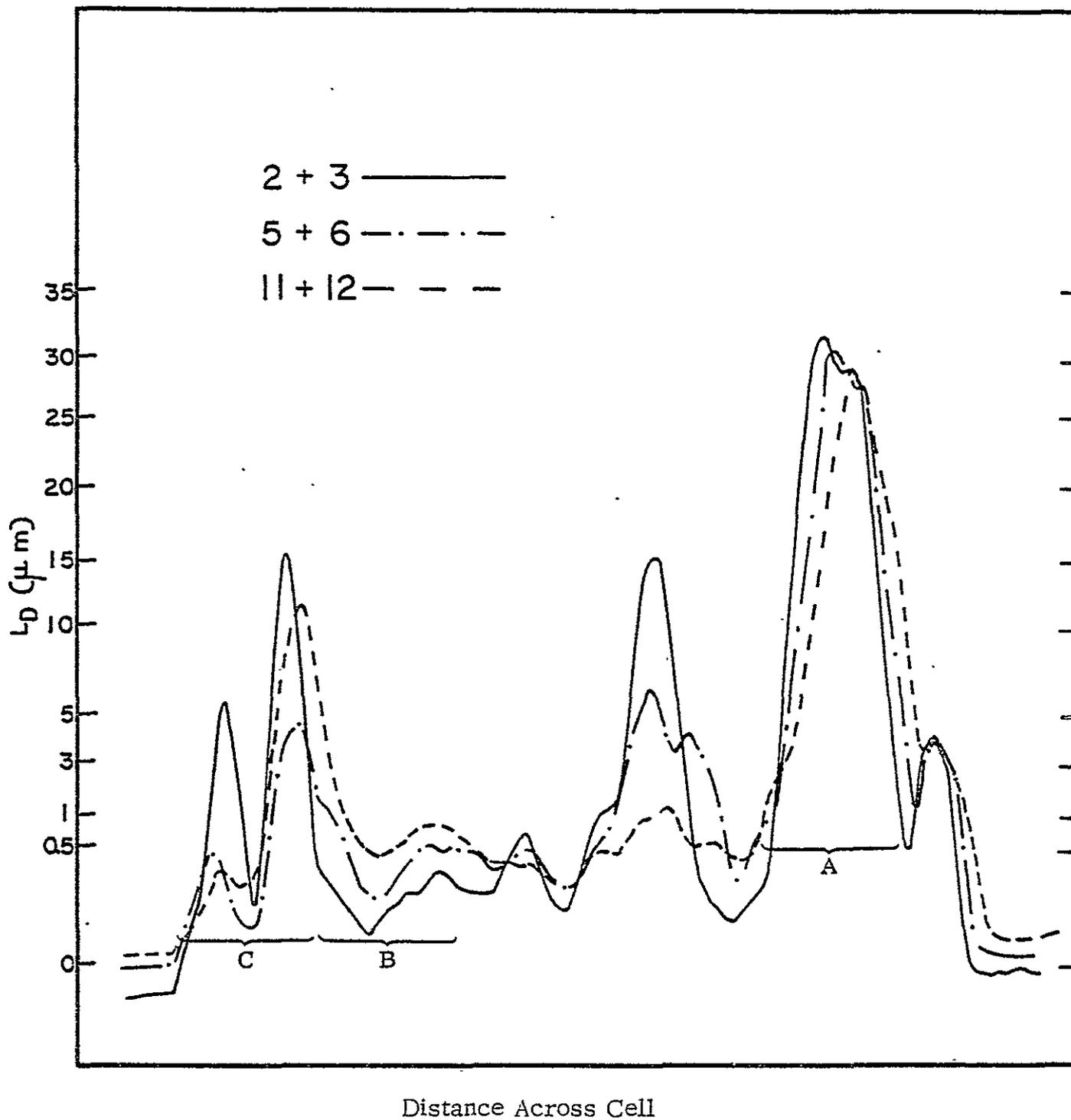


Fig. 15(a).  IR scan of Cell No. 11913.  (2 + 3, 5 + 6, etc., refer to scans
taken between those respective contact fingers.)

.2 mm
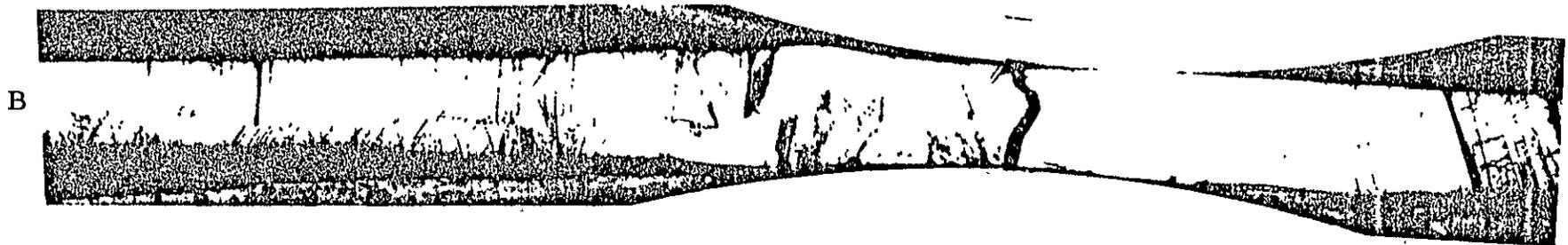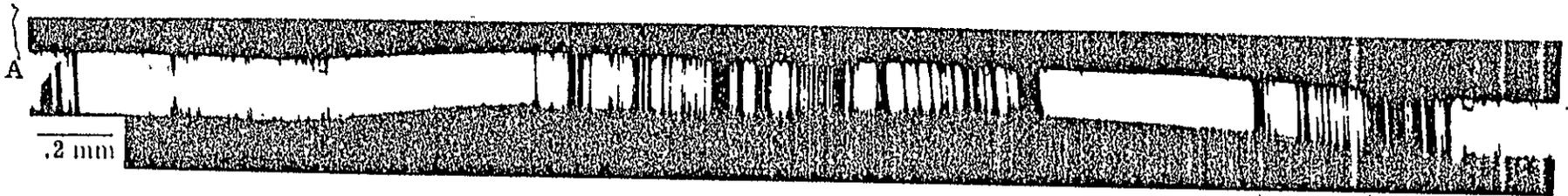
Fig. 15(b). Cross-sectional view of selected areas of Cell No. 11913, between metal contacts 5 and 6. A, B, and C refer to the corresponding regions in Fig. 15(a).

from induction heated systems. Heat treatment experiments aimed at understanding the facts found are in progress and will be reported in future reports. In addition, the effectiveness of "gettering" during the phosphorus diffusion step in initially low diffusion length material also warrants attention. Experiments aimed at understanding that are in progress as well.

REFERENCES

1.  B. Mackintosh et al., "Large Area Silicon Sheet by EFG", First Quarterly Progress Report, ERDA/JPL 954355/77-1 (March, 1977).

2.  F.V. Wald, Monthly Progress Report, May 15, 1977, ERDA/JPL Subcontract No. 954355.

3.  F.V. Wald, Monthly Progress Report, February 15, 1977, ERDA/JPL Subcontract No. 954355.

4.  R. Sahai and A.G. Milnes, Solid State Electr., 13, 1289 (1970).

PRECEDING PAGE BLANK NOT FILMED

APPENDICES

1. <u>Updated Program Plan</u>

The original program plan, shown as Table AI, is still generally in effect although several changes should be noted.

a. Tasks 5 and 6 both started later (on June 15), because the hiring of appropriate professional personnel was delayed until that date. We expect, however, that both tasks will be fully executed by the end of the contract.

b. Milestone No. 1c was not achieved, but present plans call for the first test of the three inch cartridge on July 8. Since the delay was due to delivery difficulties, this deadline is sure to be achieved because all parts are in. However, due to the decrease in the length of the shakedown period for the cartridge, it will not be possible to derive a "standard operating procedure" (SOP) before the August 1 deadline for reduced stress growth of 3 inch wide ribbon which we still intend to meet. In effect, an "SOP" will be written following achievement of that milestone.

c. A "standard operating procedure" for Machine 3A has been written, but it perhaps is a meaningless document due to the design changes required in that growth system. It has, therefore, not been delivered but is being held for review in order to incorporate any changes required.

d. So far, the milestone of multiple growth of 3 ribbons, 2 inches wide at 1.5"/min could not be achieved. The reasons for this form the bulk of the discussion on Machine 3A in this report. Significant redesign of the system is indicated and the lead times for many of the parts needed are long. However, we still plan to meet the endgoal of the contract and demonstrate 5 ribbon growth, although because of the long lead times, the goal of also achieving growth at 3"/min will be de-emphasized for this machine, since it requires procurement of a new set of cartridges, which may not be possible before the contract ends.

2. <u>Man Hours and Cost</u>

Previous man hours were 11,811 and cost plus fixed fee was $368,068. Man hours for April plus May were 3,742 and cost plus fee was $121,732. Man hours and cost plus fixed fee for June are estimated to be 2,855 and $174,117 respectively. Therefore the second quarter of 1977 man hours are estimated to be 6,597 and cost plus fee to be $295,849. Total cumulative man hours and cost plus fixed fee are estimated to be 18,408 and $663,917 respectively.

3. Engineering Drawings and Sketches Generated During the Reporting Period

    a.   Carbon crucible for JPL No. 1 system (see Figure A1).

    b.   Copy of the design of 3" belt puller (held for proper disposition).

    c.   Sketches of melt replenishment attachments for JPL No. 3A system (to be detailed, built and tested to select most appropriate design).

4. Summary of Characterization Data Generated During the Reporting Period

These data are discussed in detail in Section IV of the report. Significant findings were that the ribbons grown from resistance furnaces with widths of 2" at speeds of ~1.5" - 2.0"/min were significantly more inhomogeneous than 1" wide ribbons grown at 1"/min from induction heated systems. In particular here a very disrupted cross-sectional structure was found. Nevertheless, a number of solar cells of ~8% (AM1) conversion efficiency were prepared and it is believed that 9% - 10% are achievable if and when the problems with the severe inhomogeneities are overcome.

5. Action Items Required by JPL

None.

6. New Technology During The Reporting Period

Since all the systems designed under the contract are still being tested, new technology cannot be reported.

7. Work Not Performed Under the Contract but Introduced Here for Technical Clarification

Preprint 1: "The Edge-Defined Film-Fed Growth of Controlled Shape Crystals", by T. Surek, B. Chalmers, and A.I. Mlavsky; invited paper to be presented at ICCG-5 (5th International Conference on Crystal Growth), Boston, July 1977; accepted for publication in: Journal of Crystal·Growth. Preprint 2: "Enhancement of Diffusion Length in EFG Ribbon Solar Cells Under Illumination", by C.T. Ho, R.O. Bell and F.V. Wald; accepted for publication in: Applied Physics Letters.

Table AI.

PROGRAM PLAN

| TASKS | FEB. 1977 | MAR. | APR. | MAY | JUN. | JUL. | AUG. | SEPT. | OCT. | NOV. | DEC. | JAN. 1978 |
|---|---|---|---|---|---|---|---|---|---|---|---|---|
| 1. JPL No. 1 | | | | | | | | | | | | |
| a. Impurity Studies | | | | | | | | | | | | |
| b. Stress Analysis | | | | | | | | | | | | |
| c. Process and Machine D & D | | | | | | | | | | | | |
| d. Continuous Ribbon Growth | | | | | | | | | | | | |
| 2. Material and S.C. Characterization | | | | | | | | | | | | |
| 3. JPL No. 3 | | | | | | | | | | | | |
| a. Demonstrate Multiple Growth | | | | | | | | | | | | |
| b. Improve Quality & Growth Rate | | | | | | | | | | | | |
| c. Melt Replenishment Study | | | | | | | | | | | | |
| d. Automated Growth Development | | | | | | | | | | | | |
| 4. Automatic Control | | | | | | | | | | | | |
| a. Eval. Single Basic AWCs (Inc. Possible Interaction in Loops) | | | | | | | | | | | | |
| b. Advanced AWC D & D | | | | | | | | | | | | |
| c. Install & Evaluate 5 AWCs on JPL No. 3A | | | | | | | | | | | | |
| 5. Design of JPL No. 3B and Conceptual Design Studies | | | | | | | | | | | | |
| 6. Economic Analysis | | | | | | | | | | | | |

MILESTONES:

3   Deliver Furnace Design (JPL No. 3A)
4   Basic AWC Systems Installed
1c   3" Cartridge & Puller Design Complete
3a   Deliver JPL No. 3A SOP
1a   Achieve Intermediate Clean Conditions
3a   Demonstrate Multiple 3 x 2" x 1.5"/min
4a   Demonstrate AWC Single Basic Unit
1c   First Test 3" Cartridge
1c   Achieve 3" wide; 3" Cartridge SOP
1b   Demonstrate 3" Wide; 3"/min Reduced Stress Growth
3c   Test Melt Replenishment System
1d   First Test Belt Puller
1d   Continuous Growth SOP
3b   Demonstrate Cartridge with Growth Rate of 3"/min for 2" Wide Ribbon
1a   Achieve Clean Conditions
1b   Achieve 3" Wide; 3"/min Low Stress Growth
3a   Demonstrate Multiple 5, 2" Wide, at Least 2.5"/min
3d, 4   Demonstrate 5 AWC/1 Operator Operation of JPL No. 3A

*Financial and Technical Reports, Solar Cells and Samples will be Delivered as per the Delivery Schedule of This Contract.

B

A ←

C
L

A ←

A

A

|←—.25

$\frac{1}{32}$

1.365 RAD.

1.13 RAD.
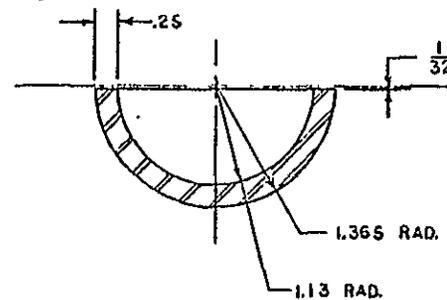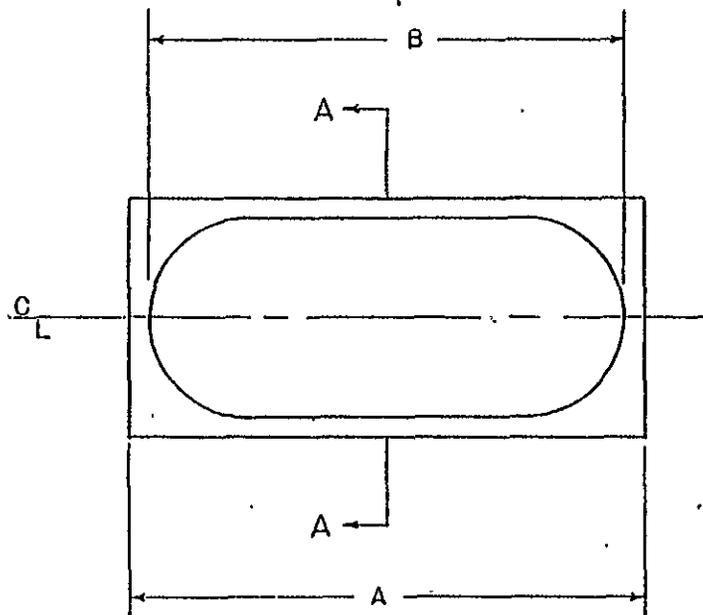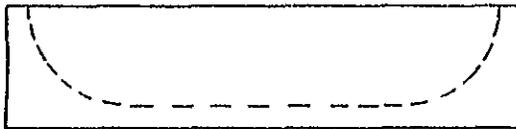
A – A

NOTE: MAKE 2 PER $2\frac{3}{4}$ DIA. ROD

| PART NO | A | B |
|---------|------|------|
| -1 | 6.00 | 5.50 |
| -2 | 4.00 | 3.50 |

| THESE DRAWINGS & SPECS ARE THE PROPERTY OF MOBIL TYCO SOLAR ENERGY CORP & SHALL NOT BE REPRODUCED, COPIED OR USED AS THE BASIS FOR MANUFACTURE OR SALE OF APPARATUS WITHOUT EXPRESSELY WRITTEN AUTHORIZATION FROM MOBIL TYCO SOLAR ENERGY CORP. | UNLESS OTHERWISE SPECIFIED DIMENSIONS ARE IN INCHES | | DR R HOGENCAMP DATE 3/5/77 | Mobil Tyco Solar Energy Corporation |
|---|---|---|---|---|
| | TOLERANCES | SURFACES | CHK | |
| | ANGLES ± | | | |
| | FRACTIONS± | 64 /MICRO- INCHES | APPD | |
| | 2 PLACE ±.01 | | APPD | |
| | 3 PLACE ±.005 | | | BOAT TYPE |
| | NEXT ASSEMBLY | | APPLICABLE DOCUMENTS | GRAPHITE CRUCIBLE |
| FINISH | MATERIAL DFP-2 | | | SIZE C 11803 REV. |
| | | | | SCALE FULL SHEET 1 OF 1 |

Fig. A1.   Graphite crucible for JPL Station No. 1.

APPENDIX 7


Preprint 1:  "The Edge-Defined Film-Fed Growth of Controlled Shape Crystals", by
             T. Surek, B. Chalmers, and A.I. Mlavsky; invited paper to be presented
             at ICCG-5 (5th International Conference on Crystal Growth), Boston,
             July 1977; accepted for publication in:  Journal of Crystal Growth.

# THE EDGE-DEFINED FILM-FED GROWTH OF
# CONTROLLED SHAPE CRYSTALS[*]

by

T. Surek, B. Chalmers and A.I. Mlavsky

Mobil Tyco Solar Energy Corporation
16 Hickory Drive
Waltham, Massachusetts 02154

. Abstract

The growth of shaped crystals is examined in the various meniscus-controlled growth processes such as Czochralski, floating zone, Stepanov, and edge-defined film-fed growth (EFG). The basic physical processes which shape the crystal are the same in these techniques; they involve the interaction of the three interfaces at the crystal-liquid-vapor junction. Specifically, for a crystal of constant dimensions, the angle $\phi$ between the meniscus and the growth axis must be $\phi_o$ (a constant; for silicon, $\phi_o = 11^o$). The degree of crystal shape control and the range of cross-sectional shapes which can be grown in a stable manner by the different techniques are shown to depend on the details of the meniscus shape and of the heat flow in the systems.

The use of a die shaper which constrains the meniscus distinguishes the EFG and Stepanov processes from the other methods. The use of a wetted die in EFG versus a non-wetted die in Stepanov growth is shown to have an additional effect on the ability to control the crystal shape and dimensions. The role of the die shaper is examined in detail from the points of view of die material selection (e.g., wettability and chemical compatibility) and die design. The advantages and disadvantages of using wetted and non-wetted dies in the shaping process are discussed from both the theoretical and practical points of view. Specific numerical examples in the paper deal with the growth of silicon ribbons.

---

# 1. Introduction

A problem which has confronted crystal growth researchers over the years has been the development of techniques to monitor and control the external shape of melt-grown crystals. Special applications of some single crystal materials have also indicated the need to grow these crystals with a pre-determined cross-sectional shape such as ribbons, tubes or filaments. Considerable progress in this area has been made by Russian workers in developing the Stepanov technique [1,2] which uses a non-wetted shaping device to control the crystal shape. The web-dendritic growth process [3,4] has been another notable development in the growth of ribbon crystals; various other shaping schemes are also described in the literature [5-7]. A significant advance in shaped crystal growth has occurred with the recognition by LaBelle and co-workers [8,9] that a die shaper which is wetted by the melt provides a means of effectively isolating the growth interface from the main melt (with capillary rise, in appropriately placed capillary slots in the die, supplying the initial melt to the shaping surface), and thus a means for better control of the cross-sectional shape of the crystal. Indeed, one of the highlights of ICCG-3 was their demonstration [10] of the "Edge-defined Film-fed Growth" (EFG) process reduced to commercial practice in the growth of variously shaped sapphire crystals using die shapers fabricated from molybdenum.

Our interest over the past few years has been to apply the EFG process to the growth of ribbon crystals of silicon; the overall effort of the program is directed toward the achievement of low-cost silicon solar cells for terrestrial applications. A detailed discussion of theoretical and experimental aspects of silicon ribbon growth by EFG, and of the crystalline and electrical characteristics of the ribbon crystals has been presented in the literature [11-30]. The theory has served to identify the parameters that control the growth of silicon ribbon by EFG and to determine the practical limits of the growth parameters, while the characterization effort has provided an insight into correlations between growth parameters, crystal quality,

electronic properties and solar cell performance. The process and material improve-
ments thus realized have led to the routine growth of long lengths (>25 meters) of
2.5 cm wide ribbon from a single graphite die at rates of 2.5 cm/min, and solar cells
of >11% (AM1) efficiency have been made from such ribbon crystals. Multiple ribbon
growth [31], i.e., simultaneous growth of several ribbons from a single crucible,
ribbon widths of 5 cm and growth rates up to 6.3 cm/min have also been achieved in
experimental systems [32].

In this paper, we briefly consider some of the underlying physical phenomena in
the growth of controlled-shape crystals (Section 2), and examine the theory of crystal
shape stability in meniscus-controlled growth processes such as EFG, Stepanov,
Czochralski and floating zone growth (Section 3). The role of the die in shaped
crystal growth is discussed in Section 4, where we examine the questions of die
material selection, die design and meniscus attachment, and the advantages and dis-
advantages of using wetted and non-wetted dies in the shaping process from both the
theoretical and practical points of view. Although much of the discussion is ap-
plicable to shaped crystal growth of any material, the specific calculations and ex-
amples will deal exclusively with silicon crystal growth and, in particular, with
silicon ribbon growth by EFG.

## 2. What is Shaped Crystal Growth?

The fundamental physical processes which determine the external shape of a
melt-grown crystal occur at the triple junction of the three interfaces, viz.,
crystal-vapor, liquid-vapor and crystal-liquid (see fig. 1a). The concept that the
shape of the growing crystal is likely to be related to that of the liquid-vapor
interface or meniscus at the triple junction has been generally recognized; the
meniscus angle $\phi$, measured between the growth axis and the tangent to the meniscus,
has been commonly assumed [5,33] to be zero for growth of a constant dimension
crystal. Experimental observations [34-37] in Czochralski and Stepanov growths of
silicon and germanium crystals have shown, on the other hand, that $\phi > 0^{\circ}$ during

constant diameter growth of these materials; the scatter in the values reported ($\sim 0^{\circ}$ to $\sim 36^{\circ}$) is probably the result of the inherent inaccuracies of these observation methods.

Recently, we described [38,39] a simple, new experimental technique which involved the analysis of radially frozen zones in thin, horizontal wafers of silicon and germanium. These experiments showed that the relative orientation of the crystal and liquid free surfaces (designated by the angle $\phi_0$ in fig. 1a) is a characteristic property of the material, and that the value of $\phi_0$ is dependent on the crystallographic orientation of the crystal-vapor interface. For {111} orientation surfaces of silicon and germanium, we have found that $\phi_0 = 11^{\circ}$ and $13^{\circ}$, respectively; the characteristic value of $\phi_0$ is likely to be lower for higher index crystal surface orientations. Experimental observations [24] of thickness changes in EFG silicon ribbons, which occurred following a change in crystal surface or growth interface orientation caused by twinning, have confirmed the anisotropic nature of the parameter $\phi_0$. These observations could be readily correlated with the expected anisotropies in the crystal-vapor and crystal-liquid interfacial free energies of silicon.

The above findings have important implications on the growth_of_shaped crystals. Firstly, a crystal cannot grow with a uniform cross-section unless the meniscus angle $\phi = \phi_0$ at all times. In view of the observed constancy of the relative angle $\phi_0$ (aside from the anisotropy effects noted above), the crystal dimension will therefore increase when $\phi > \phi_0$ and decrease when $\phi < \phi_0$. Secondly, the basic physical processes which shape the crystal are the same in EFG as in the Stepanov, Czochralski and floating zone techniques; these are all what may be termed "meniscus-controlled" growth processes. It is the degree of crystal shape control which is different in the various techniques; this, in turn, influences the range of cross-sectional shapes which can be grown, in a stable manner, by each method. As will be shown in the next two sections, the degree of crystal shape control is a function of the detailed shape of the meniscus, and of the details of the heat flow in the system in the

various techniques. In addition to the $\phi = \phi_o$ requirement at the crystal growth boundary for steady state, the manner in which the other end of the meniscus (e.g., the lower end in the schematic in fig. 1a) terminates will be shown to be of prime importance. It is this latter boundary condition which distinguishes the Czochralski and floating zone methods from the EFG and Stepanov techniques. The use of wetted versus non-wetted die-shapers in the latter processes has an additional effect on the ability to control the crystal shape.

Before proceeding to address these questions, it is worthwhile to discuss here briefly the unique requirement for steady-state growth, viz., the condition that $\phi = \phi_o$. Clearly, it is the interaction of the three interfaces at the triple junction which must somehow be involved; the thermodynamics and kinetics of this interaction are not understood at the present time. A theory proposed by Bardsley, et al. [40] considers the equilibration of surface tensions at the triple junction to determine the angular relationship of the interfaces; $\phi_o > 0$ is explained in this model (as well as in that of Pogodin, et al. [41]) as a consequence of the incomplete wetting of the solid by its own melt. The observations [38,39] that the values of $\phi_o$ for silicon and germanium are independent of crystal growth rate over nearly two orders of magnitude change in the rate tend to support the equilibrium theory [42]. The $\phi_o$ - anisotropy observations described above are also in qualitative agreement with this model if one were to include the effects of anisotropy in the crystal-vapor and crystal-liquid surface free energies into the theory [24]. At finite growth rates, however, kinetic considerations must also be involved [39]; the details of the mechanisms whereby the growth interface advances and the meniscus recedes near the triple junction to form a constant dimension crystal when $\phi = \phi_o$ are not understood.

Finally, for materials, such as silicon, with anisotropic crystallization properties, there can exist growth conditions where the crystal shape is no longer controlled by the shape of the meniscus (i.e., the $\phi = \phi_o$ requirement). This can occur when peripheral regions of the crystal-liquid interface advance by a layer

nucleation and growth mechanism. When such faceted growth occurs, the external shape
of the crystal is determined by the detailed kinetics of ledge nucleation and motion
on the peripheral facets (the {111} faces in silicon and germanium); faceted growth
is usually evidenced by the various ridge-like features on the surface of the crystal.
Such growth has been observed and analyzed in Czochralski [43], floating zone [44]
and Stepanov [2] growths of silicon and germanium crystals. Recently, we have analyzed
the effects of faceting in EFG of silicon ribbons [24]. We found that faceted growth
can compete with and, on occasion, completely override meniscus-controlled growth in
EFG, and that the effects of faceting were more deleterious at the ribbon edges than
at the ribbon sides. In the remainder of this paper, we will consider meniscus-
controlled growth in detail, and we will neglect the effects of the anisotropy of
$\phi_o$ described earlier in this section.

## 3. Theory of Crystal Shape Stability in Meniscus-Controlled Growth

The following set of equations describes the time evolution of the crystal shape
in a meniscus-controlled process such as EFG [45]:

$$\frac{dt}{d\tau} = 2V_g \tan (\phi - \phi_o), \tag{1}$$

$$\phi = \phi \ (t, \ t_d, \ s, \ h_{eff}), \tag{2}$$

$$\frac{ds}{d\tau} = V_p - V_g, \tag{3}$$

and $\quad V_g = V_g \ (t, \ s, \ \phi, \ V_p, \ H). \tag{4}$

Here $V_g$ is the component of the growth velocity along the crystal pulling axis, $V_p$ is
the velocity of pulling of the crystal, t is the crystal dimension (say, ribbon thick-
ness), $t_d$ is the edge-defining die dimension (for the purposes of the present section,
the die-edge is assumed to be a fixed point, as depicted in fig. 1b), s is the height
of the growth interface above the die top (i.e., the meniscus height), and $h_{eff}$ is the
effective height of the growth interface above the horizontal liquid level in the
crucible. The height $h_{eff}$ corresponds to the pressure difference between the at-
mosphere and a point inside the meniscus; it includes the effects of viscous flow of

melt in the capillary and in the meniscus film, as well as that of the hydrostatic

head [14,15]. The symbol H in eq (4) is used to represent heat transfer effects in

the system caused by other than the first three variables in the brackets, e.g., ex-

ternal heat input terms. The parameters $V_p$, $h_{eff}$ and H may be functions of the time

variable $\tau$, in general.

Eqs. (1) to (4) describe the growth of axisymmetric crystals by the EFG, Stepanov

and Czochralski methods, although the interpretation of some of the terms is different

in the latter case. For the floating zone process, an additional equation describing

the time rate of change of the zone volume v is required [46]; in addition, $h_{eff}$ in

eq. (2) is replaced by v, $V_g$ in eq. (4) is also a function of v, and some of the terms

have different interpretations from the present discussion. For Stepanov growth, the

parameter $h_{eff}$ is usually close to or less than zero; in principle (if not in practice),

the growth interface is below the liquid level in the crucible for $h_{eff} < 0$, i.e.,

there exists a positive hydrostatic pressure in the meniscus film (cf. the "Inverted

Stepanov Technique" [47]). It should be pointed out that we defer to Section 4

the discussion of the manner in which the lower end of the meniscus in fig. 1b

is attached to the die, and how the melt is supplied to the die top prior to seed-

ing.

Eq. (1) is, of course, a direct consequence of the meniscus angle requirement for

steady-state growth discussed in the preceding section. The functional form of $\phi$ in eq.

(2) is obtained from the solution of Laplace's capillary equation for axisymmetric menis

cus shapes [48]. The third equation expresses the time dependence of meniscus height

caused by a difference between the pulling velocity and growth velocity; the functional

dependence of the growth velocity in eq. (4) is obtained from the solution of the heat

transfer in the system and from the condition of heat balance at the solid-liquid inter-

face. The details of the assumptions which are implicit in these equations are des-

cribed in a separate publication [45]. Given the initial and boundary conditions, the

forms of the functions $\phi$ and $V_g$, and the explicit time-dependencies (if any) of $V_p$,

$h_{eff}$ and H, the above equations may be solved for the time evolution of the external shape of the crystal.

We have carried out a linear perturbation analysis, in a manner analogous to the analysis of shape stability in the floating zone process [46], to test the stability of the steady-state solution of the above equations. The necessary and sufficient conditions for stability of the dimensions of the solidifying crystal are found to be [45]

$$\alpha = \tfrac{1}{2}[(\partial V_g/\partial s) + (\partial\phi/\partial s)\cdot(\partial V_g/\partial\phi)] - V_{go}(\partial\phi/\partial t) > 0 \qquad (5)$$

and

$$\alpha^2 + \beta^2 = 2V_{go} \ [(\partial\phi/\partial s)\cdot(\partial V_g/\partial t) - (\partial\phi/\partial t)\cdot(\partial V_g/\partial s)] > 0, \qquad (6)$$

where $V_{go}$ is the steady-state growth velocity, and the quantities $\alpha$ and $\beta$ denote the natural frequencies of the system. When $\beta$ is real, perturbations to a stable system lead to an oscillation about steady state with an exponentially decaying amplitude; the decay time is given by $1/\alpha$, while the period of oscillation is $2\pi/\beta$. Typical values of the latter are ~1 sec for silicon ribbon EFG and ~100 sec for Czochralski growth of silicon crystals; the decay times are usually shorter than the periods of oscillation. Another prediction of the above theory is that fluctuations in the external (i.e., inhomogeneous) system variables (such as H, $h_{eff}$ or $V_p$ in eqs. (1) to (4)) can lead to an oscillation in the dimension of the growing crystal. When the frequency of the imposed fluctuation is >> the natural system frequencies $\alpha$ and $\beta$, the amplitude of the fluctuation in t is given by $|\Delta t| \simeq A/\omega^2$, where A is the amplitude and $\omega$ is the frequency of the oscillation in the external system variable.

It is clear from the criteria given by eqs. (5) and (6) that the existence of shape and thermal stability in a meniscus-controlled process is dependent on the explicit functional form of the variation of growth velocity with s, t and $\phi$, and on the form of the meniscus shape function $\phi$ in eq. (2). For a "thermally stable" system (i.e., $V_g$ = constant, independent of s, t and $\phi$), we have recently described [20] a qualitative analysis of shape stability in the various techniques of crystal growth from the melt. The stability criteria in eqs. (5) and (6), in this case, reduce to the requirement that $\partial\phi/\partial t < 0$. Qualitatively, shape stability thus im-

plies that if a change in crystal shape occurs (i.e., whenever $\phi \neq \phi_o$), the meniscus angle $\phi$ should approach $\phi_o$ again as a result of the shape change.

From the meniscus geometry in Czochralski growth (e.g., ref. [49]), it can be readily deduced that $\partial\phi/\partial t > 0$, where t denotes the crystal diameter; hence we concluded [20] that Czochralski growth is shape unstable (in the case where the thermal effects are neglected). A similar analysis [46] showed that shape stability is generally obtained in the usual floating zone geometries of interest; for these cases, the conditions that $(\partial\phi/\partial t)_{v,\ell} < 0$ and $(\partial\phi/\partial v)_{t,\ell} > 0$, where v is the zone volume and $\ell$ is the zone length, need to be satisfied for shape stability of the resolidifying crystal. Application to EFG ribbon growth [20,24] showed that the side of the ribbon (i.e., the thickness dimension) is stable, whereas the edge of the ribbon (i.e., the width dimension) is only conditionally stable. Shape stability in the latter case requires that the edge-defining die radius (given by $\sim t_d/2$ in fig. 1b) should not exceed approximately twice the radius of curvature of the ribbon ($\sim t/2$) at the ribbon edge. This result is exact for the EFG growth of filamentary or rod-shaped crystals; the approximation to the ribbon-edge problem provides only a lower-limit estimate of the stability. The above conclusions also apply, of course, to the growth of ribbons or rods by the Stepanov technique; in our recent analysis [20], we considered briefly the effects of $h_{eff} < 0$, which would be appropriate for the usual conditions of growth in the Stepanov process. Experimental observations [24] in EFG silicon ribbon growth provide supporting evidence for the stability of the ribbon side and the relative instability of the ribbon edges.

The complete analysis of the shape and thermal stability problem (i.e., the criteria in eqs. (5) and (6)) requires, of course, the solution of the heat transfer in the system in order to obtain the functional dependence of the growth velocity. The detailed results for EFG and Czochralski growth are given in a separate publication [45]; briefly, the heat flow in the system can lead to conditions of growth where the stability criteria are satisfied in the Czochralski process. Stability of

the ribbon sides and edges in EFG silicon ribbon growth is further enhanced by the thermal gradients under the usual conditions of growth. The problems and techniques of crystal diameter control in Czochralski growth are reviewed by Hurle [56] in this volum

## 4. The Role of the Die in Meniscus-Controlled Growth

To this point in the discussion, we have described the process of shaped crystal growth with respect to a specific boundary condition at the junction of the crystal surface and the meniscus. It is immediately obvious, however, that it is the presence of the die shaper in the EFG and Stepanov processes which sets these techniques apart from Czochralski growth. The fact that the lower end of the meniscus in the former techniques is constrained to some point on a die leads to the condition that $\partial\phi/\partial t < 0$, i.e., inherent shape stability for a wide range of growth conditions. On the other hand, in the usual Czochralski growth situation where the crystal diametei is much smaller than the diameter of the crucible, the lower end of the meniscus is not constrained; this leads to $\partial\phi/\partial t > 0$ and a condition of shape instability when heat flow effects are neglected. In this section, we examine the details of the meniscus attachment at the die top, and delineate the advantages and disadvantages of using wetted versus non-wetted dies (to be defined later) in the shaping process. For ease of exposition, we will consider the meniscus shape and attachment to the die at the side of an infinitely wide ribbon; fig. 1b is a schematic cross-section of the shaping process. The attachment to the die of the meniscus in the growth of filamentary or rod-shaped crystals and of the meniscus at the ribbon edges can be treated in an analogous manner; previous analyses have described meniscus shape calculations [14,50] and crystal shape stability [20] for these cases.

## 4.1 Meniscus Shape Considerations

In a previous paper [14], we showed meniscus shapes at the side of EFG silicon ribbons obtained by numerical integration of Laplace's capillary equation. Those calculations showed that, in the usual case where $h_{eff} > 1$ cm (and since $h_{eff} \gg s$), the meniscus radius of curvature is approximately constant and is given by $R_1 = \gamma/\rho g h_{eff}$, where $\gamma$ is the liquid-vapor interfacial free energy, $\rho$ is the density of the

liquid (for silicon, $\gamma$ = 720 ergs/cm$^2$ and $\rho$ = 2.53 gm/cm$^3$ [51]), and g is the acceleration of gravity. For $h_{eff}$ = 2 cm, which is typical for EFG silicon ribbon growth, the meniscus radius of curvature is within 7% of the above value of $R_1$ over the entire meniscus length; the approximation gets even better for larger values of $h_{eff}$. For large negative values of $h_{eff}$, the meniscus shape can be similarly approximated by a circular segment of radius $R_1$. The left and right insets in fig. 2 show the meniscus·shapes at the ribbon side for $h_{eff}$ > 0 and $h_{eff}$ < 0, respectively. Attachment of these circular menisci to a die of dimension $t_d$ can be shown to lead to the following relationship (cf. eq. (2)) among the meniscus shape variables in fig. 1b:

$$\phi = \arctan \left(\frac{t_d - t}{2s}\right) - \pi/2 + \arccos (z/2R_1), \qquad (7)$$

$$\text{where } z = [s^2 + (t_d - t)^2/4]^{\frac{1}{2}}, \qquad (8)$$

and the meniscus angle $\phi = \phi_0 = 11^o$ for steady-state growth of silicon crystals. A similar expression can also be derived for the angle $\Theta$ between the horizontal and the tangent to the meniscus (see fig. 2); as shown below, the value of $\Theta$ will be important in establishing the appropriate contact angle at the die top. These analytical expressions will be used in all subsequent calculations in this paper.

Eqs. (7) and (8) can be used to obtain the steady-state ribbon thickness as a function of meniscus height for given values of $t_d$ and $h_{eff}$. Fig. 2 shows these relationships for both positive and negative values of $h_{eff}$; for a given value of $t_d$, the ribbon thickness increases from left to right in the figure. It can be readily shown that, in the portions of the curves denoted by the solid lines, the partial derivative $\partial\phi/\partial t$ < 0, i.e., the ribbon side is inherently shape stable. The broken lines in the figure denote regions where $\partial\phi/\partial t$ > 0. The maximum meniscus height $s_{max}$ (solid points in fig. 2) for shape stability is seen to be a function of $h_{eff}$; the heights correspond to $\Theta$ = 0$^o$ and $\Theta$ = 180$^o$ for $h_{eff}$ > 0 and $h_{eff}$ < 0, respectively. For $h_{eff}$ < 0, there may not exist, of course, stable solutions to Laplace's equation

beyond some value of meniscus height which may be $< s_{max}$. For our present purposes, we will consider the practical limit $s_m$ to meniscus height (for growth with $h_{eff} < 0$) to be that where the ribbon and die dimensions are equal, i.e., $t_d - t = 0$ in fig. 2. For $s > s_m$, the ribbon thickness is greater than the die thickness.

An important consequence of the analysis in fig. 2 is that the steady-state ribbon thickness is uniquely determined by the meniscus shape variables, viz., $t = f$ $(s, t_d, h_{eff}, \phi_o)$. It follows, therefore, that in EFG, and in all other meniscus-controlled growth processes as well, there is only an indirect relationship between the crystal dimension and the growth rate; this fact is often misunderstood in the literature. The relationship arises solely via the value of the meniscus height at the edge of the crystal. The position of the tri-junction (and the detailed shape of the growth interface, as well) is, of course, determined by the heat flow in the liquid and in the crystal, and by the condition of heat balance at the growth inter-face. Therefore, in principle, a wide range of crystal growth rates can lead to the same value of s, and hence to the same value of the steady-state crystal dimension.

A quantitative measure of growth stability can be derived from fig. 2 from consideration of the quantity $\left| (\partial t/\partial s)_{t_d, h_{eff}} \right|$. Clearly, a lower absolute value of this slope implies a lesser dependence of ribbon thickness on variations in meniscus height (say, caused by changes in growth rate or thermal gradients), and hence better control of the ribbon thickness. For $h_{eff} > 0$, stability of the ribbon thickness is seen to increase as the meniscus height decreases or as $h_{eff}$ decreases. For growth with $h_{eff} < 0$, the stability increases at first as the meniscus height increases; in fact, the condition where $\left| \partial t/\partial s \right| = 0$ is reached. Beyond this height, stability decreases with further increase in meniscus height. The range of meniscus heights for which t is relatively independent of s is seen to decrease for increasingly larger negative values of $h_{eff}$.

Finally, it should be pointed out that meniscus shapes and s-t relationships can also be calculated (by numerical integration of Laplace's equation) for $h_{eff}$ in the range -1 cm to 1 cm. We are limiting our analysis to $\left| h_{eff} \right| \geq 1$ cm in order to use

the approximation that the meniscus shape is circular (i.e., eqs. (7) and (8)). Stepanov growth of shaped crystals, on the other hand, is usually carried out with $h_{eff} \approx 0$ or with $h_{eff}$ somewhat less than zero. Meniscus shape calculations appropriate to these conditions have been carried out by the Russian researchers [50,52]; we will attempt to interpolate our results to investigate this intermediate range of $|h_{eff}|$ .

## 4.2  Die Material Considerations

The selection of an appropriate die material for shaped crystal growth requires consideration of the various physical and chemical processes which can occur as a result of the intimate contact between the die and the melt. Those relevant to this discussion are:  (i) wettability (which affects capillary rise and edge-definition for shaped growth); (ii) chemical reactions; and (iii) heat and fluid flow effects. Most of these aspects of the die material problem, as they relate to silicon ribbon EFG, have been discussed in greater detail in earlier publications [14,16,21,26].

The phenomenon of capillary rise depends on the dimensions of the capillary, the surface tension of the liquid, and the wettability of the die by the melt. In all practical situations, we are dealing with systems where the die is "partially-wetted" by the melt, i.e., an equilibrium contact angle $\phi_c$ between $0^{\circ}$ and $180^{\circ}$ is established between the melt and the die surface at some point on the die. For the purposes of the present discussion, we will deviate from the classical definition of wetting and refer to "wetted" dies when $0^{\circ} < \phi_c < 90^{\circ}$ and "non-wetted" dies when $90^{\circ} < \phi_c < 180^{\circ}$; this terminology is used throughout this paper. In order for capillary rise to take place, of course, the die must be wetted by the melt; this occurs in the EFG process. For silicon ribbon growth by EFG, graphite ($\phi_c \approx 30^{\circ}$ [53]) is generally used for the die material. Stepanov growth, on the other hand, uses non-wetted dies; here, it is necessary to have a positive hydrostatic pressure (e.g., gravity) to bring the melt to the die top prior to seeding. The advantages of using wetted over non-wetted dies in the shaping process extend beyond the initial

capillary feeding problem; these essentially involve "edge-definition" aspects of the die and will be discussed in detail in Section 4.4.

The chemical compatibility of the die with the melt is a prime consideration in selecting the die material. Problems specific to silicon ribbon growth for solar cell applications have been discussed in earlier papers [14,16]. From the point of view of dissolved impurities, it should be kept in mind that a characteristic of EFG is that the effective distribution coefficient of all solutes is essentially unity [14,54]; the same holds true for Stepanov growth [55]. In general, it would be expected that dies which are not wetted by the melt would also be less reactive chemically. Chemical reaction between the melt and the die can, of course, lead to undesirable fluctuations in the contact angle $\phi_c$ (if, indeed, a contact angle can be postulated to exist under such circumstances). The mechanical integrity and long term reliability of the die are also affected by chemical reactions (e.g., reaction products or dissolution distorting the shape of the die). For silicon ribbon growth, graphite dies provide stable wetting (with $\phi_c \approx 30^o$) in spite of the continuous reaction to form silicon carbide at the die top [54]. Dies made from fused silica, on the other hand, are barely wetted by liquid silicon ($\phi_c \sim 87^o$ [14]), yet there is considerable fluctuation of the contact angle as a result of the chemical reaction to form silicon monoxide. Other considerations, from the point of view of dissolved impurities, include the effects of constitutional supercooling on crystallinity [14].

The thermal properties of the die (e.g., thermal conductivity) and the details of the die design can be used to control the shape of the crystal-liquid interface. This is very important, of course, from the point of view of crystallinity and solute distribution in the grown crystal. By arranging the capillary feeding channels in the die appropriately, we can also achieve solute redistribution (and, to a lesser extent, interface shape control) by the flow of the melt in the capillary and in the meniscus film on top of the die. In general, wetted dies (which permit growth from outer die edges for a wide range of growth conditions, as shown in Section 4.4)

provide a greater latitude in die design to effect control of the interface shape
and of the distribution of impurities in the crystal than would be possible using
non-wetted dies.

## 4.3  Die Design and Meniscus Attachment

In this section, we consider the design of the die shaper solely from the
point of view of attaching the meniscus to some point on the die top.  Fig. 3 shows
four specific cross-sectional shapes of the die top which we will examine for silicon
ribbon growth; it should be recalled that we are limiting our discussion to the
meniscus at the ribbon side, and hence we are not concerned here with the design of
the die in the ribbon width dimension.  We should point out that the designs in
fig. 3 (e.g., slopes of various surfaces) are merely used as examples, and that
many other variations are possible.  The die may be either wetted or not wetted by
liquid silicon, and the hydrostatic pressure in the meniscus film may be either
negative or positive (i.e., $h_{eff} > 0$ or $h_{eff}^{\cdot} < 0$, respectively).  We are not con-
cerned here with the manner (i.e., capillary rise, gravity, etc.) in which the die is
filled by the melt before seeding.

We will be considering the attachment of the meniscus to the edges denoted by
AD, BA, CA, BD, ED and CE in fig. 3; the edge AD, for example, corresponds to the
junction of the vertical inner surface D and horizontal surface A, as shown in the
figure.  The utility of the above notation will be apparent from the subsequent dis-
cussion.  Fig. 3a is a typical EFG die shape; the bevel at the outer edge BA may be
varied (cf. vertical outer surface at edge CA in fig. 3b).  The die-top surface
(i.e., AD to BA) may also be varied in extent, and it need not be horizontal.  Fig. 3c
shows the limiting case of a knife-edge die; the die top surface in fig. 3d is sloped
toward the center capillary.  The latter die design has been particularly useful in
controlling the interface shape and solute distribution in the growth of sapphire
ribbons from molybdenum dies [57].  In considering the point of attachment of the
meniscus to the die, it is useful to consider each of the edges in fig. 3 to be

consisting of a rounded corner with some finite radius of curvature. An example of this is shown in fig. 3e for the edge BD in fig. 3c. Each point on the die can now be characterized by the angle $\psi_d$ (defined in fig. 3e); the range of $\psi_d$-values for each die-edge of interest is listed in the caption to fig. 3. Although neither the simplification in fig. 3e nor the assumption of perfectly sharp edges is entirely correct, the former is clearly a better approximation to a real system. Also, it is the range of $\psi_d$-values (rather than the detailed shape) at each corner which will be relevant to our discussion.

On a magnified scale of the die surface, such as shown in fig. 3e, the meniscus will seek out a point of attachment where the equilibrium contact angle $\phi_c$ between the melt and the die surface is satisfied; this is illustrated in fig. 3e. The parameters which are relevant to finding this point, for a given value of $\phi_c$, are the angle $\Theta$ between the meniscus and the horizontal and the angle $\psi_d$ which characterize: the contact point on the die; with reference to fig. 3e, it can be readily shown that

$$\phi_c = \Theta + 90^o - \psi_d. \tag{9}$$

For steady-state growth (i.e., $\phi = \phi_o$), the angle $\Theta$ has a predictable variation with meniscus height for a given value of $h_{eff}$. The results of the calculation are shown in fig. 4 for the approximation of a circular meniscus at the ribbon side. We next consider the attachment of the meniscus to wetted and non-wetted die shapes of the type shown in fig. 3 in view of the contact angle requirement expressed by eq. (9).

4.4  Comparison of Wetted and Non-Wetted Dies

We can combine the $\Theta$-variation in fig. 4 and the $\psi_d$-ranges of the various die edges in fig. 3 with the expression for $\phi_c$ in eq. (9) to determine the range of contact angles which can be obtained, for given values of meniscus height and $h_{eff}$, at each of the die edges. The resulting curves are shown in figs. 5a and 5b for $h_{eff}$ = 2 cm and $h_{eff}$ = -2 cm, respectively. The region between curves B and A in the figures denotes possible growth conditions from edge BA in fig. 3, that between curves A and D denotes growth conditions from edge AD, and so on. The broken lines denoted

by $s_{max}$ in fig. 5 represent the limit of shape stability (i.e., $\partial\phi/\partial t \leq 0$), as discussed previously. The second broken line in fig. 5b denotes the meniscus height ($s_m$) where $t = t_d$; recall that we have selected this value of meniscus height as the practical limit for growth under positive hydrostatic pressure (i.e., $h_{eff} < 0$). We now proceed to examine briefly the use of graphite and fused silica dies for the growth of silicon ribbons.

For graphite dies ($\phi_c = 30^o$) and a negative hydrostatic pressure corresponding to $h_{eff} = 2$ cm (fig. 5a), we see that growth can take place from the outer die edges BA and CA up to a maximum meniscus height of about 0.098 cm. For $s > 0.098$ cm, the meniscus would tend to recede toward the inner edge AD. Growth from AD, however, is possible only for $0.098 < s < s_{max} = 0.117$ cm. Whether or not growth would continue in this case, depends on the capillary spacing in the die, which now becomes the effective value of $t_d$. From fig. 2, we see that $t_d - t = 0.14$ cm when $s = 0.098$ cm; thus, for a typically narrow capillary spacing, the ribbon thickness would tend to become zero. It should be emphasized that the curves in fig. 2, which relate the ribbon thickness to meniscus height for a given edge-to-edge die dimension, should always be considered in conjunction with the analysis of fig. 5. Growth from edges BD and CE in fig. 5a can occur up to $s_{max}$ for graphite dies, but growth is not possible from the inner edge ED. It is interesting to point out in fig. 5a that, for very small values of the contact angle, the meniscus height must be above a certain minimum value before growth can take place from edge BA. For example, for $\phi_c = 0^o$, it is necessary that $s \gtrsim 0.045$ cm for growth from BA.

Graphite dies do not function as satisfactorily under a positive hydrostatic pressure of $h_{eff} = -2$ cm (see fig. 5b). Growth from CA and CE is possible up to the meniscus height $s_m$ (this is a somewhat arbitrary limit, as explained earlier), whereas growth from BA and BD can occur up to a meniscus height of about 0.027 cm. If this value of meniscus height were exceeded, the meniscus would tend to spread beyond the edges BA and BD, i.e., "flooding" would tend to occur. Growth cannot

occur from the inner edges AD and ED with $\phi_c = 30^o$.

From fig. 5a, we see that fused silica dies cannot be used under a negative hydrostatic pressure of $h_{eff} = 2$ cm for growth from edges BA and CA, but that growth is possible for all $s \leq s_{max}$ from BD and AD. For $s \lesssim 0.051$ cm, growth can occur from CE, while it is necessary that $0.051$ cm $< s < s_{max}$ for growth from edge ED. Under a positive hydrostatic pressure of $h_{eff} = -2$ cm (fig. 5b), fused silica dies can be used for growth from all die edges with the exception of ED. For growth from AD, s must be less than about $0.019$ cm; for s greater than this value (up to the limit $s_m$), the meniscus would spread across the die-top surface to the edges BA and CA. Such spreading growth, with the concomitant thermal changes, may be undesirable, since it may lead to a possible "flooding" situation. Growth from BD and CE can occur up to the limiting height for $\phi_c = 87^o$.

Fig. 6 summarizes the results for graphite and fused silica dies as a function of $h_{eff}$. The curves denoted by A to E have the same meaning as in fig. 5; the subscripts "c" and "s" are used to denote graphite and fused silica dies, respectively. Several of the curves coincide with the $s = 0$ line, as noted in the figure. The interpretation of the curves is the same as for fig. 5; e.g., the region between $B_c$ and $A_c$ denotes possible growth conditions from edge BA (for graphite dies), that between $A_s$ and $D_s$ denotes possible growth from AD (for fused silica dies), and so on. The broken lines in fig. 6 denote the limiting height $s_{max}$ and the practical limit $s_m$ for growth under positive hydrostatic pressure; for $h_{eff} > 0$, the curve for $s_{max}$ coincides with that denoted by $D_c$, $E_c$ and $D_s$.

It is apparent from the above analysis that a useful basis for comparison of wetted and non-wetted dies is the range of meniscus heights for which growth can occur from a given die edge. Clearly, a greater range of s-values can be translated, in practice, into less stringent control of the growth parameters, i.e., a greater range of experimental operating conditions or less precisely controlled production conditions (growth rates, thermal gradients, etc.) for stable crystal growth. On

this basis, then, we can make the following statements regarding the use of wetted and non-wetted dies for shaped crystal growth, as evidenced by the examples shown in figs. 5 and 6:

(i)  Growth from inner die edges (e.g., AD and ED) is favored by non-wetted dies.

(ii)  Growth from outer die edges (e.g., BA, CA and CE) is favored by wetted dies.

(iii)  Growth from knife-edge dies (e.g., BD) is favored by non-wetted (or less wetting) dies for positive hydrostatic pressure, and by wetted (or more wetting) dies for negative hydrostatic pressure.  Although a knife-edge die can be used for either wetted or non-wetted dies in most situations, it appears likely that some deterioration of the knife-edge would always occur in practice, in which case the die-top would soon resemble that in fig. 3a.

(iv)  The use of negative hydrostatic pressure generally favors the use of more wetting dies (i.e., $\phi_c$ decreasing); advantages of $h_{eff} > 0$ include stability against flooding, larger range of s-values, and easier control of the pressure.

(v)  The use of positive hydrostatic pressure generally favors the use of less wetting dies (i.e., $\phi_c$ increasing); advantages of $h_{eff} < 0$ include greater shape (or si stability (i.e., lower $|\partial t/\partial s|$), and obviating the need for capillary rise to effect the initial filling of the die.

(vi)  For wetted dies, the full extent of the die top (i.e., large $t_d$-range) is generally available for growth when $h_{eff} > 0$; the same holds true for non-wetted dies when $h_{eff} < 0$.

(vii)  The $h_{eff} \simeq 0$ case would fall somewhere in-between the curves in figs. 5a and 5b; it is readily seen that outer die edges are more useful for growth from wetted dies, while inner edges are preferred for growth from non-wetted dies.

It should be noted that many of these advantages of wetted and non-wetted dies are already inherent in the usual practice of the EFG and Stepanov methods, respectively.

Other advantages of wetted dies (e.g., interface shape and solute distribution control via the wetted top surface, and capillary rise) and of non-wetted dies (e.g., better chemical compatibility, in general) have been discussed in a previous section. For ribbon growth with $h_{eff} > 0$, non-wetted dies would tend to provide very little stability at the ribbon edges. Even if the die were initially filled in some manner, for example, the melt in the capillary at the die edges would tend to recede as soon as the ribbon tapered (i.e., the width decreased). It seems unlikely that full-width growth could be re-established under these conditions. On the effects of the "roughness" of the die surface, which is likely to be the case in most shaped crystal growth situations, it should be pointed out that the effective or apparent angle of contact at the die surface decreases with increasing surface roughness for $\phi_c < 90^{\circ}$, while it increases with roughness for $\phi_c > 90^{\circ}$ [58].

In summary, it may be said that either wetted or non-wetted dies can be used for shaped crystal growth, but that the necessary conditions may be easier to achieve and maintain when wetted dies are used. The EFG process has evolved, in a relatively short period of time, to become a viable commercial technology for the growth of sapphire crystals; every indication suggests that the same should occur for the growth of silicon crystals by EFG.

Acknowledgments

We are grateful to S.R. Coriell, D.N. Jewett, H.E. LaBelle, Jr., K.V. Ravi, and F.V. Wald for many helpful comments and discussions.

References

1. A.V. Stepanov, Bull. Acad. Sci. USSR, Phys. Ser. 33 (1969) 1775.

2. P.I. Antonov, J. Crystal Growth 23 (1974) 318.

3. A.I. Bennett and R.L. Longini, Phys. Rev. 116 (1959) 53.

4. S. O'Hara and A.I. Bennett, J. Appl. Phys. 35 (1964) 686.

5. G.K. Gaule and J.R. Pastore, in: "Metallurgy of Elemental and Compound Semi-conductors", Ed. R.O. Grubel (Interscience, New York, 1961) p. 201.

6. J.C. Boatman and P.C. Goundry, Electrochem. Tech. 5 (1967) 98.

7. C.E. Bleil, J. Crystal Growth 5 (1969) 99.

8. H.E. LaBelle, Jr., U.S. Patent 3, 471, 266 (October 1969); H.E. LaBelle, Jr., U.S. Patent 3, 591, 348 (July 1971).

9. H.E. LaBelle, Jr. and A.I. Mlavsky, Mater. Res. Bull. 6 (1971) 571; H.E. LaBelle, Jr., Mater. Res. Bull. 6 (1971) 581; B. Chalmers, H.E. LaBelle, Jr. and A.I. Mlavsk; Mater. Res. Bull. 6 (1971) 681.

10. B. Chalmers, H.E. LaBelle, Jr. and A.I. Mlavsky, J. Crystal Growth 13/14 (1972) 84.

11. H.E. Bates, F.H. Cocks and A.I. Mlavsky, in: "Proc. Ninth IEEE Photovoltaic Specialists Conf." (IEEE, New York, 1972) p. 386.

12. H.E. Bates, D.N. Jewett and V.E. White, in: "Proc. Tenth IEEE Photovoltaic Specialists Conf." (IEEE, New York, 1974) p. 197.

13. H.B. Serreze, J.C. Swartz, G. Entine and K.V. Ravi, Mater. Res. Bull. 9, (1974) 1421.

14. J.C. Swartz, T. Surek and B. Chalmers, J. Electron. Mater. 4 (1975) 255.

15. B. Chalmers, A.I. Mlavsky, T. Surek, J.C. Swartz, R.O. Bell, D.N. Jewett, D.A. Yate K.V. Ravi and F. Wald, Mobil Tyco Solar Energy Corp., Final Technical Report NSF/RANN/SE/GI-37067X/FR/75/1, August 1975 (NTIS Accession No. PB247228/AS).†

16. K.V. Ravi, H.B. Serreze, H.E. Bates, A.D. Morrison, D.N. Jewett and J.C.T. Ho, in: "Proc. Eleventh IEEE Photovoltaic Specialists Conf." (IEEE, New York, 1975) p. 280.

17. C.V. Hari Rao, H.E. Bates and K.V. Ravi, J. Appl. Phys. 47 (1976) 2614.

18. K.V. Ravi and A.I. Mlavsky, in: "Sharing the Sun: Solar Technology in the Seventies", Vol. 6, Ed. K.W. Boer (ISES, 1976) p. 23.

19. L.C. Garone, C.V.H. Rao, A.D. Morrison, T. Surek and K.V. Ravi, Appl. Phys. Lett. 29 (1976) 511.

20. T. Surek, J. Appl. Phys. 47 (1976) 4384.

21. A.D. Morrison, D.N. Jewett, B.H. Mackintosh, W.T. Little, V.E. White and D.A. Yates, in: "Proc. of the International Symposium on Solar Energy", Ed. J.B. Berkowitz and I.A. Lesk (The Electrochemical Soc., Princeton, 1976) p. 216.

22. A.K. Sood, G.M. Freedman, R.O. Bell and F.V. Wald, in: "Proc. of the International Symposium on Solar Energy", Ed. J.B. Berkowitz and I.A. Lesk (The Electrochemical Soc., Princeton, 1976) p. 227.

23. A.K. Sood, C.V. Hari Rao, H.E. Bates and K.V. Ravi, 424 RNP, J. Electrochem. Soc. 122 (1975) 181C.

24. T. Surek, C.V. Hari Rao, J.C. Swartz and L.C. Garone, J. Electrochem. Soc. 124 (1977) 112.

25. K.V. Ravi, F.V. Wald, R. Gonsiorawski, H. Rao, L.C. Garone, J.C.T. Ho and R.O. Bell, in: "Proc. Twelfth IEEE Photovoltaic Specialists Conf." (IEEE, New York, 1976), p. 182.

26. K.V. Ravi, J. Crystal Growth, in print.

27. K.V. Ravi and F.V. Wald, in: "Semiconductor Silicon, 1977", Ed. by H.R. Huff and E. Sirtl (The Electrochemical Soc., Princeton, 1977) p. 820.

28. T.F. Ciszek, Mater. Res. Bull. 7 (1972) 731.

29. T.F. Ciszek and G.H. Schwuttke, Phys. Status Solidi A 27 (1975) 231.

30. T.F. Ciszek, J. Appl. Phys. 47 (1976) 440.

31. B.H. Mackintosh, A.D. Morrison, C.V.H.N. Rao, K.V. Ravi, H.B. Serreze, T. Surek, F.V. Wald and D.A. Yates, Mobil Tyco Solar Energy Corp., First Quarterly Report ERDA/JPL/954355/77-1, March 1977.†

32. A.D. Morrison, K.V. Ravi, C.V. Hari Rao, T. Surek, D.F. Bliss, L.C. Garone and R.W. Hogencamp, Mobil Tyco Solar Energy Corp., Annual Progress Report ERDA/JPL/954355/76-11, September 1976.†

33. R.J. Pohl, J. Appl. Phys. 25 (1954) 668.

34. P.I. Antonov, in: "Growth of Crystals", Vol. 6a, Ed. N.N. Sheftal (Consultants Bureau, New York, 1968) p. 145.

35. P.I. Antonov and A.V. Stepanov, Bull. Acad. Sci. USSR, Phys. Ser. 33 (1969) 1805.

36. P.I. Antonov and A.V. Stepanov, Bull. Acad. Sci. USSR, Phys. Ser. 33 (1969) 1813.

37. Yu. M. Shashkov and E.V. Melnikov, Russian J. Phys. Chem. 39 (1965) 1364.

38. T. Surek and B. Chalmers, J. Crystal Growth 29 (1975) 1.

39. T. Surek, Scripta Met. 10 (1976) 425.

40. W. Bardsley, F.C. Frank, G.W. Green and D.T.J. Hurle, J. Crystal Growth 23 (1974) 341.

41. A.I. Pogodin, I.M. Tumin and A.M. Eidenzon, Bull. Acad. Sci. USSR, Phys. Ser. 37 (1973) 32.

42. F.C. Frank, private communication (1976).

43. M.G. Milvidskii and A.V. Berkova, Sov. Phys. Solid State (Eng. Transl.) 5 (1963) 374.

44. T.F. Ciszek, J. Crystal Growth 10 (1971) 263.

45. T. Surek and S.R. Coriell, to be published.

46. T. Surek and S.R. Coriell, J. Crystal Growth 37 (1977) 253.

47. K.M. Kim, G.W. Cullen, S. Berkman and A.E. Bell, RCA Laboratories, Quarterly Report No. ERDA/JPL/954465/76-1, June 1976.†

48. S.R. Coriell and M.R. Cordes, Proceedings of ICCG-5, this volume.

49. K. Mika and W. Uelhoff, J. Crystal Growth 30 (1975) 9.

50. V.A. Tatarchenko, A.I. Saet and A.V. Stepanov, Bull. Acad. Sci. USSR, Phys. Ser. 33 (1969) 1782; V.A. Tatarchenko and A.V. Stepanov, Bull. Acad. Sci. USSR, Phys. Ser. 33 (1969) 1788; V.A. Tatarchenko, D.I. Levinzon and A.V. Stepanov Bull. Acad. Sci. USSR, Phys. Ser. 36 (1972) 429.

51. M. Neuberger, "Group IV Semiconductor Materials", Handbook of Electronic Materials Vol. 5 (IFI/Plenum, New York 1971).

52. L.P. Egorov, L.M. Zatulovskii, P.M. Chaikin and D.I. Levinzon, Bull. Acad. Sci. USSR, Phys. Ser. 37 (1973) 22.

53. J.A. Champion, B.J. Keene and S. Allen, J. Mater. Sci. 8 (1973) 423.

54. B. Chalmers, M.C. Cretella, C.V. Hari Rao, T. Surek, F.V. Wald and K.V. Ravi, paper presented at ICCG-5, Boston, Mass. July 17 - 22, 1977.

55. A.I. Gubanov and S. Yu. Davydov, Bull. Acad. Sci. USSR, Phys. Ser. 35 (1971) 405.

56. D.T.J. Hurle, Proceedings of ICCG-5, this volume.

57. H.E. LaBelle, Jr., private communication (1977).

58. R.E. Johnson, Jr. and R.H. Dettre, in: "Surface and Colloid Science", Vol. 2, Ed. E. Matijevic (Wiley-Interscience, 1969) p. 85.

---

†These reports are avialable from the National Technical Information Service (NTIS), Springfield, Va. 22151, U.S.A., or from the sponsoring U.S. Government Agencies.
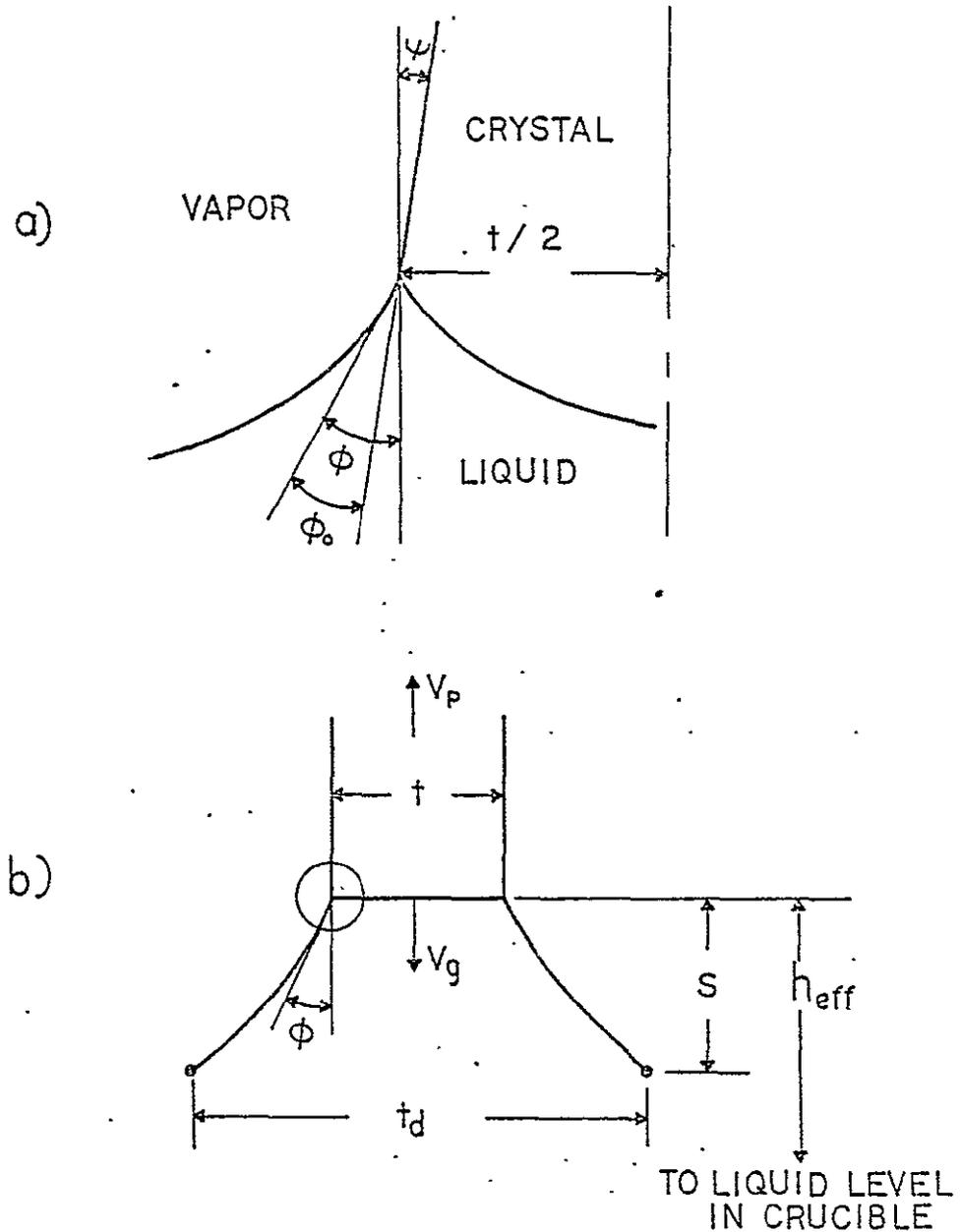
Fig. 1. (a) Schematic of interfacial configuration at crystal-liquid-vapor junction (magnified view of circled region in (b)) in crystal growth from the melt. The crystal grows with a uniform dimension t when the meniscus angle $\phi = \phi_0 = 11^\circ$ for silicon crystal growth. (b) Schematic cross-section of ribbon growth from a die-shaper of thickness $t_d$ showing geometrical variables which determine the ribbon thickness.
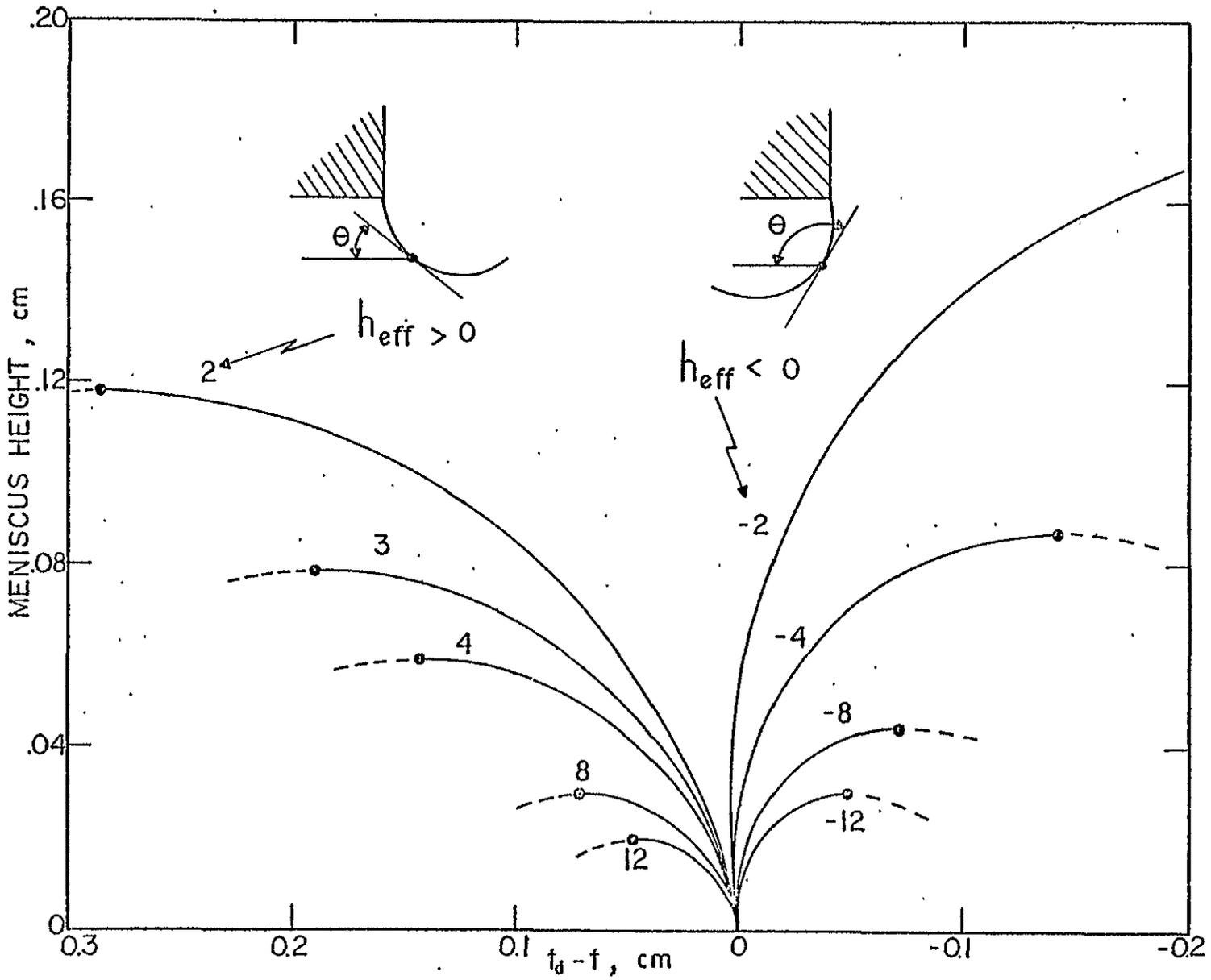
Fig. 2. Meniscus height-ribbon thickness relationships in silicon ribbon growth as a function of $h_{eff}$ ($t_d$ is the die thickness). The curves correspond to steady-state growth conditions, i.e., $\phi = \phi_o = 11^0$. The insets in the figure show the circular menisci at the side of the ribbon for positive and negative $h_{eff}$.
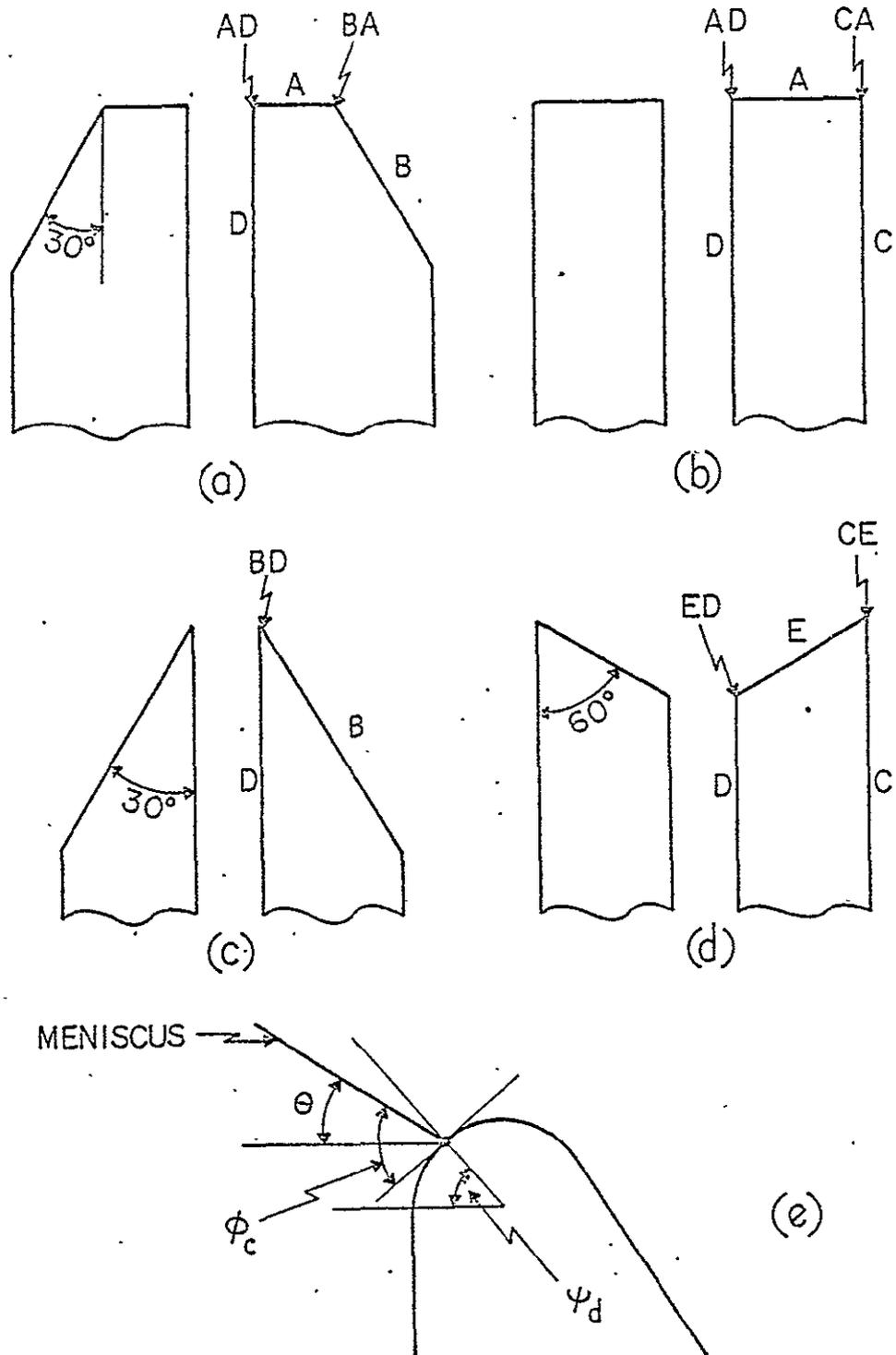
Fig. 3. (a) - (d) Examples of cross-sectional shapes of die top examined for silicon ribbon growth. The symbols A to E in the figures designate the various surface types under consideration. (e) Magnified view of edge BD in (c) showing attachment of meniscus to die top with contact angle $\phi_c$. The range of $\psi_d$-values for the various die edges are: AD ($0^\circ$ to $90^\circ$), BA ($90^\circ$ to $150^\circ$), CA ($90^\circ$ to $180^\circ$), BD ($0^\circ$ to $150^\circ$), ED ($0^\circ$ to $60^\circ$), and CE ($60^\circ$ to $180^\circ$).
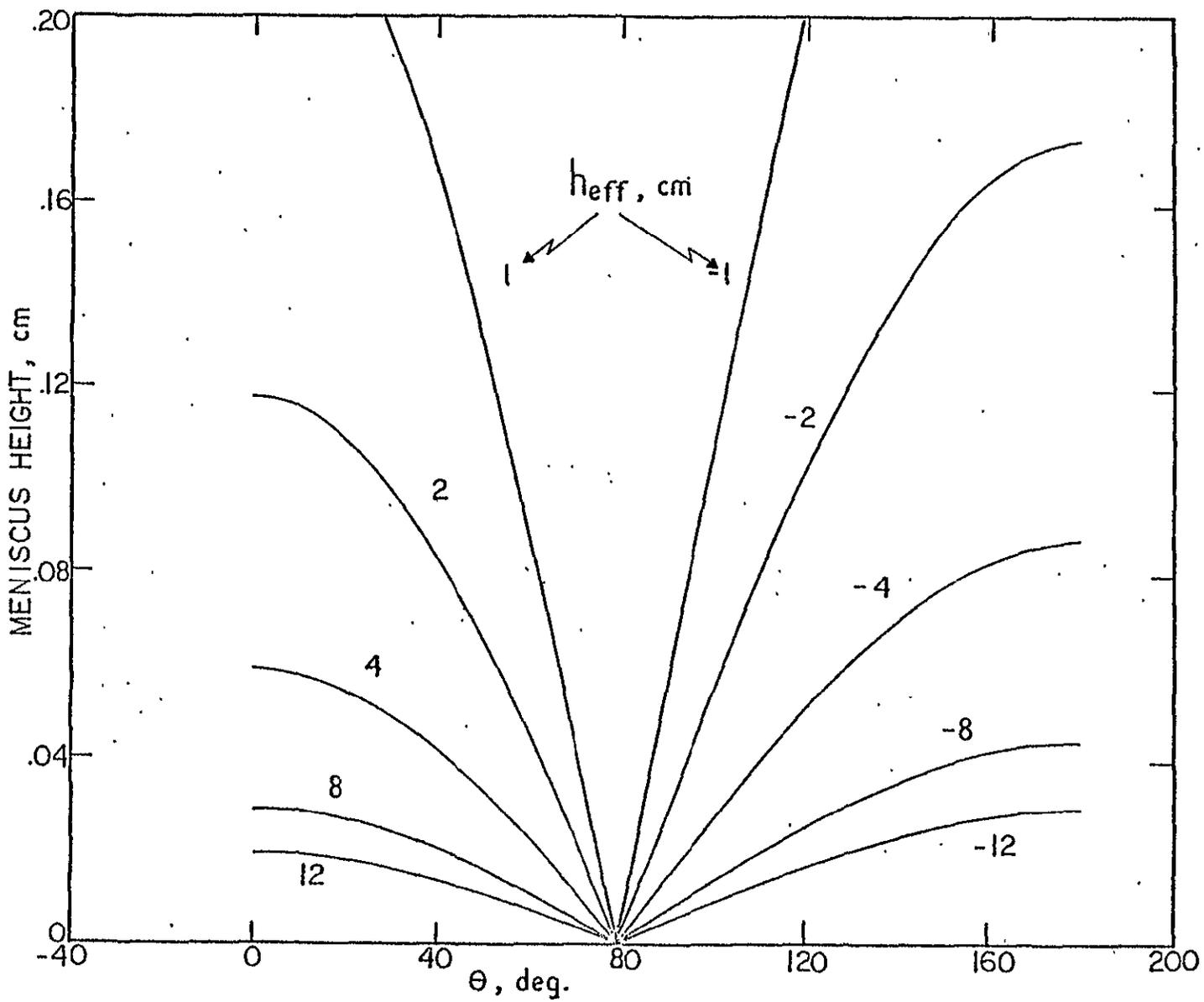
Fig. 4. Variation of the angle $\Theta$ between the meniscus and the horizontal with meniscus height as a function of $h_{eff}$ for the growth of silicon ribbons. At $s = 0$, $\Theta = 79°$; the maximum meniscus height ($s_{max}$) for shape stability occurs at $\Theta = 0°$ for $h_{eff} > 0$ and $\Theta = 180°$ for $h_{eff} < 0$.
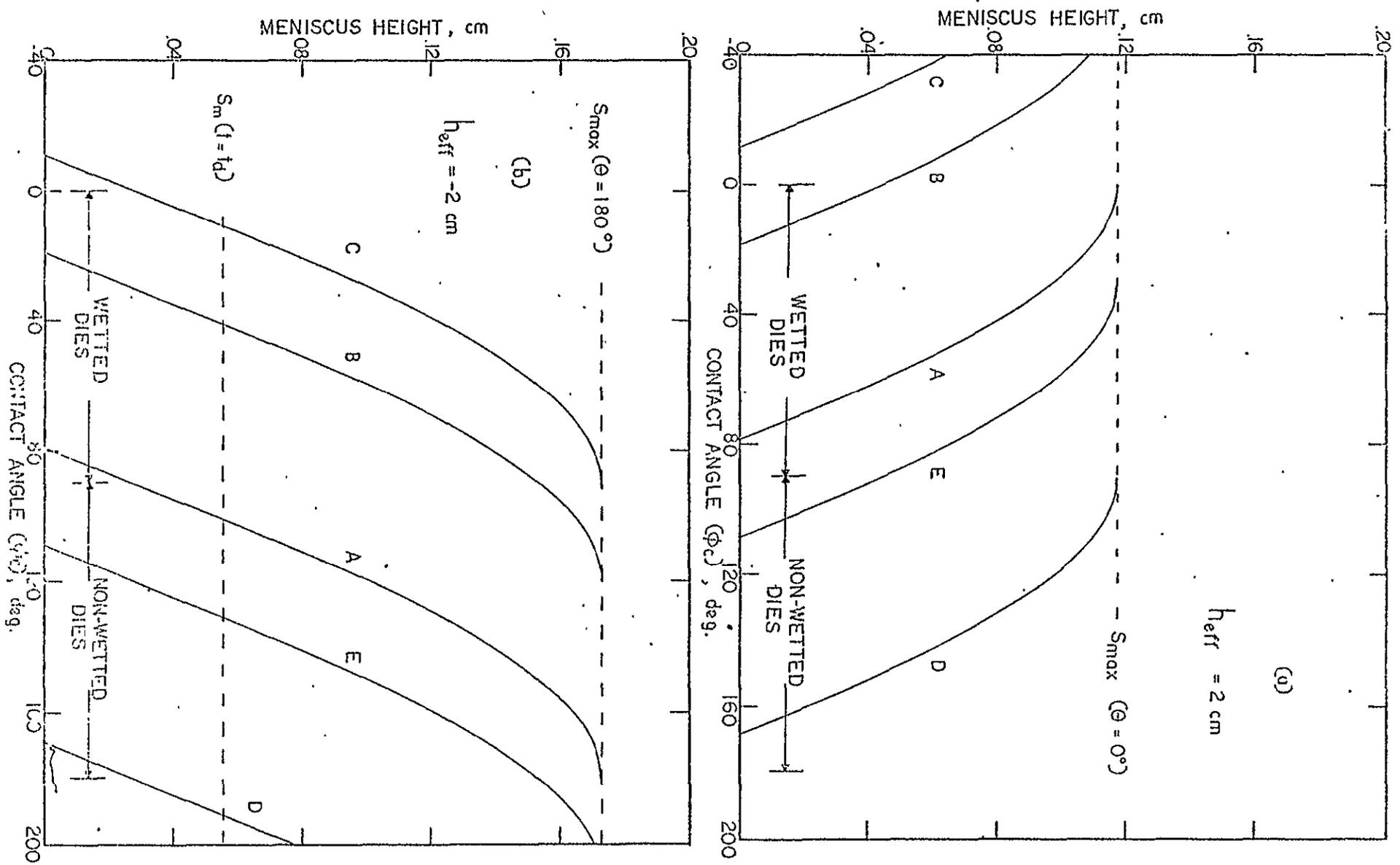
Fig. 5. Meniscus height limits as a function of contact angle for growth of silicon
ribbon from the various die edges in fig. 3. The region between curves A
and D, for example, denotes possible growth conditions from edge AD. (a)
$h_{eff}$ = 2 cm; (b) $h_{eff}$ = -2 cm.
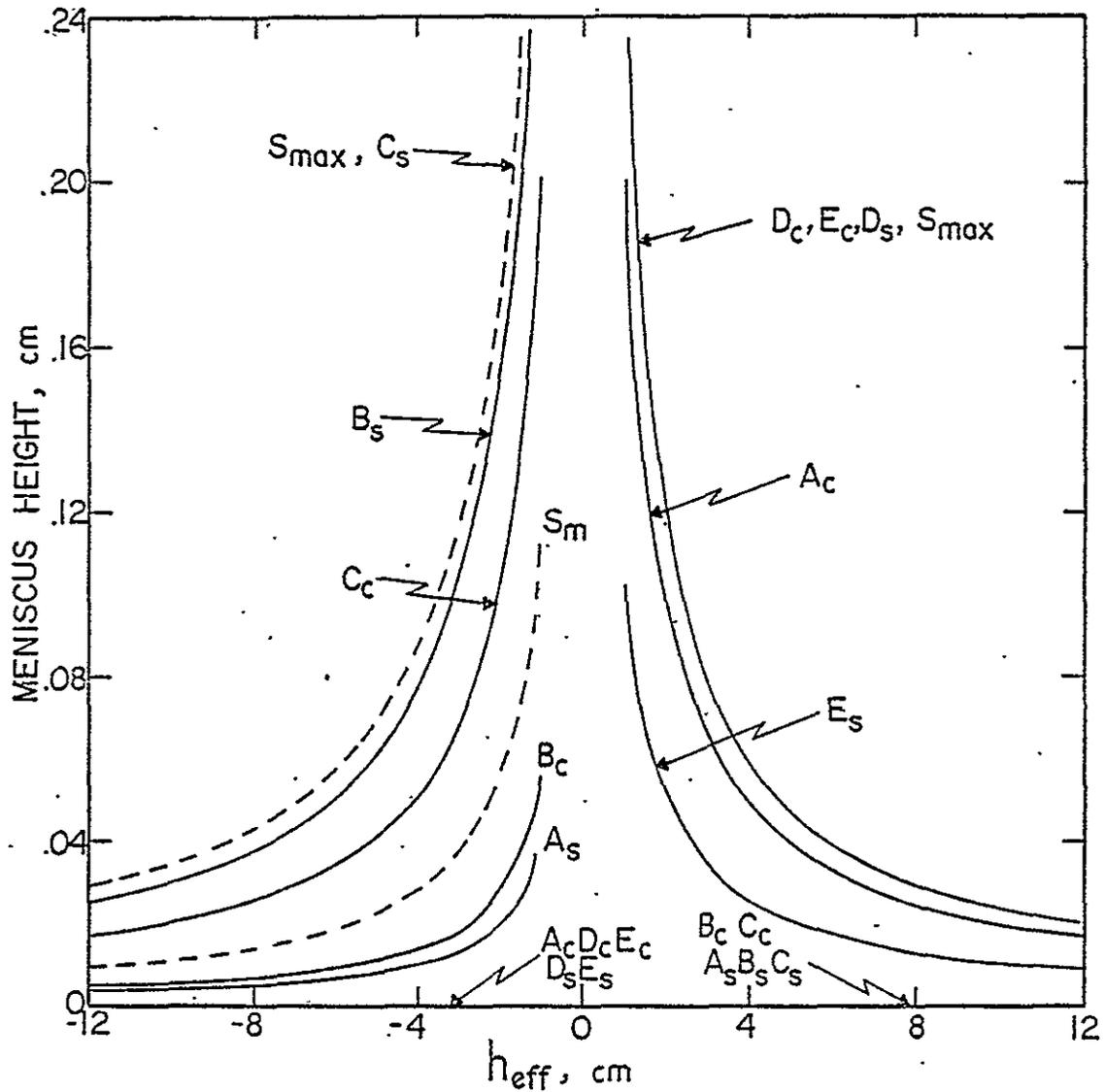
Fig. 6. Meniscus height limits as a function of $h_{eff}$ for growth of silicon ribbon from graphite (subscript "c") and fused silica (subscript "s") dies. Curves denoted by $B_c$ and $A_c$, for example, represent the range of allowed meniscus heights for growth from edge BA in fig. 3 (for a graphite die). The curves for $B_c$, $C_c$, $A_s$, $B_s$ and $C_s$ (for $h_{eff} > 0$) and $A_c$, $D_c$, $E_c$, $D_s$ and $E_s$ (for $h_{eff} < 0$) coincide with s = 0.

APPENDIX 7


Preprint 2: "Enhancement of Diffusion Length in EFG Ribbon Solar Cells Under Illumi-
nation", by C.T. Ho, R.O. Bell and F.V. Wald; accepted for publication
in:  Applied Physics Letters.

# ENHANCEMENT OF DIFFUSION LENGTH IN EFG RIBBON
# SOLAR CELLS UNDER ILLUMINATION

by

C. T. Ho, R. O. Bell and F. V. Wald

Mobil Tyco Solar Energy Corporation
16 Hickory Drive
Waltham, Massachusetts 02154

## ABSTRACT

The short circuit current, efficiency and minority carrier diffusion length of EFG ribbon silicon solar cells have been measured as a function of illumination level between zero and 5 suns and found to increase. The faster rate of increase of the current in ribbon cells compared to CZ we attribute to the enhancement of the minority carrier diffusion length under illumination. A quasi-continuous deep trap model with a Gaussian distribution of compensated donor states is proposed to account for these observations.

Minority carrier diffusion length is the single most important parameter·characterizing the performance of a photovoltaic converter such as silicon solar cell. With present advanced technologies, silicon crystals grown by the conventional Czochralski (CZ) or the float zone methods can have diffusion lengths of a hundred microns or longer. However, the ribbon-shaped crystals grown by the edge-defined, film-fed growth technique (EFG), typically have diffusion lengths of 20 to 30 $\mu$m.[1] In general one expects that crystallographic structural imperfections (twins, slip bands, dislocations, etc.) and metallic impurities (transition metals) present in EFG ribbons might behave as recombination centers, adversely affecting the diffusion length of the crystals, and consequently influencing the conversion efficiency of solar cells fabricated from ribbon material. In.this letter we show that this reasoning may not hold in operating cells because of a significant enhancement of the diffusion length even under low illumination levels.

As a model to explain this behavior we adopt a viewpoint commonly used in describing photoconduction processes[2,3] and demonstrate that a Gaussian or normal distribution of deep traps within the energy gap can account for the observations. Although somewhat similar findings have recently been reported by Fabre et al.[4] as well as Dalal and Moore,[5] who worked with Czochralski material, no detailed model for the effect has been given.

In our experiments both CZ and ribbon solar cells were fabricated by using conventional phosphorous diffusion and aluminum metallization

2

on p-type 1 to 5 Ω·cm materials. Back surface fields and antireflection coatings were not incorporated in the fabrication. The ribbon samples were chosen from various growth runs and only well behaved cells with good fill factors (> 0.7) were used.

Figure 1a shows the conversion efficiency of the cells as a function of illumination level up to about 5 suns. The conversion efficiency of the CZ cells increases only slightly as the light intensity increases, before the power loss from internal series resistance dominates. However, the ribbon cells show a substantial increase in efficiency even at very low illumination levels. In Fig. 1a, group A represents the averaged value of three cells with the highest photovoltaic output, and group C, three cells with the lowest photovoltaic performance. When the average short circuit current densities are plotted as a function of light intensity, a slope greater than unity (superlinearity) is found for the ribbon cells whereas the CZ cells maintain a slope of one. By superlinearity we mean that the short circuit current is proportional to the incident power to an exponent $\alpha$ , where $\alpha$ is greater than 1. Figure 1b shows the short circuit current per unit power plotted as a function of power. We find that the ribbon cells of group C exhibit a greater superlinearity ($\alpha = 1.07$) than group A ($\alpha = 1.04$).

Subsequently, the minority carrier diffusion lengths under different incident light levels were measured. By employing a standard lock-in amplifier the spectral response of the short circuit current was obtained

3

from a mechanically chopped, low intensity monochromatic light with a superimposed dc white light of intensities between 0 and 170 mW/cm$^2$. The charge collection efficiency was determined for wavelengths between 0.4 and 1.0 $\mu$m and the diffusion length, $L_n$, was calculated by using a non-linear least squares analysis to fit the photoresponse. The solar cell model used to relate the charge collection to the diffusion length is similar to the low injection level one outlined by Sahai and Milnes.[6] The minority carrier diffusion length in the p-region and the junction depth were used as the variable fitting parameters.

Figure 2a shows the diffusion lengths as a function of the white light intensities for one sample selected from each of the typical groups of good, medium, and poor performing solar cells. In this semilogarithmic plot we label $L_D$ as the diffusion length measured with only the mono-chromatic light present. A calibrated photodiode indicated this to have an intensity of 4 x 10$^{-5}$ mW/cm$^2$ at 0.95 $\mu$m. In all cases, the diffusion length increases monotonically as the photoexcitation increases, and at 100 mW/cm$^2$ it is much higher than in the "dark". In the few cases where measurements beyond one sun were made, a slow but continuing increase to at least 500 mW/cm$^2$ could be seen. A plot of the data for the same cells on a linear scale (Fig. 2b) reveals more clearly the fact that the main increase in $L_D$ occurs at very low intensities followed by a much slower rate of increase about 5 mW/cm$^2$.

One can use a model which postulates the presence of deep trapping states in the bandgap to explain the above observations. These deep

4

trapping centers have a "sensitizing effect" in analogy to the sensitizing centers discussed for II-VI compound photoconductors. For instance, the characteristic behavior of the sensitizing centers in an n-type CdS photoconductor is associated with the presence of compensated acceptors.[2] These centers are negatively charged, so that they have a much larger cross section for the capture of free holes than they subsequently have for the capture of free electrons.

In our case, we assume that deep, compensated donor states exist in the p-type substrate of the ribbon cell. Under essentially dard conditions, the minority carrier (electron) lifetime is controlled entirely by the density and capture cross section of these unoccupied and thus positively charged centers. As the illumination level increases, however, these states progressively trap electrons and become neutral. Their capture cross section is thus reduced significantly which decreases the electron recombination rate, thereby enhancing the lifetime and diffusion length.

Since the illumination intensity is not high enough to greatly perturb the majority carrier density, this concept is even simpler to apply here than in a photoconductor because in the base of a solar cell the carrier density at thermal equilibrium is high. Thus, we do not need to invoke the concept of optical charge transfer between fast recombination (type I) and sensitizing (type II) centers[2,3] because the change of occupancy of the defect states has little effect on the majority carrier density.

5

We assume that due to the high defect densities in ribbon silicon, the position of the deep trapping states is "smeared out" in energy and becomes quasi-continuous with a distribution function $N(E)dE$ within the band gap. If $N_t$ is the total density of the traps, $n_{td}$ and $n_{t\ell}$ are the densities that are filled by electrons in the dark and under illumination, respectively, we find

$$\frac{\tau_\ell}{\tau_d} = \frac{(N_t - n_{td})}{(N_t - n_{t\ell})} = \frac{\int_{E_v}^{E_c} N(E)dE - \int_{E_v}^{E_{fd}} N(E)dE}{\int_{E_v}^{E_c} N(E)dE - \int_{E_v}^{E_{f\ell}} N(E)dE} = \frac{\int_{E_{fd}}^{E_c} N(E)dE}{\int_{E_{f\ell}}^{E_c} N(E)dE} \quad (1)$$

where $\tau_d$ and $\tau_\ell$ are the electron minority carrier lifetimes, and $E_{fd}$ and $E_{f\ell}$ are the quasi-Fermi levels for electrons measured from the valence band edge $E_v$ toward the conduction band edge $E_c$ in the dark and under illumination, respectively.

Several different distributions of trapping states within the gap have been considered, including uniform, linear and exponential. However by far the most successful, both from the point of view of fitting the theory to experiment and yielding a reasonable physical interpretation, is a Gaussian distribution,

$$N(E)dE = N_o \exp\left[-((E - E')/\Delta E)^2\right] dE \quad (2)$$

where $E'$ is the mean value and $\Delta E / \sqrt{2}$ is the variance of the distribution (Fig. 3).

6

Assuming that the electron mobility does not change with intensity, using Eq. (1), we can write the ratio of the diffusion length in light $L_{n\ell}$ to the diffusion length in dark $L_{nd}$ in terms of error functions,

$$L_{n\ell}/L_{nd} = (\tau_\ell/\tau_d)^{\frac{1}{2}} = \left[ \frac{\text{erf}(\epsilon_c) - \text{erf}(\epsilon_d)}{\text{erf}(\epsilon_c) - \text{erf}(\epsilon_\ell)} \right]^{\frac{1}{2}} \tag{3}$$

where $\epsilon_c = (E_c - E')/\Delta E$, $\epsilon_d = (E_{fd} - E')/\Delta E$, and $\epsilon_\ell = (E_{f\ell} - E')/\Delta E$.

In order to calculate $L_{n\ell}$ we must choose $E'$ and $\Delta E$ to fit the measurement data. It is also necessary to know how $E_{f\ell}$ varies as a function of illumination intensity. This was calculated by assuming that the minority carrier concentration, $n$, was equal on average to the product of the dark lifetime and the generation rate of the light one diffusion length deep in the silicon. The familiar expression $E_f = kT\ell n(N_c/n)$ is used to determine $E_{f\ell}$. The calculated values of $L_{n\ell}/L_{nd}$ are shown in Figure 2 as solid lines, and the parameters used to fit the experimental data are given in Table I. For any given sample only $E'$ and $\Delta E$ are required to fit the data but to relate different samples to each other the relative number of traps is given by $N_o$ (Eq. (2) and Fig. 3).

Currently, other experiments including thermal and optical quenching measurements are being conducted to test this model. Preliminary low temperature measurements for group A samples show that at $80^\circ$K, $L_n$ is slightly larger - about 25% in the dark and 5% under 1 sun illumination - than $L_n$ at room temperature which is evidence for thermal quenching. There is also evidence for optical quenching when we compare the photo-response using only 0.95 $\mu$m monochromatic light ($E_\lambda > E_g$) to light con-

7

taining a wide band of infrared wavelengths.

In summary then, we show that the enhanced diffusion length under illumination is probably caused by a distribution of deep donor state, centered 0.55 eV from the conduction band. We feel that it is entirely logical to consider that such a state, which might be caused by an unintentional impurity, would be broadened (and might assume a Gaussian form) in EFG material due to the various imperfections found. These include twins, dislocations, dissolved or precipitated carbon and residual stress, which all would likely act to "smear out" the state of even a single impurity. Also some apparent broadening is produced by the nature of our simple model. The actual situation in an operating ribbon solar cell is more complicated. Since radiation with a wide distribution of wavelengths is present, thus the rate of generation of minority carriers and the position of the quasi-Fermi level is varying with depth below the surface of the base region of the cell. A more exact model requires knowledge of the recombination processes and the solution of a non-linear differential equation.

Nevertheless, the overall picture is quite clear. As the intensity increases, the minority carrier lifetime (or diffusion length) increases as deep donor levels are filled. This causes an improvement in solar cell performance which is most evident at very low light levels, where the shift of the Fermi level is most rapid. However, enhancement is still continuing at 5 suns with no evidence of total saturation.

## Acknowledgements

9

# REFERENCES

1. K. V. Ravi, H. B. Serreze, H. E. Bates, A. D. Morrison, D. N. Jewett, and C. T. Ho, 11th IEEE Photovoltaic Specialists Conference Record, Phoenix, Arizona, 1975, p. 280.

2. R. H. Bube, "Photoconductivity of Solids", John Wiley and Sons, New York (1960).

3. A. Rose, "Concepts in Photoconductivity and Allied Problems", Wiley-Interscience, New York (1963).

4. E. Fabre, M. Mautref, and A. Mircea, Appl. Phys. Letters $\underline{27}$, 239 (1975).

5. V. L. Dalal and A. R. Moore, J. Appl. Phys. $\underline{48}$, 1244 (1977).

6. R. Sahai and A. G. Milnes, Solid State Electronics $\underline{13}$, 1289 (1970).

TABLE I. Parameters used to fit experimental data in Figure 2 using the distribution function given by Eq. (2). $N_o$ is normalized with respect to cell group A.

| Cell Group | $L_D$ ($\mu$m) | $N_o$ (Rel) | E' (eV) | $\Delta E$ (eV) |
|------------|----------------|-------------|---------|-----------------|
| A | 38 | 1 | 0.64 | .21 |
| B | 15 | 6 | 0.55 | .26 |
| C | 6.2 | 38 | 0.55 | .22 |
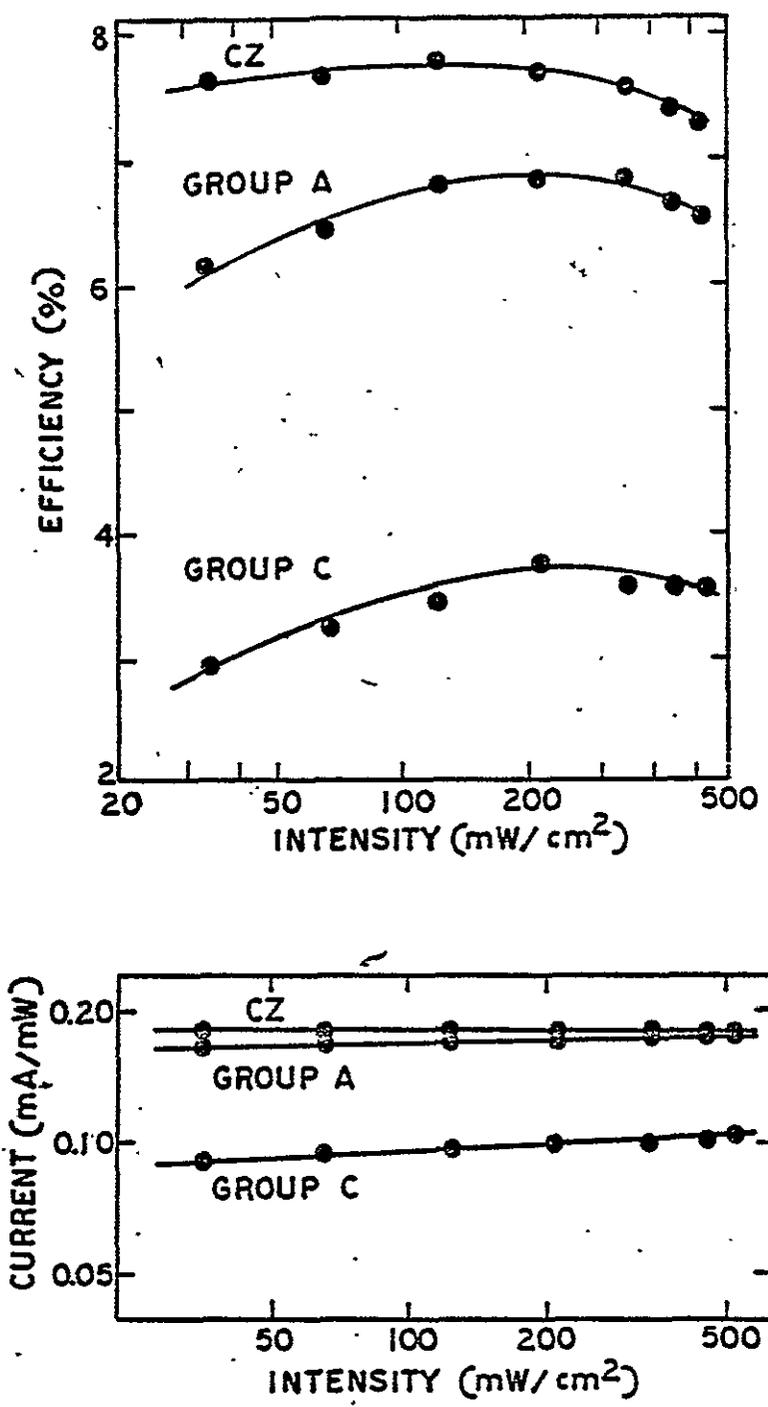
Figure 1. Behavior of EFG and CZ silicon solar cells as a function of illumination intensity. a) Efficiency. b) Short circuit current.
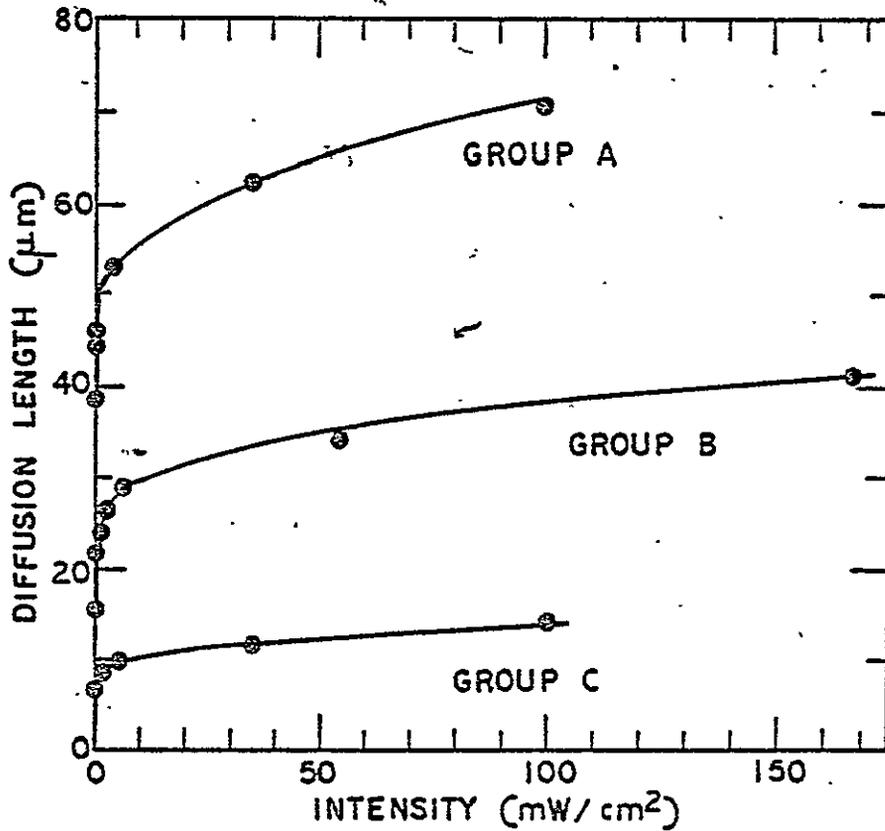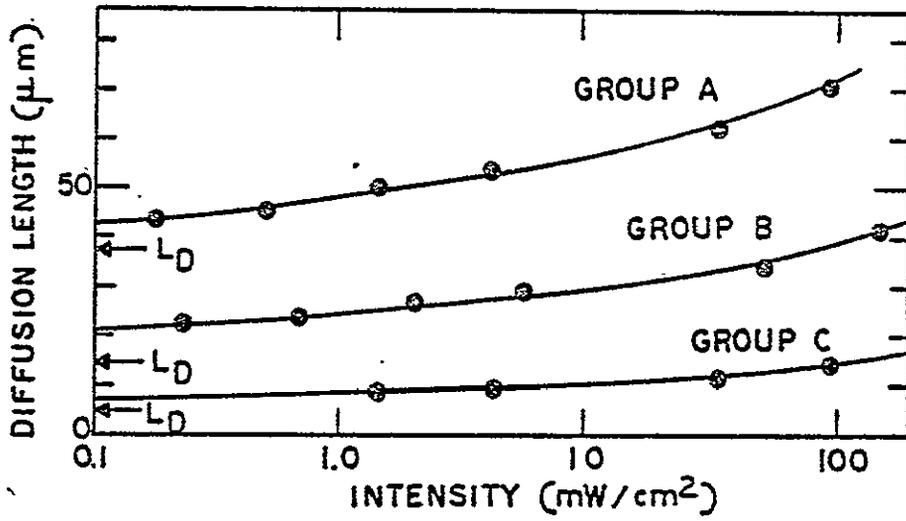
Figure 2. Diffusion length of EFG silicon solar cells as a function of illumination intensity. The solid lines are calculated and the points are experimental data. a) Semi-logarithmic scale. b) Linear scale.
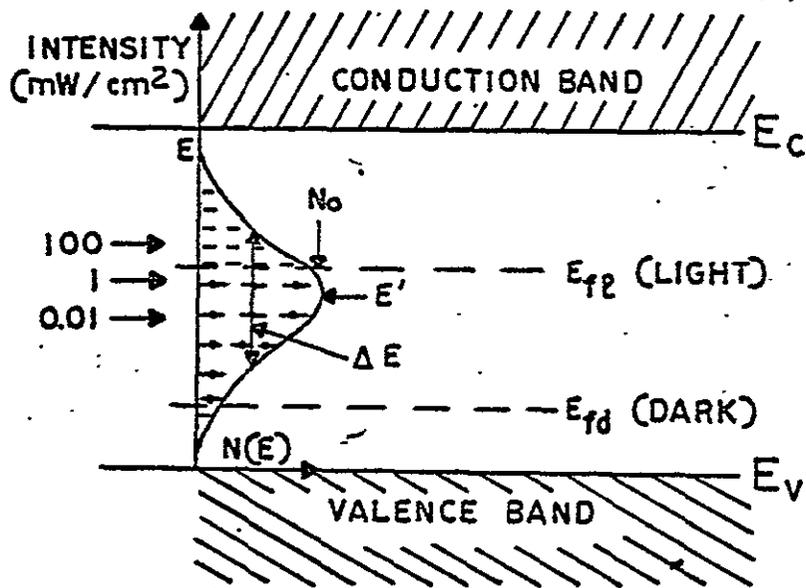
Figure 3. Energy level diagram of the density of donors within the band
gap. The position of the quasi-Fermi level for electrons is
shown in the light, $E_{f\ell}$ (light) and dark, $E_{fd}$ (dark). $E_{fd}$
(dark), the equilibrium Fermi level, is fixed by the doping
concentration in the p-type material. Also indicated is the
approximate position of the quasi-Fermi level of electrons
for different illumination levels.